UNIVERSITY OF WITWATERSRAND

CNT Doped PAN Nanofibre Strengthened Aramid-PP Composites: Improved interlaminar Properties

by

Mkhululi Ncube

A thesis submitted in partial fulfillment for the
degree of Master of Science in Engineering

in the
Faculty of Engineering
School of Mechanical Industrial and Aeronautical Engineering

September 2018

Declaration of Authorship

I, MKHULULI NCUBE, declare that this thesis titled, 'CNT doped PAN nanofibre strengthened aramid-PP composites: Improved interlaminar properties' and the work presented in it are my own. I confirm that:

- This work was done wholly or mainly while in candidature for a research degree at this University.
- Where any part of this thesis has previously been submitted for a degree or any other qualification at this University or any other institution, this has been clearly stated.
- Where I have consulted the published work of others, this is always clearly attributed.
- Where I have quoted from the work of others, the source is always given. With the exception of such quotations, this thesis is entirely my own work.
- I have acknowledged all main sources of help.
- Where the thesis is based on work done by myself jointly with others, I have made clear exactly what was done by others and what I have contributed myself.

Signed:
Mkhululi Ncube

Date:
12 June 2018

"Fear not, for I am with you."

Isaiah 41:10

Abstract

This study focused on the strengthening of aramid polypropylene hybrid composites using both electrospun PAN and CNT doped PAN nanomat. The strengthening of the aramid-polypropylene (PP) composites with both aligned and randomly distributed nanofibres resulted in the improvement of the tensile strength, flexural strength, impact energy absorption and interlaminar shear strength (ILSS). However, compared to the randomly distributed 0.5% PAN nanofibre strengthened aramid-PP composites, the aligned PAN nanofibre strengthened aramid-PP composites had higher mechanical properties with improvements in tensile strength by 6%, flexural strength by 5%, impact energy absorption by 7% and ILSS by 3%. The doping of PAN nanomat with pristine and functionalized CNTs resulted in an improved mechanical properties of the hybrid composites with those strengthened with functionalized CNTs achieving higher mechanical properties. With the increase in CNT concentration in the CNT doped PAN nanomat strengthened hybrid composite the mechanical properties increased. Compared with PAN reinforced aramid-PP composites, the addition of PAN doped with 0.5% functionalized CNTs resulted in an increase in tensile strength by 15%, flexural strength by 35%, impact absorption energy by 26% and ILSS by 32%. It was found that the dominant mechanism of failure for aramid-PP composites without PAN/CNT reinforcement was due to interfacial debonding.

This study shows that the use of aligned electrospun nanofibres help to improve the imterlaminar properties of the the hybrid composites. Functionalization of CNTs greatly improves the fibre-matrix interaction and thus greatly reducing failure by interfacial debonding. Overall, the doping of aligned PAN nanofibres with functionalized CNTs resulted in improvement in interlaminar and mechanical properties of the hybrid composites.

Acknowledgements

I would like to thank merSETA for funding my studies and making it possible for me to pursue this research. I would also like to thank Centre of Excellence in Strong Materials for financial support to purchase the equipment necessary to conduct this research.

Thanks to my family, colleagues and friends for their unwavering support through the hard and challenging times. Without their support I wouldn't have managed to go through this journey.

I would also like to thank my lab partner, Muhammad Arif, for all the support and assistance. This research wouldn't have been interesting without having you by my side. Thank you my friend.

I would also like to thank Mr. Shaun Riekert and his laboratory stuff for their help with the manufacturing of the equipment. I would also like to thank Dr Rudolph Erasmus for assisting me with Raman spectroscopy. Thanks to Dr Prakash Murthiyamma Gangatharan and Prof. Neil Coville for assisting me with CNT functionalization and analysis equipment.

Lastly I would like to thank my supervisor, Prof. Jacob Muthu, for his support and guidance throughout this journey. He gave me advise not only about research but life in general and made me feel welcome in this institution.

Contents

List of Figures

List of Tables

Dedicated To my Parents

Chapter 1

Introduction

1.1 Background

A composite is made of two or more constituents with different physical or chemical properties, when combined forms a material with characteristics different from its individual components. Typical engineered composite materials include concrete and reinforced plastics such as fibre composites [1].

Fibre reinforced polymer composites (FRPCs) have been used commercially for many decades in structural applications, including in aerospace, construction and automotive industries [2]. FRPCs consist of a polymer matrix reinforced with fibres such as aramid, glass, and carbon. The use of FRPCs have significantly increased in the last few decades due to their ease of processing, reduction in cost and weight savings when compared to conventional materials like metals [3]. The FRPC's properties depend mainly on the the properties of the individual constituents, geometry and their distribution[4]. The common shortcoming with FRPCs is their failure in matrix-rich interlaminar region where the load transfer between load-bearing fibres occur. The interlaminar region within a composite material is the area around the fibre where its in contact with the matrix. A strong fibre-matrix bond improves the strength of composite leading to better interlaminar properties. In an effort to improve the mechanical properties of fibre composites, researchers incorporated two or more fibres into a single matrix leading to the development of hybrid composites. The behaviour of hybrid composites is a weighed sum of the individual components in which there is a more favourable balance between the inherent advantages and disadvantages [5]. Hybrid composites offer a wide range of benefits such as low cost, better strength to weight ratio and fatigue performance that has led to most material engineers tailoring the hybrid materials to suit their exact structural design requirements [6]. Despite all these remarkable properties, hybrid composites are

still susceptible to failure at the interlaminar regions. As a result, many researchers have focused on the nano-strengthened-hybrid composites whereby nanoparticles are used as secondary reinforcement in an effort to improve both interlaminar region and overall properties of composites. Nanostrengthened hybrid composites are commonly called multi-scale reinforced hybrid composites [7]. Various carbon-based nanoparticles such as carbon nanotubes (CNTs) have been widely used as secondary reinforcement in hybrid composites because they posses attractive mechanical properties.

Carbon nanotubes (CNTs), first reported by Iijima in 1991, have received a lot of attention due to their unique properties. These properties include superior mechanical, electrical and thermal properties such as good stiffness, improved strength, and electrical conductivity [8]. CNTs are classified into single-walled CNTs (SWCNTs), double-walled CNTs (DWCNTs) and multi-walled CNTs (MWCNTs). SWCNTs and DWCNTs can be visualised as a single sheet of graphenfe rolled into a seamless cylindrical shape with diameter of 1-1.5 nm [9]. As a result to the covalent bonding between carbon atoms arising from sp^2 hybridisation, CNTs have high surface area to volume ratio and thus very high elastic modulus (200 - 1000 GPa) and tensile strength (200 - 900 MPa) [10].

Due to their extraordinary properties, CNTs are now used in a wide range of applications especially as advanced filler materials in composites [11]. Presently there is a great interest in exploiting the exciting properties of CNTs by incorporating them into polymer matrix [12]. They have been mainly used as a secondary reinforcement in hybrid composites resulting in the improved interlaminar region and overall mechanical properties of these composites. Despite the excellent properties displayed by CNTs, their potential as a secondary reinforcement in FRCs have not been fully realised. This is mainly because CNTs tend to entangle due to an interaction with each other and eventually aggregate. This results in poor dispersion and alignment of CNTs within the matrix [13]. In addition, since CNTs are carbon allotropes, they have few functional groups for chemical bonding, strong interfacial adhesion of CNTs with other polymer molecules is a challenge such as[14]:

1. Poor dispersion
2. Alignment of CNTs
3. Poor adhesion

1.1.1 Poor Dispersion

Various dispersion methods have been used in an effort to disperse carbon nano-particles such as stirring, sonication but with little success. A number of challenges must be

overcome before producing a homogeneous dispersion of CNTs in a polymer matrix, including processing methods for fabricating CNTs/polymer composites [15]. The attraction between CNTs by van der Waals forces causes the the CNTs to agglomerate into bundles. These aggregated bundles tend to act as defect sites which adversely affect mechanical properties of the hybrid composites. Thus, effective dispersion of CNTs is required. In recent years, researchers have been focusing on finding the effective method of dispersing nano-particles with more attention being given to electrospinning process because this technique is simple and inexpensive to manufacture sub-micron fibers and nanofibers (NFs). It also provides a potential way to fabricate continuous NFs. In a typical electrospinning process, an electrical potential is applied between a droplet of polymer solution, or melt, held through a syringe needle and a grounded target. Electrostatic charging of the droplet results in the formation of the well-known Taylor cone [16]. When the electric forces overcome the surface tension of the droplet from the apex of the cone, a charged fluid jet is ejected. The jet exhibits bending instabilities due to repulsive forces between the surface charges, which is carried with the jet, and follows a looping and spiraling path [17]. The electrical forces elongate the jet thousands of times and the jet becomes very thin. Ultimately, the solvent evaporates, or the melt solidifies and very long nanofibers are collected on the grounded target [18].

Thus, electrospining can be utilised to disperse nano-particles through doping of the polymer fibers. The doping concept involves dispersion of the CNTs within a polymer such as PAN(polyacrylonitrile) at a specified concentration, and the entire mixture is fabricated into CNT doped PAN nanofibres. Electrospun PAN nanofibres have a high degree of molecular orientation and significantly less structural imperfections [19]. Doping PAN nanofibres with CNTs could be an effective approach to disperse CNTs using electrospinging process. The continuous nanofibres will result in the formation CNT doped electropun nanomat. The nanomat could allow for good adhesion between the composite matrix and reinforcing fibers, which may, among others, reduce delamination tendency. The addition of the nomat into the interface of the composite can lead to nanofibers-bridging resulting in better nanofibres and microfibres interaction.

1.1.2 CNTs Alignment

The other key challenge is the poor alignment of CNTs and this is mainly due to the fact that the nanotubes have asymmetric structure and properties. The mechanical properties of CNT strengthened hybrid composites are strongly influenced by the alignment of the CNTs in the matrix. In order to take full advantage of the properties of CNTs, they should be aligned in a particular direction [20]. Electrospinning is one of the effective

methods that can be used to disperse and align CNTs. However, the conventional electrospinning technique produce randomly distributed fibers which show poor alignment. The randomly oriented composite nanofibers lead to low molecular orientation, and as a result, materials with poor mechanical properties are obtained [21, 22]. Thus, it is desirable to generate aligned composite nanofibers to improve the interlaminar region. The modification of the electrospinning process to produce highly aligned nanofibres is necessary.

1.1.3 Interfacial Adhesion

The other key challenge is in creating a good interface between nanotubes and the polymer matrix. Many researchers have shown that the structure and properties of filler-matrix interface plays a major role in determining the structural integrity and mechanical performance of composite materials. CNTs are relatively nonreactive and as such there is a lack of interfacial bonding between the CNT and the polymer chains that limits load transfer. Hence the benefits of high mechanical properties of CNTs are not utilized properly. Cooper et al. [23] were the first researchers to investigate the interfacial interaction between the CNTs and polymer. They investigated the detachment of CNTs from the epoxy matrix using a pull out test for individual CNTs and observed that the interfacial shear stress varied between 35-376 MPa. They attributed this variation in interfacial stress to poor interfacial adhesion and hence the inefficient load transfer between the CNTs.

There are three main mechanisms for load transfer from the matrix to the CNTs. The first is weak van der Waal interaction between filler and polymer. The second mechanism is micromechanical interlocking which is difficult in CNTs nanocomposites due to their atomically smooth surface. The third mechanism for better adhesion between CNTs and polymer is ionic or covalent bonding (chemical functionalization). Chemical fuctionalization is basically the introduction of functional groups to the surface of nano-particles which can help to improve the interaction between the nano-particle and the matrix. Chen et al. [24] reported that introducing functional groups such as -COOH and -OH groups to the surface of CNTs reduces agglomeration and can improve the dispersion into the matrix [25]. Recent research reports also indicated that carbon nanotubes functionalized with -COOH groups have strong interfacial interactions with many polymer matrices [26–28]. However, these approaches require multi-step reactions to achieve the desired functionality and in most cases chemical functionalization is conducted in solvents like strong acids that can damage the CNTs structure. This can affect the CNTs unique properties and thus proper consideration need to be done when functionalizing CNTs.

1.2 Manufacturing Technique

Lastly, the manufacturing technique also plays a significant role on the mechanical properties of the nano-particle strengthened hybrid composites. The type of matrix to be used also plays an important role in the selection of manufacturing technique. For this research, a thermoplastic will be used. Polypropylene (PP) was chosen due to its various properties and advantages including low production cost, excellent corrosion resistance, good retention of mechanical properties and less recycling challenges in comparison to other matrix systems such as thermosets [29]. There are several manufacturing methods used in the composite industry and these include compression molding, injection molding, calendering and extrusion. However, compression molding is one of the preferred methods for the fabrication of composites. The advantage of compression molding over other techniques is that it can produce composite plates with uniform material distribution. When using extrusion technique to fabricate composites for-instance, nano-fibers are generally oriented parallel to the extrusion flow direction and this increases the probability of fiber breakage due to abrasion [30]. However, in compression molding the fiber orientation cannot be altered and thus the risk of fiber breakage is reduced. However there are some problems associated with compression molding that result in defects in the fabricated hybrid composites and these include blisters, short shots, porous parts, orange peel or wrinkly surface,gas burns and gas blush [31].

Many of these issues can be addressed using compression molding trouble shooting techniques. However, blistering is very difficult to resolve using the trouble shooting techniques. Blistering is the area of gas entrapment caused by incomplete curing of the part. It forms a bulge on opposite sides of the thickest cross-sectional area of the part. If the blistering region is broken apart, there will be a large void in the center of the bulge. To address this, it is proposed that compression molding be coupled with other processing techniques like calendering especially for thermoplastics fabrication as they are recyclable.

Calendering, which is commonly known as three roll mill, is a manufacturing method that employs shear force created by the rotating rolls to mix, disperse or homogenize viscous materials. The shear force is applied with a short residence and this shearing process can be repeated many times since PP can be reprocessed. The calendering process offers the flexibility of multiple entries as milling cycles can be repeated several times. This could ensure better penetration of the matrix into the microfibers and prevent the formation of blisters in the process. This will greatly reduce chances of voids developing on the compression molded composite part. Furthermore, it could maximise the binding between fiber (both primary reinforcement i.e micro-fiber and secondary reinforcement i.e nano-fibers) and the matrix.

1.3 Research Problem

FRPCs have taken a central role in engineering design for the last few decades due to their ease in processing, tailorable properties and weight savings compared to metal alloys. The main issue limiting the FRPCs have been their failure at the interlaminar region. Firstly, the researchers tried to address this issue by adding 2 or more macrofibres in matrix resulting in the formation of hybrid composites. However, the mechanical properties achieved were lower than those anticipated. In an effort to address this issue, researchers added a second reinforcement in the form of nano-particles mainly CNTs leading to the formation of nano-strengthened hybrid composites which are generally called multiscale hybrid composites. This has lead to the improvement of the interlaminar region and overall mechanical properties. However this improvement in interlaminar properties is marginal when considering the potential properties of CNTs.

This is largely a result of poor interlaminar region due to inadequate dispersion, poor alignment and weak interfacial adhesion between CNTs and the polymer matrix. Electrospinning is currently the most used technique to disperse and align fibers. However, the traditional electrospinning technique produces randomly aligned fibers. Thus, it is very crucial to research on how best to modify the electrospinning equipment to achieve aligned nanofibres. The weak interfacial adhesion of CNTs with the polymer matrix have been addressed using functionalization. However, functionalization can damage CNTs resulting in the degradation of CNTs. Thus, it is worth researching the optimal ways of functionalizing CNTs without degrading them. Furthermore, the manufacturing technique is also important and in this research focus will be placed on the coupling of the compression molding and calendering techniques as fabrication methods. The coupling of the two methods could improve penetration of the matrix into the fibers. Addressing these issues may lead to significant improvement of the interlaminar region of the nano-strengthened hybrid composites.

1.4 Objectives

The objectives of the proposed research are to:

1. Determine the effect of dispersion, alignment and functionalization of CNT doped PAN nanomat on the interlaminar region of the aramid fibre composites
    - Use of the electrospinning process to improve the alignment and dispersion of CNT doped PAN nanofibres.

- Design and development of calendering manufacturing method to be coupled with compression moulding for the fabrication of CNT doped polyacrylonitrile (PAN) nanofibre strengthened aramid-PP hybrid composite.
- Understanding functionalization of CNTs and their effect on the interlaminar properties of hybrid composite.

2. Characterization of mechanical properties of CNT doped PAN nanofibre strengthened aramid polypropylene hybrid composite.
    - Characterizeation of the interlaminar properties of the CNT doped PAN nanofibre polypropylene hybrid composite.

1.5 Chapter Layouts

The chapter layout of the thesis is as follows:

1. Chapter 1: Introduction

   This chapter introduces the 3 main issues that need to be addressed to improve the interlaminar region of nano-strengthened hybrid composites. The three issues are poor dispersion of the CNTs into the polymer matrix, improper alignment of CNTs and weak interfacial bond between nano-particle reinforcement and the matrix. The research problem is introduced and explained in detail. The objectives are clearly defined.

2. Chapter 2: Literature Survey

   This chapter looks into what other researchers have done and the existing techniques being used to address the poor interlaminar region in composites especially the hybrid composites. The electrospinning working principle as a technique to disperse and align nanofibres is discussed in detail. Functionalization of CNTs is also discussed in great detail

3. Chapter 3: Methodology

   Methodology details the procedure of all the experiments conducted. This involves the use of the electrospinning process to attain the aligned PAN nanofibres, functionalization of CNTs, doping of PAN nanofibers and the fabrication of the aramid-PP hybrid composites. It also includes mechanical and morphological characterization of the fabricated nanofibers and CNT strengthened hybrid composite. Mechanical tests include tensile, flexural, impact and short beam test. Morphological tests include the use Raman Spectroscopy (RS), Scan Eletron

Microscopy (SEM), Transmission Electron Microscopy (TEM), Fourier-Transform Infrared (FTIR) Spectroscopy and Thermogravimetric analysis (TGA).

4. Chapter 4: Results and Discussion

   This section presents results and the discussion of the results obtained from the experiments conducted. The improvement in interlaminar properties and overall mechanical properties of the hybrid composites is quantified in this section.

5. Chapter 5: Conclusions and Recommendations

   This section outlines the conclusions drawn out of the research conducted. Recommendations are also made on what further research can be conducted to aid further development of this research.

Chapter 2

Literature Review

2.1 Fiber Reinforced Polymer Composites (FRPCs)

Fiber reinforced polymer composites (FRPCs) possess superior specific strengths and stiffness in comparison to other structural composites, such as metal or ceramic-reinforced composites [13, 32, 33]. They have many advantages including superior mechanical properties, light weight, high corrosion resistance, ease of manufacturing, etc. FRPCs consist of two parts; matrix and reinforcement. The matrix is continuous and holds the fibers in their position, transfer loads between fibers, provides interlaminar shear strength and protects the fibers from abrasion. Reinforcements, as the name suggests, are discontinuous, stronger and stiffer, and play a significant role in improving the structural characteristics of the composites [34]. [35]

FRPCs are typically categorised according to the nature of the matrix material which are either thermoplastic and thermoset matrix composites. Thermoset matrices such as polyester and epoxy are inherently brittle as they have immobile chemical bonds and form crosslinks during cure stage of manufacturing process forming rigid intractable solid product [36]. Thermoplastics are saturated polymers which do not form crosslink during processing as they do not undergo chemical reaction during cure. Most common thermoplastics include polyethylene, nylon, polyvinyl chloride (PVC) and polypropylene (PP). In this research emphasis is placed on thermoplastics and specifically PP. Thermoplastics offer a number of benefits in comparison with thermoset composites including low cost per part, superior handing and formability and they are reprocess-able and recyclable [37]. Other advantages of thermoplastics include high damage tolerance, improved fracture toughness and resistance to micro cracking.

Reinforcements have varying forms; continuous and chopped forms with different lengths or discontinuous in form to meet different properties and processing methods [38]. The

most commonly used fibers in polymer matrices as reinforcement are glass, carbon and aramid fiber. The region between the reinforcement and the matrix which forms due to chemical interaction or effects of processing between the two is called interface or interlaminar region. Figure 2.1 shows the schematic cross-section of the fiber-reinforced composite and the detailed fiber surface region respectively of the composite interface [39].

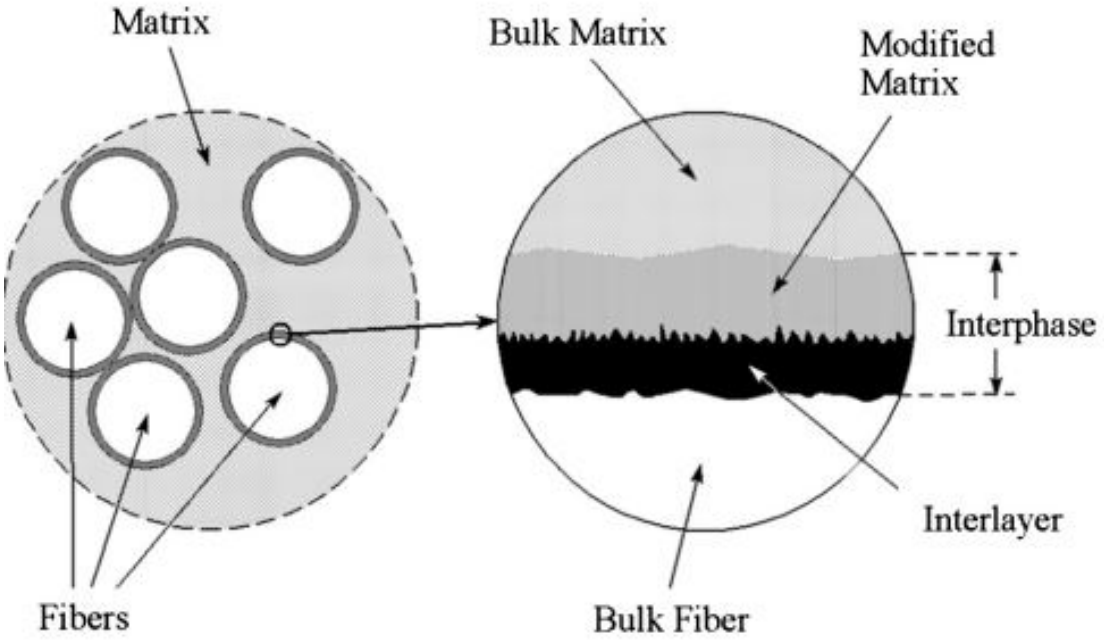

FIGURE 2.1: Schematic illustration of a composite interface [37].

2.1.1 Reinforcement - Aramid Fibre

Aromatic polyamide fibre or aramid fibre was the first organic fibre to be used as a reinforcement of composites [40]. It is commonly known under its Dupont trade name Kevlar, but there has been an increase in numbers of suppliers of the fibre. Aramids are generally produced by a reaction between an amine group and a carboxylic acid halide group. The chemical composition of Kevalar aramid fibre is poly para-phenyleneterephthamide (PPTA) and the chemical structure is shown in Figure 2.2. Aramid has higher mechanical properties than other synthetic fibres and aramid fibres have displaced metal and inorganic fibres in various applications such as aircraft, bullet proof vests, watercraft and automobiles [41]. This fibre not only has better mechanical properties than glass fibre and steel per weight basis but it is able to maintain these properties at high temperatures due to its excellent resistance to heat.

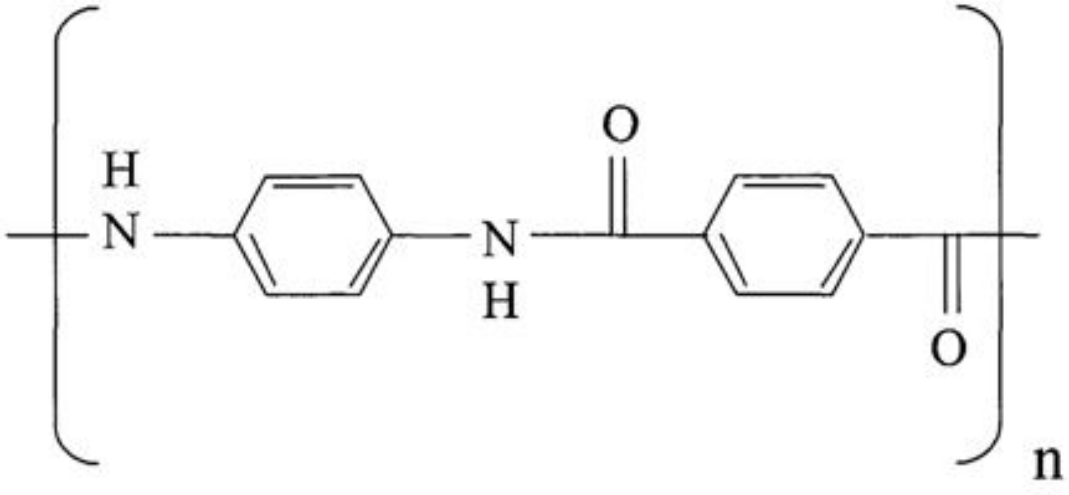

FIGURE 2.2: Chemical structure of Kevlar [40]

2.1.2 Matrix - Polypropylene (PP)

Polypropylene has been chosen as a matrix for this research because of various reasons. Firstly, it is one of the cheapest industrial polymers in the market and thus very cost effective. PP is thermoformable and recyclable and thus allows for new approach and fabrication methods [42]. Varga et al. [43] proved that PP composites combine very well by a process similar to welding and this is useful in improving the adhesion between the matrix and reinforcement. Unlike most thermosets, thermoplastics do not have cross links; hence, they can be reprocessed. During the heating of thermosets, the molecular weight increases which in turn affect the mechanical properties. Conversely, there is no change in molecular weight in thermoplastics and thus no compromise on mechanical properties. It has also been shown that with adequate pressures, thermoplastic fabricated parts have low void content and can be recycled if need be [44].

2.1.3 Hybrid composites

Hybrid materials are composites consisting of two or more reinforcements in a composite system. Hybridization has enabled the realization of the advantages of the heterogeneous composites while also eliminating their undesirable features. For example, the introduction of carbon fillers into the composition of the material of rotor blades which were traditionally made of glass fibre reinforced plastic resulted in a significant increase in their fatigue strength, torsional rigidity and service life [45]. One of the most important benefits of hybrid composites is the attainment of higher order properties through

the rule of mixtures (ROM). Other benefits include excellent strength and stiffness, reduced weight and cost, improved fracture toughness, improved impact resistance and increased service life [46–48]. There are five types of hybrid composite materials and are characterised as [49–51]:

- Inter-ply, in which two or more fibres of different types are mixed in a random manner
- Sandwich hybrids, where one material is sandwiched between two layers of another
- Laminated, in which alternate layers of two or more materials are staked in regular manner
- Averaged or intimately mixed hybrids, where fibres of different types are made to mix as randomly as possible such that no macro-concentrations of any fibre type are available

There has been strong suggestions that CNTs are the most suitable secondary reinforcement of the matrix-rich interlaminar region, mainly due to their exceptional mechanical, electrical and thermal properties [52]. It has been proven that combination of primary reinforcement (traditional fibers such as carbon and glass) with CNTs resulted in improved fiber/polymer matrix interfacial load transfer [53]. CNTs are discussed in detail in the following section.

2.2 Carbon nanotubes (CNTs)

A carbon nanotube can be visualised as a hollow cylindrical rolled graphite sheet [54]. Since their discovery by Ijima in 1991, CNTs have attracted huge attention in the fields of science and engineering due to their extraordinary mechanical, thermal and electrical properties [55]. Due to their extraordinary properties, CNTs are now applied in a wide range of applications especially as advanced filler materials in composites [56]. Researchers are envisaging exploiting their high aspect ratio and conductivity to produce conductive plastics with extremely low percolation thresholds. It is also envisaged that high thermal conductivity can be taken advantage of to produce thermally conductive plastics [57, 58]. However, CNTs research has mainly focused on their use in composite materials to enhance mechanical properties of plastics by using them as reinforcing fillers [8, 59].

2.2.1 Types of CNTs

There are two main types of nanotubes, single-walled nanotubes (SWNT) and multi-walled nanotube(MWNT). SWNT can be visualised as a single sheet of graphene rolled into a seamless cylindrical shape with diameter of 1-1.5 nm [60, 61]. The van der Waals interaction between the SWNTs side walls result in close-packed bundles [62]. On the other hand, MWCNTs consists of multiple layers of concentrically formed cylindrical graphene sheets separated by 0.35 nm where the interaction between the individual shells is van der Waals forces [63, 64]. They have diameters ranging from 2 to 100 nm and tens of microns in length [65].

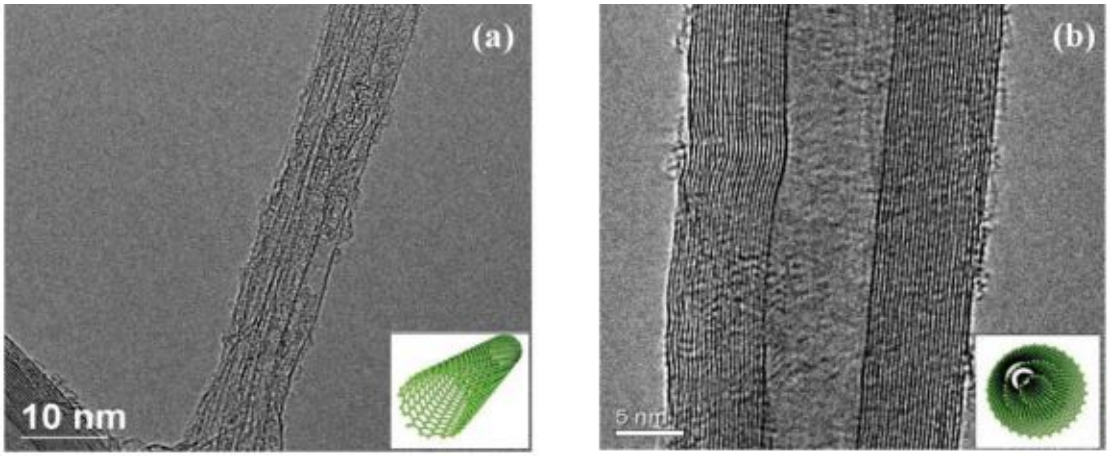

FIGURE 2.3: TEM images of a) SWNT. b) MWCNT [58].

The anatomic structure of carbon nanotubes is generally described in three different forms. These are armchair, zigzag, and chira and are shown in Figure 2.4.

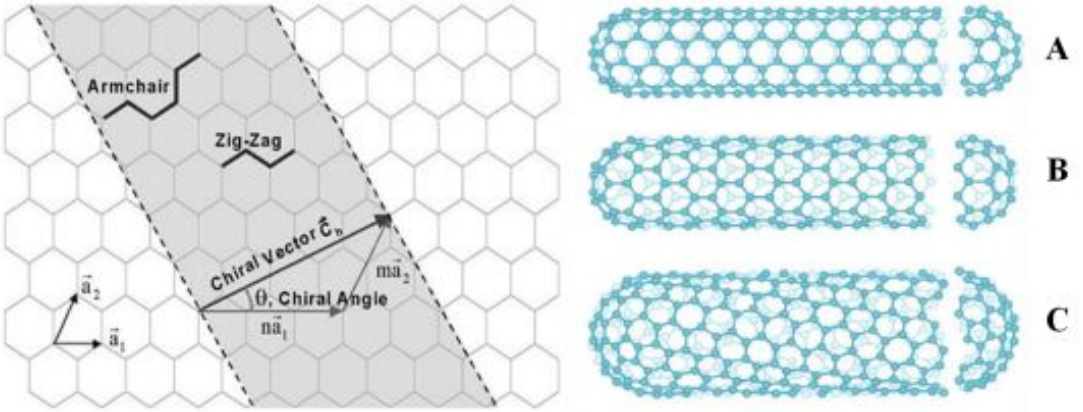

FIGURE 2.4: Hexagonal sheets of graphite rolled to form CNTs with different chiralities, A) armchair. B) zigzag. C) chiral [59].

2.3 Critical issues in CNTs reinforced polymer nanocomposites

Polymer composites are widely used in various industries but their use have been severely limited due to their failure at the fiber-matrix interlaminar region. The extraordinary mechanical, thermal and electrical properties of CNTs has made them the preferred candidate as secondary reinforcement fillers in composites [66, 67]. SWCNTs and MWCNTs have been used as secondary reinforcement in both thermosetting polymers including epoxy, polyurethane (PU) and phenol formaldehyde (PF) resins as well as the thermoplastics polymers such as polypropylene (PP), polystyrene (PS), polyvinyl alcohol (PVA), polymethyl methacrylate (PMMA), polyvinylidene and many others to improve strength and conductivity among other properties [68, 69]. The secondary reinforcement of polymer composites with CNTs has resulted in a significant improvement in hybrid composites. However, the expected mechanical properties have not been achieved due to various challenges and problems associated with CNT/Polymer composites such as poor dispersion, poor CNT alignment and inadequate interface adhesion of CNTs in polymer matrix. These critical issues are discussed in detail in the following subsection

2.3.1 Fibre/matrix interfacial interaction

The mechanical behaviour of composites not only depends on the properties of the constituents (matrix and fibre) but also interface between its constituents [70]. The interface region is the contact region between the matrix and reinforcement in a composite. The interfacial interaction between the constituents of the composite plays an important role in load transferring between the fibers and matrix [71]. Poor interfacial strength results in poor mechanical and chemical properties of a resulting composite. Composite constituents interact with each other through physical, chemical and mechanical ways. Physical interaction mainly refers to inter-molecular forces between polymer matrix and fibers such as H-bonds and electrostatic forces [72, 73]. Mechanical interaction of the fibres and the matrix occurs through the friction between composites constituents against the applied force. Chemical interaction refers to chemical bonding between the fibers and matrix which result in increased adhesive bond strength by preventing breakage at a sharp interface [74, 75]. A lot of researchers have focused on the strengthening of the matrix-reinforcement adhesion particularly in thermoplastic composite materials[76].

Different kinds of treatments have been considered in trying to improve interfacial adhesion by either fiber surface treatment, making changes to the polymer matrix or both. This helps in increasing compatibility between the matrix and reinforcement [76–78]. There has been a strong focus on functionalization of CNTs to improve both the

microfiber/matrix and nano-particle/matrix interaction. The section below discusses functionalization in detail. Functionalization is divided into chemical and physical functionalization depending on the inter-molecular interaction between active molecules and the carbon atoms on the CNTs.

Physcical functionalization involves the use of covalent bond method which can introduce functional groups to the surface of the CNTs [79]. There are major drawbacks with this method of functionalization: the first one being the existence of defects on the CNT walls and even having CNTs fragmented into smaller pieces in some extreme cases created by the functionalisation reaction and the damaging ultrasonication process which result in the degradation of mechanical properties. It can also lead to disruption of p electron system in CNTs [25] and this will have adverse effect on the transport properties of CNTs as the deffects scatter the photon and electrons responsible for thermal and electrical conduction respectively. The second issue is that CNT functionalization uses highly concentrated acids and strong oxidants which are environmentally unfriendly [25, 80]. There has been a lot of effort that has been made to develop methods that can have less damage to CNTs structure, convenient to use and low cost. Non-covalent functionalisation is an alternative process that can be able to tune interfacial properties of nanotubes. A typical example of non covalent functionalization is the suspension of CNTs in the presence of polymers, such as polystyrene resulting in polymer wrapping around the CNTs forming supermolecular complexes of CNTs [81, 82].

Chemical functionalization is another method used to modify the chemical properties of the nanoparticles. CNTs are generally inert and they interact with the surrounding matrix mainly through van der Waals forces. This is due to the fact that the carbon on CNT walls are chemically stable as a result of the aromatic nature of the bond [79]. This hinders their ability to efficiently transfer load across the CNT/matrix interface resulting in premature failure of the composite. There has been a lot of research output into chemical functionalized CNTs and the reaction pathway between CNTs and functional groups[83]. These are performed at the termin or sidewalls of the CNTs[84]. Indirect covalent bonding takes advantage of the carboxylic group's chemical alerations at open ends and holes in sidewalls of the CNTs. The carboxylic group is mainly generated during oxidative purification. Hiura et al. [85] functionalized CNTs by treating them with mixture of sulfuric acid and potassium permanganate, however, this process is not suitable for large scale separation.

Paiva et at. [86] functionalized CNTs using poly (vinyl alcohol) (PVA) and found that the mechanical properties of the nano-composites strengthened with these CNTs significantly improved. They concluded that functionalization of CNTs resulted in improved distribution and interaction of nanotubes with the matrix leading to improved

mechanical properties. Tohji et al. [87] suggested a purification process which involves hydrothermal treatment of fulerenes, themal oxidation and dissolution in 6M hydrocloric acid. In order to prevent CNTs destruction during purification, Bandow et al. [88] and Bonard et al. [89] dispersed CNTs in polar solvents with surfactants such as as sodium dodecyl sulfate followed by micro-filtration and size exclusion chromatography. The addition of oxygen-containing functionalities on to the graphitic surfaces is very important as it enhances the interfacial adhesion. Thus, CNTs functionalization is very crucial if they are to be used as reinforcements in composites.

2.3.2 Carbon Nano-Particles Alignment (CNPs)

The alignment of CNPs is very important and various researchers have shown that CNPs alignment can improve the mechanical properties of composites. Lau et al. [90] showed that nano-composites with randomly orientated CNPs did not show the full potential of the mechanical properties when compared to those with aligned CNPs. Zhou et al. [71] measured superior mechanical properties for nanocomposites with aligned CNPs when compared to those with randomly dispersed CNPs. There are various techniques used to align CNPs including spray winding, slicing and chemical vapour deposition [91]. However, there are shortcomings associated with these techniques such as variation in alignment, defects on the fibre surface which greatly reduce the mechanical properties of resulting nano-composites [92]. In contrast, electrospinning alleviates most of the above limitations and has garnered much attention in the last decade due to increased interest in nanoscale particles and technologies and also due to its simplicity and cost effectiveness [93].

2.3.3 Electrospinning

Electrospinning process is a simple and cost effective method of fabricating polymer fibres when compared to traditional or conventional techniques such as extrusion moulding, wet spinning and melt spinning. It is a versatile method capable of producing uniform diameter nanofibres on a mass scale from different polymers [94]. Electrospinning, developed by Anton Formhals in 1934 is derived from electrostatic spinning in which electrical charges are employed to produce filament [35].

Electrospinning setup typically consists of a syringe pump with a 0.5 mm to 1.5 mm nominal diameter range, a high voltage supply and a collector as shown in Figure 2.5a. The process begins when a polymer solution is held at a needle tip and subjected to an electric field and charge is induced of the liquid surface which results in charge repulsion within the solution [71]. The resulting electrostatic force has an opposing effect on the

surface tension which it overcomes resulting in the initiation of the polymer jet. The solvent evaporates as the polymer jet travels and producing polymer fibres which are collected on the grounded charge. Figure 2.5b shows typical fibres produced through this process.

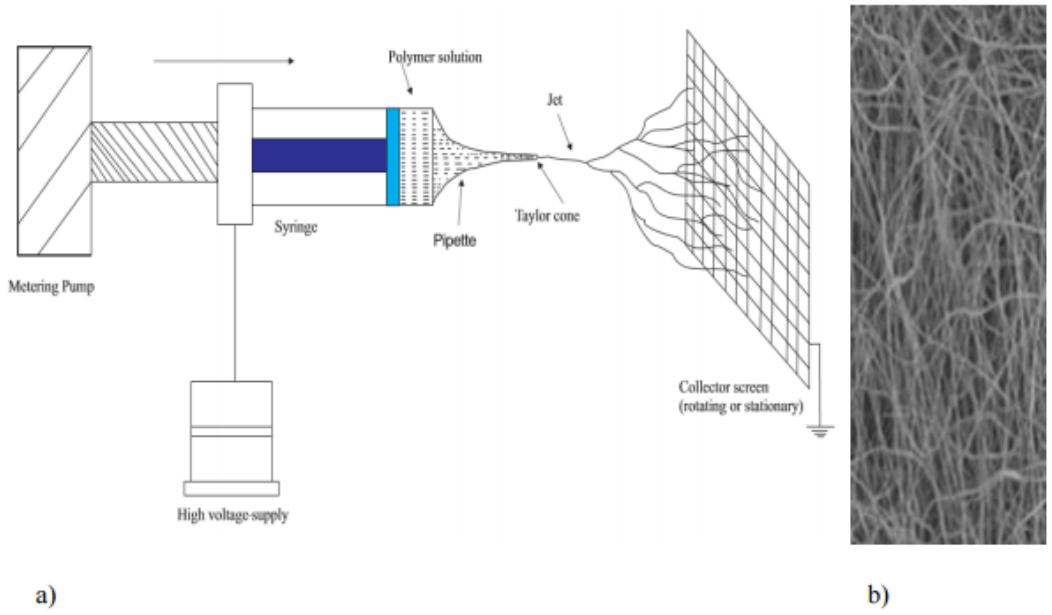

FIGURE 2.5: a)Electrospinning Apparatus. b) PAN-based ECNFs.[68]

2.3.4 Electrospinning process parameters

Doshi and Reneker [16] studied the parameters of electrospinning in detail and they stated that the process can be influenced by a number of variables. They classified the parameters into three different categories and these are Solution properties, Processing or controlled parameters and ambient parameters [18]. Solution properties include properties of viscosity, surface tension, polymer molecular weight and dielectric constant. However, the effect of solution is not easy to vary as any change of one property affects other solution properties. Processing parameters include flow rate, electric field strength, distance between tip and collector, collector composition and geometry [19]. Ambient parameters include humidity, temperature and air velocity. Table 2.1 shows the summary of the effect of the electrospinning parameters on the fiber morphology. Most of the above mentioned parameters will be optimised during the investigation in order to achieve the best nanofiber morphology.

TABLE 2.1: Parameters affecting the configuration of electrospun fibers [19].

Fabrication parameters	**Effect on fibre morphology**
Solution concentration	A low concentrated solution result in bead formation while a highly concentrated solution result in larger fibres
Solution charge density	The more dense the solution charge the more uniform bead-free fibers and smaller fibers are produced
Polymer molecular weight	An increase in molecular weight result in reduced number of beads
Flow rate	Low flow rates results in smaller fibres while high flow rate result in larger fibres
Field strength	Stronger field strength result in larger fibres while a weak field has an opposite effect
Distance between the needle tip and collector	The smaller the distance between the needle tip and collector the smaller the fibers produced. Larger fibers are produced with the larger distance
Needle tip design and diameter	An increase in needle diameter result in larger fibres
Collector geometry	This defines the fibre orientation and shape
Ambient parameters	An increase in temperature causes a reduction in viscosity and this will result in bead formation and larger fibres
Surface tension	No conclusive link

2.3.5 CNTs Dispersion

Introduction of CNTs into conventional fibre reinforced composites has shown an improvement in mechanical properties. However, their full potential influence or effect has been severely limited due to difficulties associated with dispersion of entangled CNTs during processing [95–97]. Dispersion plays an integral role in the production of CNT/polymer composites and thus, better dispersion will result in more filler surface available for bonding with the matrix [98]. This will also greatly help prevent the aggregated filler from acting as stress concentrator which have adverse effects on composite performance.

There are mainly two aspects that affect the dispersion in CNT/polymer nanocomposites and the first one is micro or macroscopic dispersion which is uniform dispersion of individual CNTs or their agglomerates in the strengthened nanocomposites [99]. The second aspect is nanoscopic dispersion which is the disentanglement of CNT agglomerates or bundles. Various methods have been used to disperse CNPs in the matrix and these include ball milling, calendering, sonication, stirring and extrusion. Most of these processes have limitations and calendering is the least researched technique of them all.

The technique chosen in processing CNT/polymer nanocomposites is vital as it has influence on mechanical properties. A closer look at calendering technique shows that it might have a potential to improve the dispersion of CNPs in the matrix. The following section discusses calendering method technique in detail.

2.4 Manufacturing techniques

2.4.1 Compression molding

Compression molding is one of the well known method used for manufacturing plastic and composites products. Figure 2.6 shows the compression molding apparatus [100]. The mold consists of a female (lower mold plate) and male (upper mold plate) mold parts. The heat, pressure and time are the main parameters being varied as per specific product being molded for a definite period of time. The material being molded takes the shape of the mold. The molded product is cured at room or higher temperature. Advantages and disadvantages of compression molding include the following:

Advantages

1. Minimum material wastage during manufacturing
2. Low maintenance cost
3. Negligible residual stress in the molded component
4. Good surface finishes can be achieved
5. The production rate is usually high as the mold cycle time is low

Disadvantages

1. The molded component sometimes requires trimming or machining after compression
2. The process is labour intensive
3. Sometimes voids are present

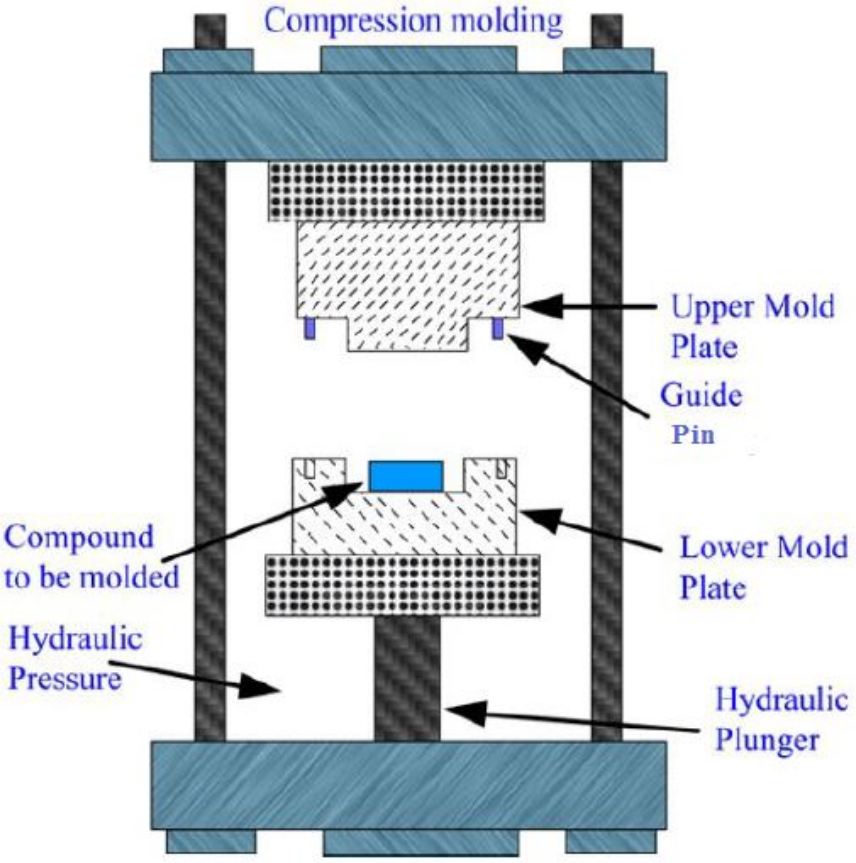

FIGURE 2.6: Compression molding equipment [100]

The controlling parameters in compression molding are temperature, pressure and time as shown in Figure 2.7 [101].

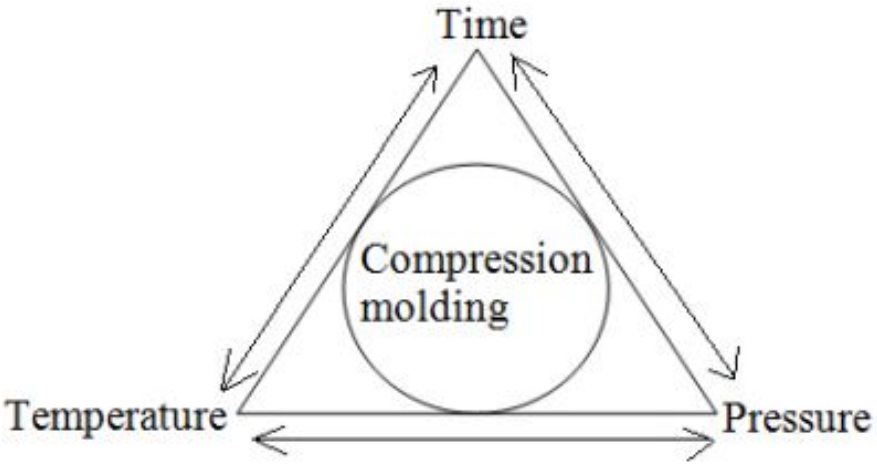

FIGURE 2.7: Compression molding controll paramters [101].

2.4.2 Calendering

The calendering technique, widely known as a three roll mill is a processing method which uses shear force created by rollers rotating in different directions and speed to mix, homogenize mainly viscous material [102]. It is also used as a finishing process in various industries such as rubber, plastic and paper industries to achieve desired thickness and surface finish [103]. A typical calender is shown in Figure 2.8 [104]. The most common configuration consists of three adjacent cylindrical rollers. The first and the third rollers are called feeding and apron rollers respectively and they rotate in the same direction. The central (center) roller rotates in the opposite direction. The narrow gaps between the rollers together with the angular velocity result in high shear forces in a short residence time [105].

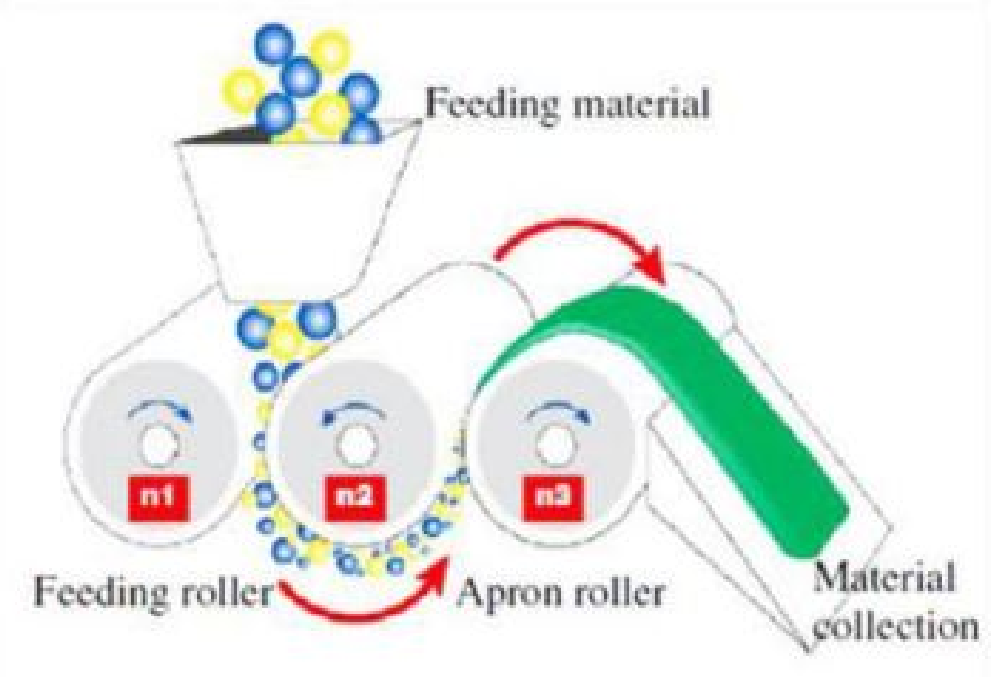

FIGURE 2.8: Schematic of the calendering technique and its working mechanism [105].

The contact zone between two rolls is called a nip and is shown in Figure 2.9. When the materials pass through the nip, it is pressed between the rotating rollers under heavy load and high temperature [106]. This temperature is controlled using the heated rollers.

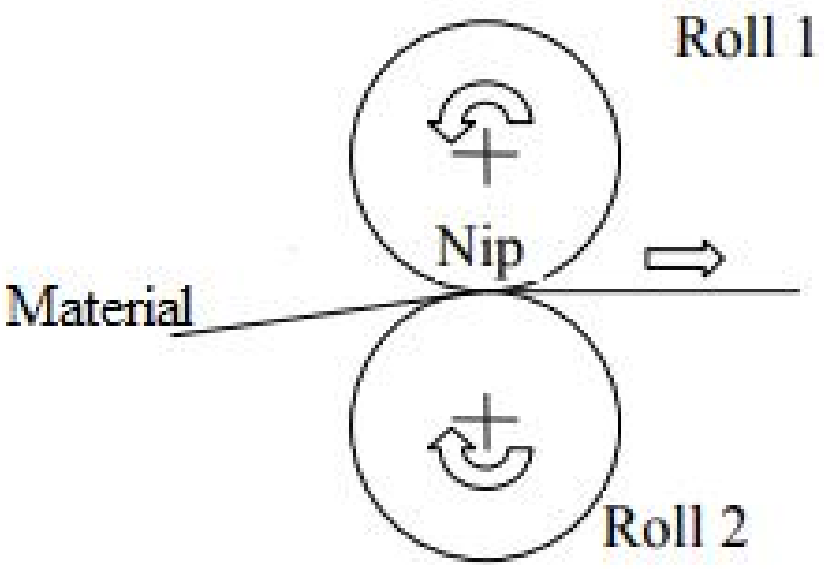

FIGURE 2.9: Material travels between two rolls [106].

Chapter 3

Methodology

This chapter outlines the detailed experimental procedure including the fabrication and characterization of both aramid polypropylene (PP) composites and CNT doped PAN nanomat strengthened multiscale hybrid composites. A detailed functionalization procedure is also presented along with the combined compression molding and calendering fabrication methods. At first the aramid fibre composites with 25%, 30% and 35% volume fractions were tested to obtain the optimum aramid fibre volume fraction. Secondly, the optimum aramid fibre volume fraction were then used to fabricate the PAN nanomat (0.1%, 0.5% and 1% volume fraction) strengthened hybrid composites and tested to obtain the best PAN nanomat volume fraction. This was done for both random and aligned nanofibres. Finally, the best PAN nanomat (0.5%) strengthened aramid (30%) polypropylene composites was then used to fabricate the CNT doped PAN nanomat strengthened hybrid composites. The three different CNT concentrations used were 0.1%, 0.25% and 0.5%. This was done for both pristine and functionalized CNTs.

3.1 Materials

Polypropylene was used as a matrix and was purchased from AMT Composites Pty Ltd (South Africa). PP is thermo-formable and thus allows for reprocessing with different fabrication methods. The properties of Polypropylene are summarized in Table 3.1. Aramid fiber was chosen as the primary reinforcement and was purchased from AMT Composites Pty Ltd (South Africa). The properties of aramid fiber are given in Table 3.2.

Table 3.1: Properties of polypropylene

Property	**Value**
Density (g/cm^3)	0.91
Modulus of elasticity (GPa)	1.6
Tensile strength(MPa)	30
Elongation(%)	>50
Melting temperature (°C)	165

Table 3.2: Physical and mechanical properties of the aramid fibre (Twaron 2200)

Property	**Value**
Specific Gravity (g/cm^3)	1.44
Young's Modulus (GPa)	80 - 190
Tensile Strength (GPa)	2.8 - 3.6
Tensile Elongation (%)	2 - 4

Continuous CNT doped electrospun PAN nanofibres were used as secondary reinforcement. Electrospinning was used to produce the continuous CNT doped PAN nanofibres with an average diameter of about 100 nm. The SWCNTs, PAN polymer and DMF solvent were purchased from Sigma Aldrich Pty Ltd (South Africa). Properties of the CNTs used are shown in Table 3.3.

Table 3.3: CNTs Properties

Property	**Value**
Relative Density (g/cm^3)	1.7 - 2.1
Diameter Range (nm)	1.3 - 2.3
Purity (%)	70

3.2 Fabrication Methods

3.2.1 Compression Molding Process

The aramid-PP composite specimens were fabricated using both the compression molding and calendering technique. The reason for using two methods is for the proper matrix penetration into the fibre and also for removing voids within the specimen. The PP sheets and the aramid fibre woven mats for the different volume fractions (25%, 32%

and 35%) were layered alternatively inside the female part of the compression molding jig before processing inside the compression molding furnace. Figure 3.1 shows the compression molding furnace and jig respectively.

Before starting the manufacturing process, both the male and female parts were polished and waxed with RAM wax to prevent PP sticking to the mold walls. The compression molding process was started by varying parameters (temperature,pressure and time) in an effort to attain optimum manufacturing parameters. At first, the mold was heated to 175 °C resulting in poor matrix penetration. The temperature was increased to 185 °C and this improved matrix penetration. Similar trials were conducted to obtain the required pressure value and at low pressure (190 bar), there was poor matrix penetration resulting in specimens with voids. With the increase in pressure to 200 bar, the compression molding process has produced specimens with improved matrix penetration without voids.

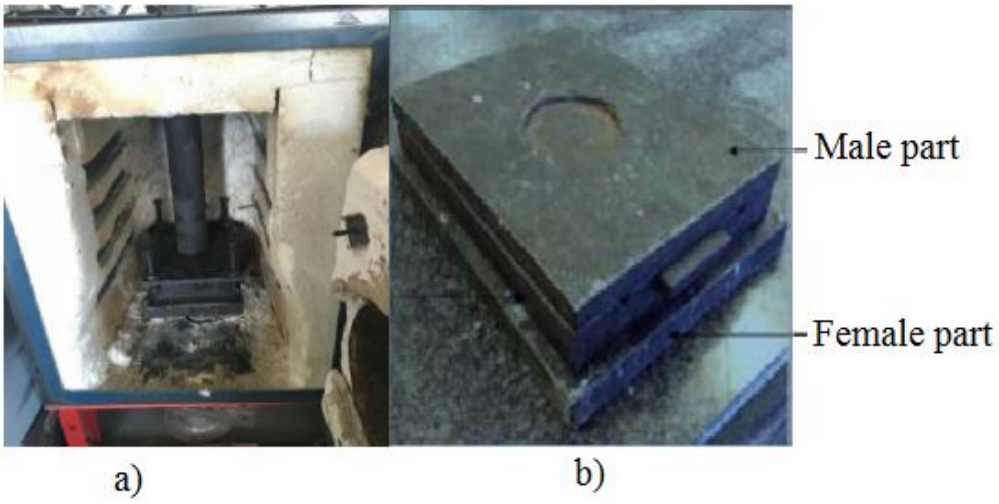

FIGURE 3.1: a) Compression moulding furnace and b) Compression moulding die.

Once the matrix and the fibre mats were placed inside the mold, the furnace was heated to 185 °C and subsequently, the pressure of 200 bar was applied on to the mold. The temperature and the pressure was maintained for an hour and then the molded specimen was removed using the heat protective gloves for the second stage of calendering manufacturing.

3.2.2 Calendering Techniques

The calendering equipment was designed and fabricated at the Witwatersrand University (mechanical engineering laboratory). The calendering equipment consists of 3 rolls mounted on bearings supported by side frames. The flexible heaters which can reach

to a maximum temperature of 200 °C inserted inside the rolls and the temperature was measured using a thermocouple. The calendering equipment used in this experiment is shown in Figure 3.2.

The compression molded specimen was passed through the calendering roll to remove any air bubbles, voids and also improve the matrix penetration. The calendering technique roll's temperature was set at 190 °C. Thereafter it was put back into the compression molding promptly for another hour of compression molding at a temperature of 185 °C and pressure of 200bar. The molded specimen was then allowed to cool to room temperature before being removed from the compression molding jig.

FIGURE 3.2: Calendering equipment.

3.2.3 Fibre Composites Fabrication

The aramid composite was fabricated with three different aramid fiber volume fractions of 25%, 32% and 35% respectively. According to the ASTM D4762-16, the polymer matrix composite needs to have a minimum thickness of 3 mm. In this experiment, initially, the matrix thickness was fixed at 3 mm. Aramid fibre content was then varied to determine the approximate number of layers required and the detailed fibre volume fraction calculations were done as follows.

The mass of the single polypropylene sheet was calculated using the below formula:

$$m_{pp} = V_f \times \rho_{pp} \tag{3.1}$$

where V_f is the volume fraction of PP given by the dimensions of the compression molding jig of $17 \times 13cm$ and the overall thickness of PP which is 0.3 cm. The density of PP is $0.91g/cm^3$, thus the mass of PP is $60g$

Using the thickness of both the matrix and fiber, fibre volume fraction can be calculated as follows:

$$V_f = \frac{t_f}{t_m + t_f} \tag{3.2}$$

where V_f is fibre volume fraction given as 25%, 30% and 35%, t_f is fiber thickness and t_m is the matrix thickness given as $0.3cm$. Where t_f, the fibre thickness is given as follows:

$$t_f = \frac{n_f \times m_f}{\rho_f} \tag{3.3}$$

where n_f is the number of fiber(aramid) layers, ρ_f is the aramid fibre density given as $1.44g/cm^3$ and m_f is fiber mass per unit area given as:

$$m_f = \frac{M_f}{A_{mold}} \tag{3.4}$$

where M_f is the aramid fibre weighed at 4.45g and A_{mold} is the area of the mould given by $17cm \times 13cm$

Solving equations 3.1 to 3.4, the number of aramid fibre layers required for each volume fraction is shown in Table 3.4.

TABLE 3.4: Number of aramid layers required for each volume fraction

Volume fraction	**Number of layers**
25%	7
30%	9
35%	11

The number of layers were rounded off to the whole number. It was then decided to work backwards using the number of layers, fibre volume fractions, fibre mass and density to calculate the amount of polypropylene required. I was determined that the polypropylene required for 25%, 30% and 35% is 59.06g, 59.06g and 57.45g respectively. Thus, two 1mm thick solid polypropylene sheets were used together with powder polypropylene.

Figure 3.3 shows the neat aramid-PP composite panel. The panel underwent both the compression molding and calendering processing. The fabricated composites had no voids such as blisters and showed good matrix penetration.

FIGURE 3.3: Aramid/Polypropylene composite.

3.3 Electrospinning Process

3.3.1 PAN Solution Preparation

PAN is one of the most used polymers in various areas such as in composites materials, tissue engineering and filtration. In this study, PAN solution was prepared by mixing PAN powder with dimethylformamide (DMF) solvent. Both PAN and DMF were purchased from Sigma-Aldrich. Figure 3.4 shows the PAN and DMF used in this study.

FIGURE 3.4: DMF solution (left) and PAN powder (right)

The average molecular weight of PAN was 150,000. PAN solutions of 8.4% concentration were prepared. The decision to use 8.4% concentration was made based on the best PAN/DMF concentration found in the literature [10, 18, 107]. Magnetic stirrer hot plate with stirring-level 4 and heating-level 2 was used and mixing duration was 24 hours. The well dissolved solution was transparent and had a light yellow colour as shown in Figure 3.5.

FIGURE 3.5: PAN solution: (a) before stirring and heating; (b) after mixing

3.3.2 Electrospinning

Electrospinning was used to fabricate both the aligned PAN and randomly distributed nanofibres. The schematic and the actual electrospinning equipment is shown in Figure

3.6 and Figure 3.7 respectively. It was observed from the manufacturing of the PAN nanomat that keeping other parameters constant and increasing the collector distance resulted in a decrease in fiber diameter showing no signs of beading. This was due to the fact that the stretched polymeric solution had more time to reach the collector and produced PAN nanofibres with diameters of 100 nm. However, a further increase beyond the optimum distance resulted in broken fibers.

The solution (PAN/DMF) concentration also has a significant effect on the fiber diameters and quality. The concentration was varied between 8% and 9% based on the the literature. The diameter decreased with the increase in solution concentration up until the 8.3% concentration. Beyond this concentration, the fiber diameters started to increase rapidly. It was also noted that an increase in voltage resulted in an increase in fiber diameter but the beading decreased significantly and fibers were of better quality

Following the experimentation with varying electrospinning parameters, PAN concentration of 8.3%, needle tip to collector distance of 20 cm, needle diameter of size 22G, voltage of 25 kV, drum collector speed of 800 rpm and solution flow rate of 0.36ml/h; were found to be producing quality PAN nanofibres. At first, the randomly distributed nanofibres were produced using the conventional electrospinning process. Then, the aligned nanofibres were produced using an electrospinning process modified with 2 positively charged electrodes perpendicular to the needles and at a distance of 12 cm from the needle. The distance of the auxiliary electrodes was then varied in the X and Y directions and the results are presented in Table 3.5. Figure 3.8 shows the SEM image of the electrospun PAN nanofibres produced by varying the auxiliary electrodes in the X-Y directions

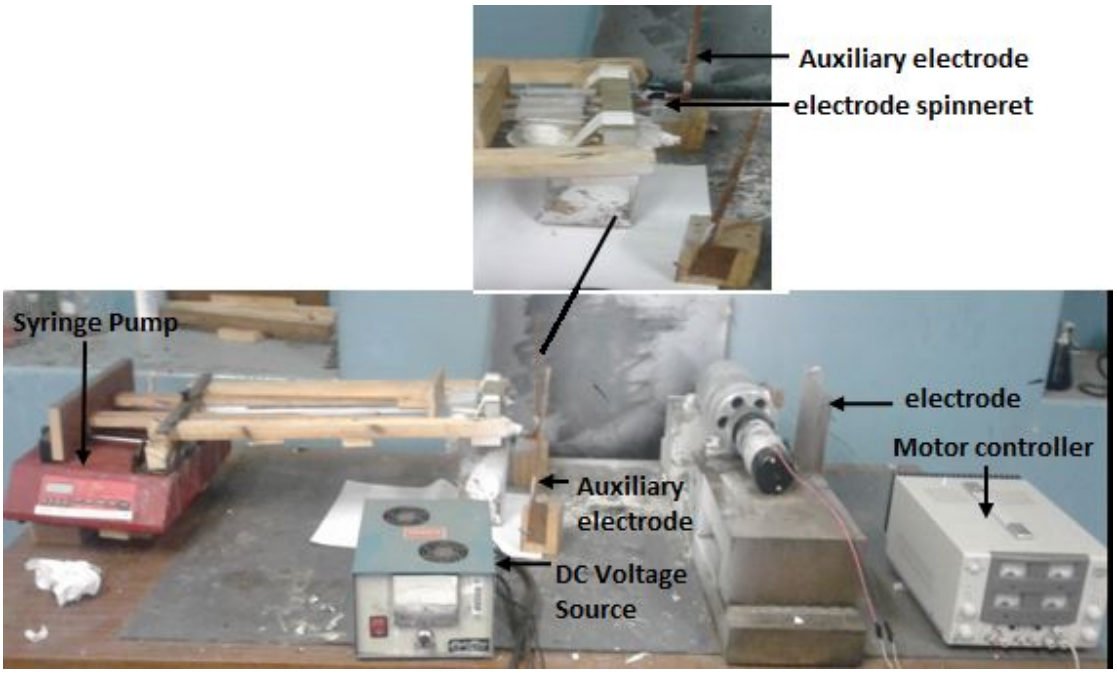

FIGURE 3.6: Modified electrospinning process (MEP)

Figure 3.7 shows the schematic of the the electrospinning equipment used to produce aligned nanofibres. The distance of the auxiliary electrodes was varied in the X and Y directions and the results are shown in Table 3.5. Figure 3.8 shows the SEM image of the electrospun PAN nanofibres produced by varying the auxiliary electrodes in the X-Y directions.

TABLE 3.5: Processing parameters of electrospinning of aligned PAN nanomat

X{_1} (cm)	**Y{_1} (cm)**	**Average diameter (nm)**	**Obeservations**
0	15	140	Broken fibers with beads
0	20	147	Aligned fibers with small beads
0	25	198	Good quality aligned fibers
0	30	256	Poor quality fibers showing random distribution
10	15	282	broken beaded fibers
10	25	293	Aligned fibers with a lot of beads
10	30	333	Aligned fibers with large beads
20	15	352	Broken fibers with beads
20	25	361	Randomly distributed fibers with beads
-10	15	288	Fibers showing random distribution
-10	25	336	Fibers randomly distributed

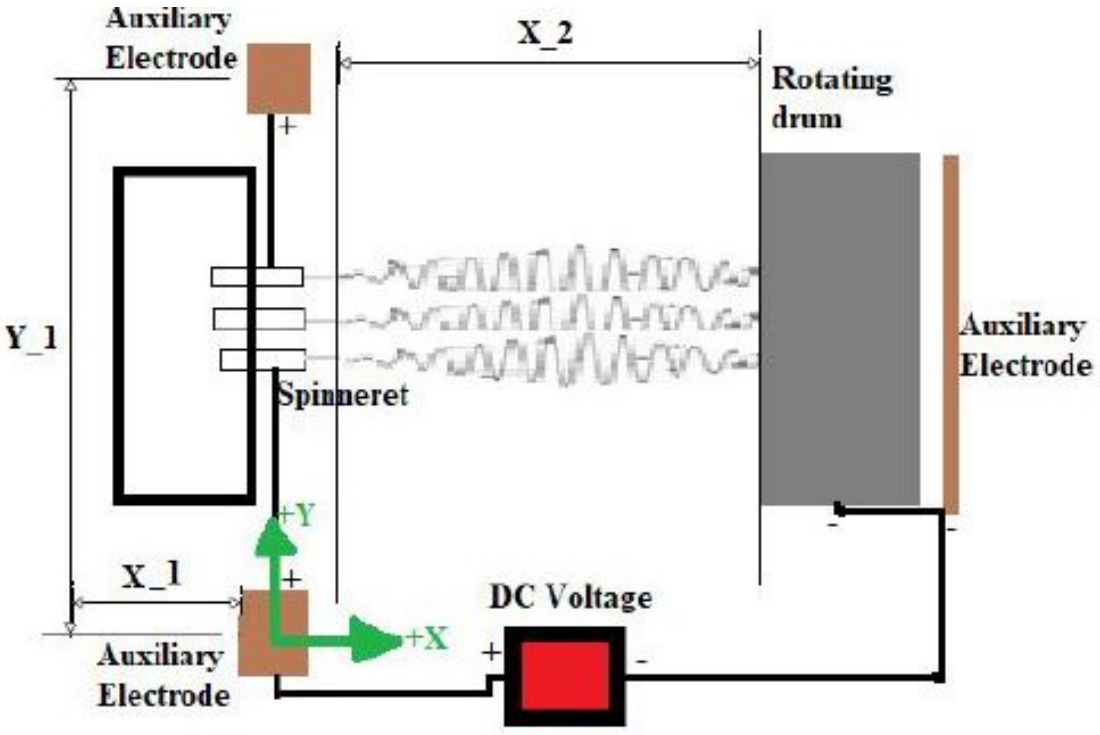

FIGURE 3.7: Schematic of the electrospinning equipment used to produce aligned nanofibres

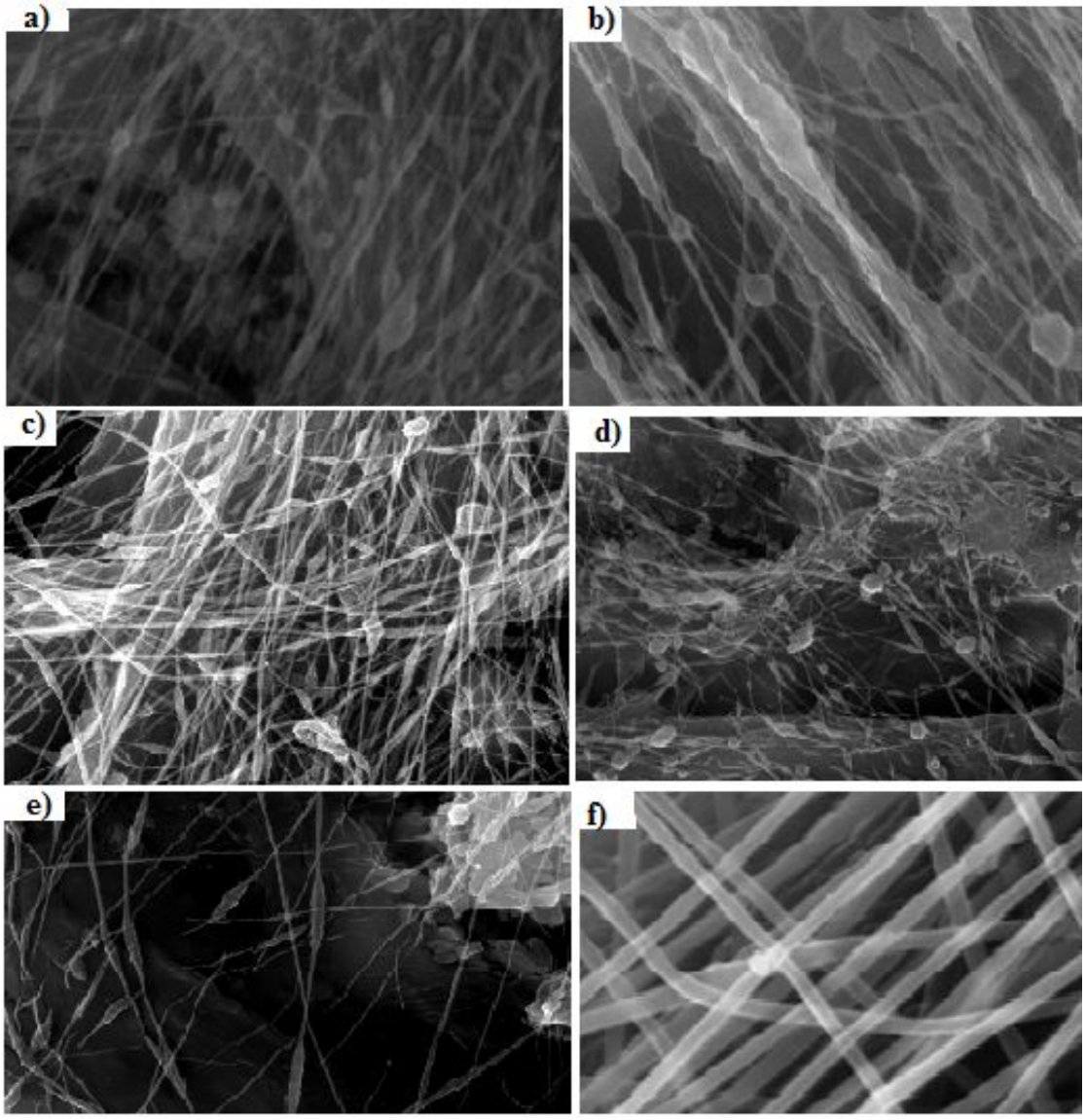

FIGURE 3.8: SEM micrograph of electrospun nanofibre produced using Electrospinning with varying of auxiliary electrodes X (distance from the rotating collector and Y (distance from the spinneret to auxiliary electrode coordinates: (a) X = 10 cm and Y = 25 cm (b) X = 10 cm and Y = 30 cm, (c) X = 0 cm and Y = 30 cm, (d) X = 20 cm and Y = 25 cm (e) X = 0 cm and Y = 15cm and (f) X = 0 cm and Y = 25 cm (Optimal)

3.3.3 Aligned and Randomly Distributed Nanofibre Analysis

Figure 3.9 illustrate SEM images of PAN aligned and randomly distributed nanofibres. The aligned nanofibres showed a decrease in the nanofibre diameter, enhance the diameter distribution, and improved nanofibre alignment.

To determine the diameter distribution of nanofibres, 50 nanofibres from the SEM images similar to the ones shown in Figure 3.9a) and b) were analyzed using ImageJ software.

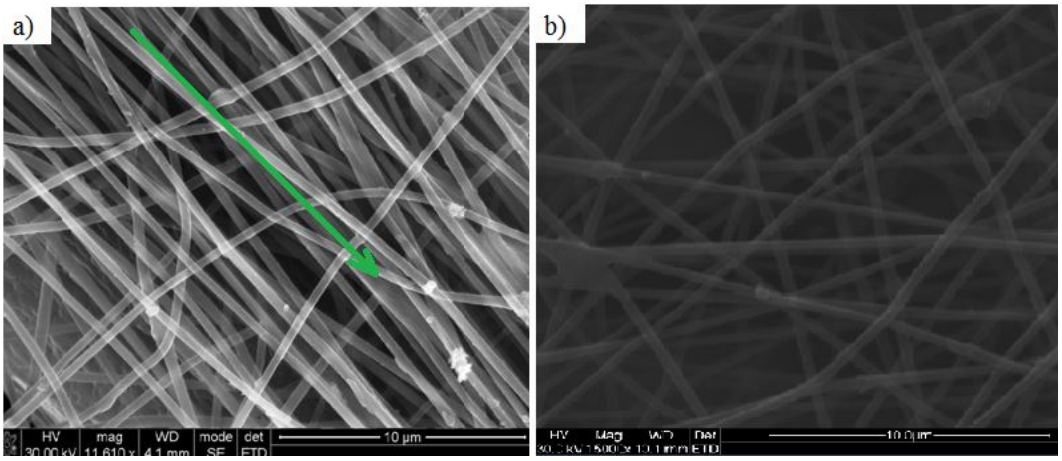

FIGURE 3.9: a) aligned nanofibres and b) randomly distributed nanofibres.

The aligned nanofibres had smaller diameters than the randomly distributed nanofibres with 84% of the aligned nanofibres having diameter less than 200 nm as shown in Figure 3.9a). The distribution range is also very narrow as smallest and highest diameters are 150 nm and 300 nm respectively. The average diameter of the aligned nanofibres is approximately 190 nm. This is indication that the introduction of auxiliary electrodes to modify the electrospinning equipment resulted in the production of good quality aligned nanofibres with small diameters and enhanced diameter distribution. Contrary, the nanofibres produced using the existing electrospinning equipment are randomly distributed with big diameters and poor nanofibre diameter distribution. The nanofiber diameter distribution ranges from 300 to 900 nm and the average diameter is 527 nm.

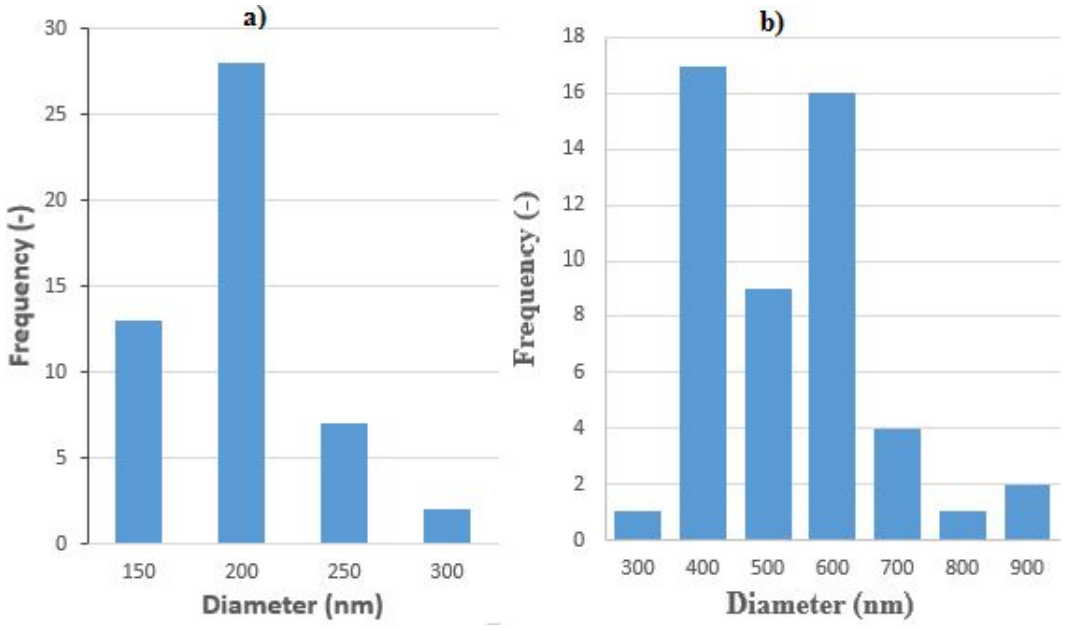

FIGURE 3.10: (a) Diameter distribution of aligned and (b) randomly electrospun PAN nanofibres produced using electrospinning equipment with and without parallel electrodes.

Furthermore, ImageJ software was used to mesasure the degree of alignment by analysing SEM images for both aligned and randomly dispersed nanofibres. Figure 3.11a) and b) displays the degree of alignment of the composite nanofibres. In this research, the angle between the long axis of the nanofibres and its expected direction (the vectors of parallel electric field) was used as the parameter to quantify the alignment. The degree of nanofibre alignment was defined as the ratio of the number of nanofibres, whose angle of alignment is between -10° and 10° to the total number of nanofibres. The degree of nanofibre alignment of the randomly dispersed nanofibres is 6% which is very poor. The nanofibres are randomly dispersed in different angles ranging between 100° and -300°. Furthermore, the degree of alignment of the 86% of the aligned nanofibres is between -20° and 20° and this shows that the nanofibres are well aligned. Finally, it can be concluded that the modified electrospinning process (MEP) decreases the PAN nanofibre diameter, enhances the diameter distribution, and improves the composite nanofibre alignment.

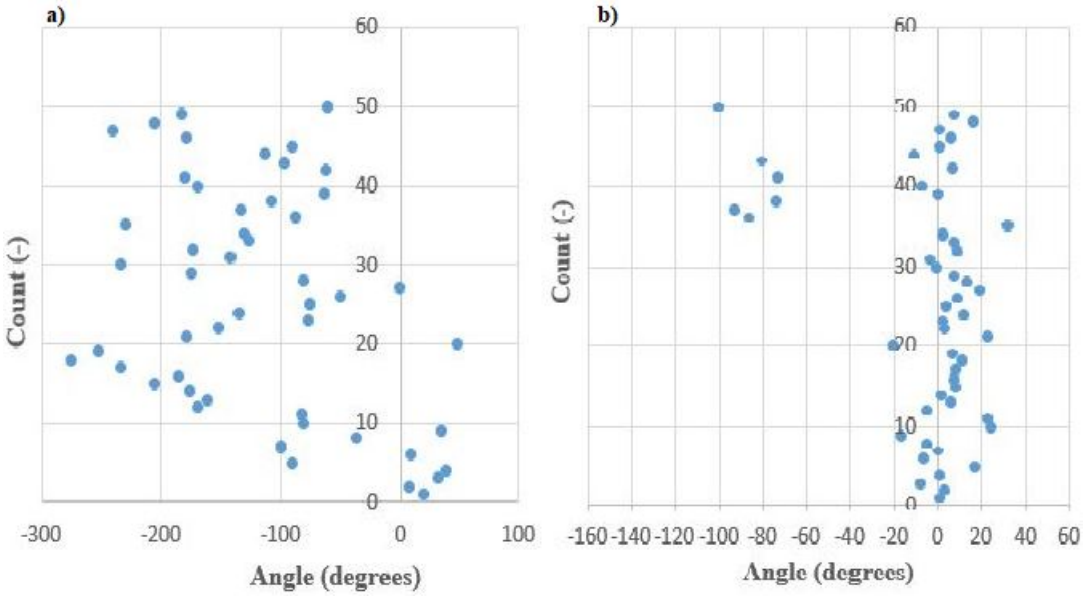

FIGURE 3.11: (a) Diameter distribution of aligned and (b) randomly electrospun PAN nanofibres.

3.3.4 PAN Nanomat Manufacturing

In an effort to determine the optimum PAN nanomat volume fraction required to reinforce the aramid polypropylene composite, three PAN nanomat volume fractions were used and these are 0.1%, 0.5% and 1%. In order to determine the amount of PAN needed for each volume fraction, the rule of mixtures for laminate composites was used as described next.

The first step was the determination of the density of the overall composites which is given by the equation:

$$\rho_c = V_{faramid}\rho_f + V_{pp}\rho_{pp} + \rho_{PAN}V_{PAN} \tag{3.5}$$

where

$V_{faramid} = 30\%$ is the optimum aramid fiber volume

$\rho_f = 1.44g/cm^3$ is the density of aramid fiber

$V_{pp} = 1 - V_{faramid} - V_{PAN}$ is the Volume fraction of polypropylene

$\rho_{pp} = 0.91g/cm^3$ is the density of polypropylene

$\rho_{PAN} = 1.184g/cm^3$ is the density of PAN

$V_{PAN} = 0.1\%$, 0.5% and 1% is the volume fraction of PAN

Substituting the above values, it was found that the overall composite density for each PAN volume fraction of 0.1%, 0.5% and 1% is $1.069g/cm^3$, $1.070g/cm^3$, $1.072g/cm^3$ respectively

It is clear that the PAN nanofibre volume fractions has little effect on the overall density of the composite. The mass of the composite was determined using quation 3.6:

$$m_c = \rho_c \times V_{mould} \tag{3.6}$$

where

$\rho_c = 1.07g/cm^3$

$V_{mould} = 13 \times 17 \times 0.3 = 66.3cm^3$

The weight fraction, W_f, of the amount of PAN that is needed is given by quation 3.7:

$$W_{fpan} = \frac{\rho_{pan} \times V_{pan}}{\rho_c} = \frac{1.184 \times V_{fpan}}{1.07} \tag{3.7}$$

By substituting the V_{fPAN} values into the above equation, the PAN weight fraction for 0.1%, 0.5% and 1% were calculated as 0.11%, 0.55% and 1.11% respectively.

The mass of the required PAN is given by equation 3.8.

$$m_{pan} = m_c \times W_{pan} \tag{3.8}$$

Solving equation 3.7 and substituting W_{fpan} variables into the above equation, the mass of PAN for each PAN volume fraction of $0.1\%, 0.5\%$ and 1% is calculated as $0.0785g, 0.3925g$ and $0.78g$ respectively.

The next step is to find the required volume of PAN using the following equation:

$$Volume_{pan} = \frac{m_{pan}}{\rho_{pan}} \tag{3.9}$$

By substituting m_{PAN} variables calculated in equation 3.7 for $0.1\%, 0.5\%$ and 1% PAN volume fractions, the PAN volume of $0.066ml, 0.33ml$ and $0.66ml$ respectively. However, PAN was in solid form and it needed to be dissolved in DMF. The volume of PAN/DMF solution is determined as follows:

$$Volume_{pan/DMF} = \frac{Volume_{pan}}{PAN_c onc.} \tag{3.10}$$

Where $PAN_conc. = 0.083$ is the concentration of the solution.

The volume PAN/DMF solution for PAN volume fraction of $0.1\%, 0.5\%$ and 1% were $0.8ml, 3.98ml$ and $7.95ml$. At dispensing speed of $0.36ml/hr$ and using 6 syringes, these volumes were fully dispensed in $25mins, 110mins$ and $248mins$ respectively. However, there are 9 aramid layers/sheets per composite and this means electrospinning for $2.8mins/sheet$, $12.2mins/sheet$ and $27.6min/sheet$. In summary the amount of PAN/DMF solution needed to be dispensed was determined by dividing the volume of PAN/DMF (calculated using equation 3.9) by the dispensing speed, number of syringes and the number of sheets (which is equal to 9). The next step was to electrospin PAN nanomat onto the aramid fiber using the elctrospinning equipment described in detail in section 3.2.1. The initial step of the electrospinning procedure was filling the syringes with the required amount 8.4% DMF/PAN solution. The syringes were then loaded into the syringe holder designed to hold the syringes tightly in place and to prevent them moving.

Woven aramid fiber sheets were then cut into the mould dimensions ($17cm \times 13cm$) and secured onto the drum collector using duct tape. The syringe pump was then adjusted into the required flow rate and volume of solution to be dispensed. The drum rotational speed was then set at $800rmp$ using the motor controller. The voltage was then set to 25 kV using the voltage source. The PAN nanofibres were then spun onto the aramid wrapped collector for the duration of the required time. Figure 3.12 shows the PAN nanofibres collected on the aramid fiber. The PAN reinforced aramid polypropylene

FIGURE 3.12: PAN nanomat electrospun onto aramid wrapped collector

composite was then fabricated using both compression molding and calendering. The

processing parameters were also kept the same. The only difference was that PAN nanofibre coated polypropylene sheets were placed with the electrospun nanomat.

3.3.5 Fuctionalization Procedure

Functionalization was carried out by ultrasonically dispersing 100 *grams* of SWCNTs for 30 minutes at 25 $^{\circ}C$ in 1000 *ml* of 95 *wt*% aqueous methanol using an Integral Systems UD 80SH-2L Digital Sonifier shown in Figure 3.13a.

The ultrasonically treated SWCNTs were allowed to deposit (Figure 3.13b) for 3 hours and then filtered through a 1.0 *microm* pore size filter paper. Thereafter, the filtered SWCNTs were dried using the oven at 90 $^{\circ}C$ for 5 hours. The dried SWCNTs from the

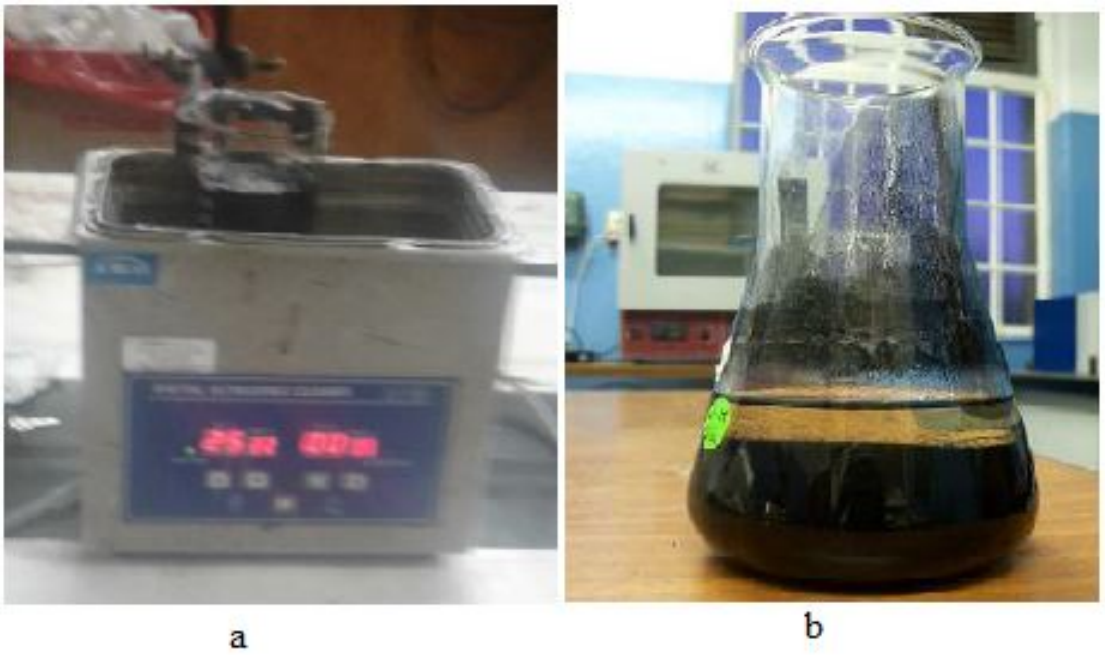

FIGURE 3.13: SWCNTs ultrasonic treatment process.

ultrasonication treatment were then acid treated using a solution made of nitric (HNO_3) and sulphuric (H_2SO_4) acid, both at 50% concentration. The ratio of HNO_3 and H_2SO_4 used was 1:2. The SWCNTs and acid mixture was then mixed at 45 $^{\circ}C$ for 12h, 24h and 36h using the combined hot plate magnetic stirrer stove at atmospheric controlled chamber as shown in Figure 3.14.

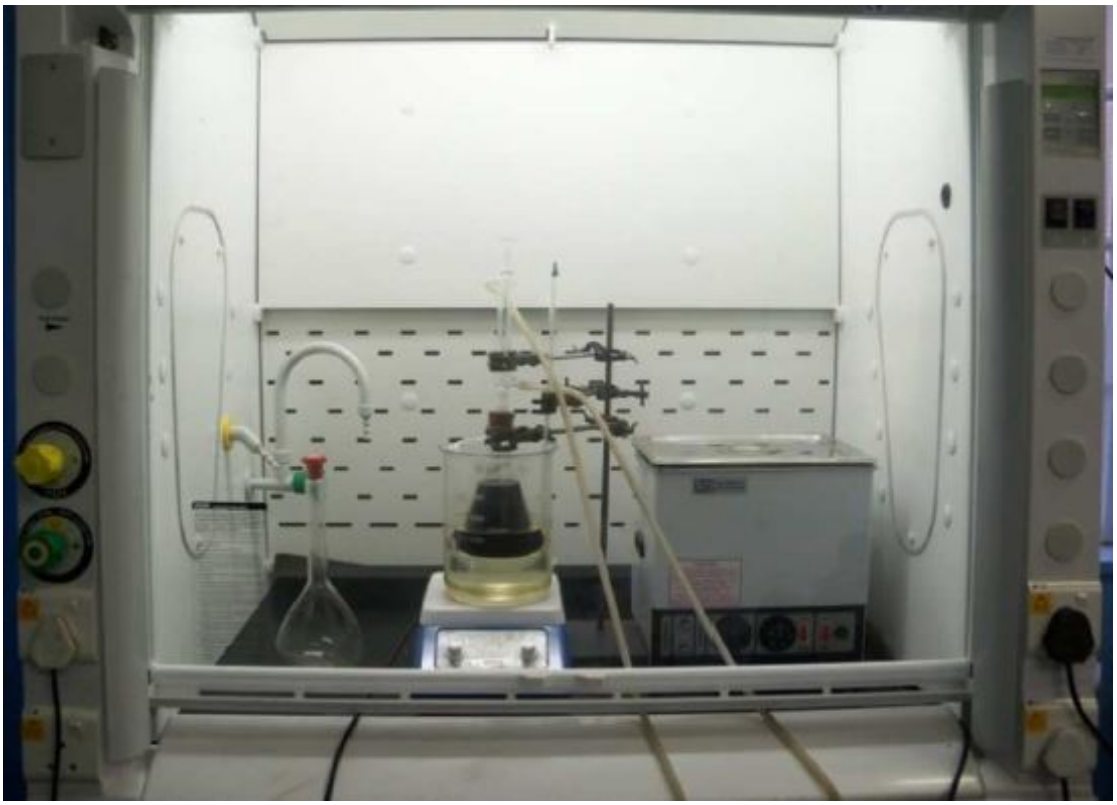

FIGURE 3.14: Acid treatment of SWCNTs.

After the acid treatment was completed, the mixture was ultrasonically treated for 30 minutes at 25 $^{\circ}C$ to ensure good dispersion of SWCNTs. Thereafter, the acid treated SWCNTs were filtered and washed 5 times using a 1.0 *microm* pore size and deionised water respectively. This was done to remove excess acid and neutralize the solution. The SWCNTs were then dried in an oven at 90 $^{\circ}C$ for 24 hours and the dried functionalized SWCNTs is shown in Figure 3.15.

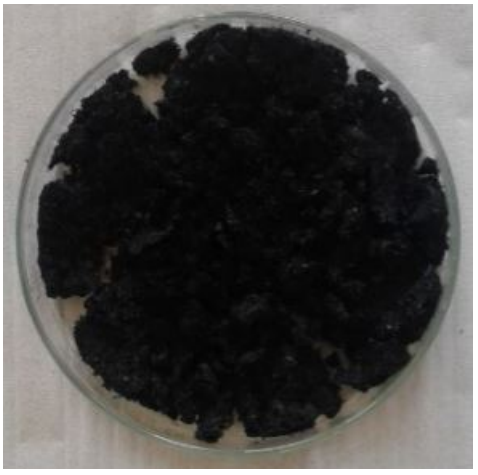

FIGURE 3.15: Dry functionalized SWCNTs.

3.3.6 FTIR, Raman and Thermogravimetric(TGA) Analysis

FTIR microscopy was used to identify the OH and -COOH functional groups which are supposed to be attached to CNTs during functionalization. Figure 3.16 shows the FTIR results of the pristine(untreated), $12h$, $24h$ and $36h$ functinalized SWCNTs. Following functionalization, peaks were observed at $2250cm^{-1}$ and $3150cm^{-1}$ which indicate that COOH and OH groups had been successfully grafted onto the surface of the SWCNTs. The graph also shows that the extent of functionalization increased with time of functionalization.

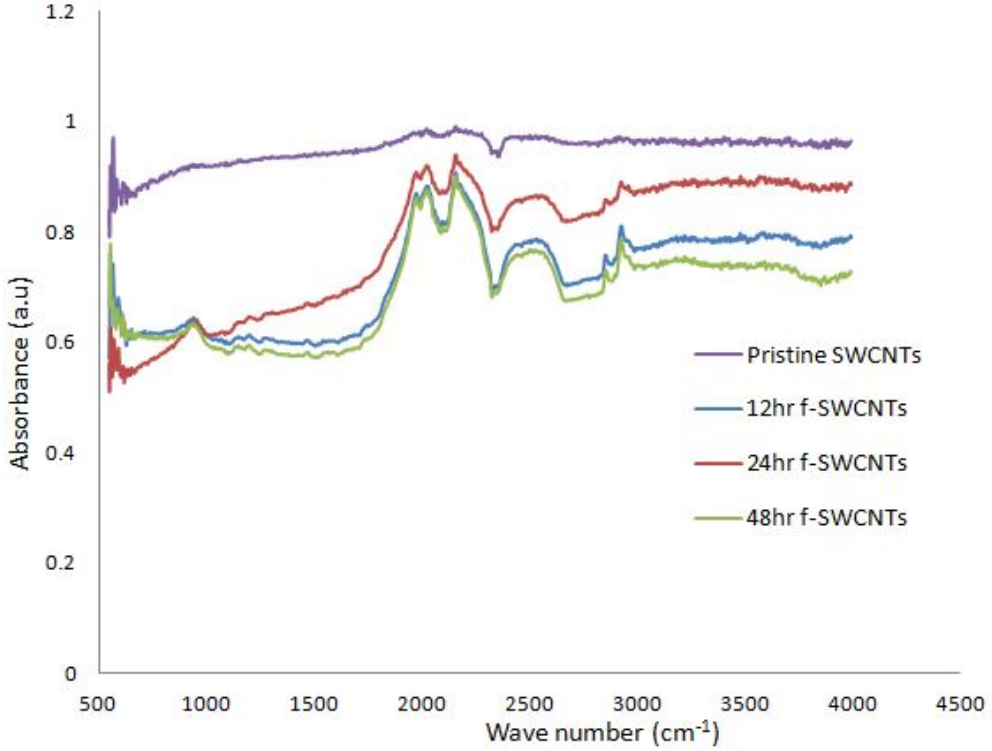

FIGURE 3.16: FTIR results of the pristine and functionalized SWCNTs

Furthermore, FTIR was also used to determine if PAN was indeed doped with CNTs. This was done by conducting FTIR analysis on pure PAN nanofibres, SWCNT doped PAN and Pristine SWCNTs as shown in Figure 3.17 . FTIR analysis shows minor changes in the spectra of pure PAN nanofibre upon addition of SWCNTs (CNT doped PAN nanofibres). One of these changes were observed at the 2540 cm^{-1} region which indicates that the π bonds present in SWCNTs interact with the hydrogen attached to the nitrogen in the urethane bond, thus changing the shape of the bond. The spectra also showed sharp peaks at $1040cm^{-1}$ and 1600 cm^{-1} which could be due to the C=C stretch mode in SWCNTs. These results serve to confirm that the PAN nanofibres are doped with CNTs. Raman Spectroscopy was also conducted on both pristine and

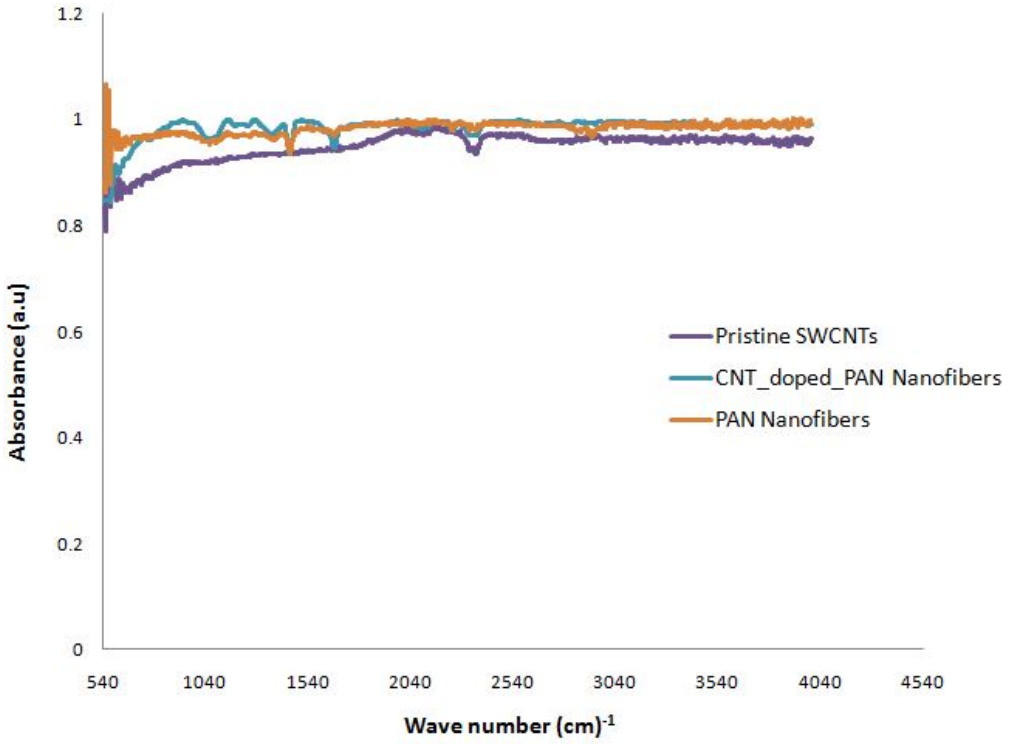

FIGURE 3.17: FTIR analysis of PAN nanofibres, SWCNT doped PAN and Pristine SWCNTs

fucntionalized CNTs. Figure 3.18 shows the Raman spectrum of pristine, $12h$, $24h$ and $36h$ functinalized SWCNTs. The two Raman peaks at D and G band were observed in both pristine and functinalized SWCNTs. This is attributed to the disorder in hexagonal framework of the SWCNTs walls. The comparison of the Raman spectrums of pristine SWCNTs with that of functinalized SWCNTs shows that intensities of G and D bands of pristine SWCNTs are greater than those of functionalized SWCNTs. This difference is an indication of the functionalization of SWCNTs as a result of acid treatment. It is also worth noting that the G and D bands of both the pristine and functinalized SWCNTs are similar. This suggests that the acid treatment did not damage or alter the graphine layers of the SWCNTs. Furthermore, the purity and the crystalline CNTs can be found by attaining the ratio of the intensity of the G band and that of the D band (I_G/I_D ratio). The I_G/I_D ratio can reveal the disorder in the CNTs structure and the higher the ratio, the more crystalline the CNTs. This makes Raman spectrum suitable to be used to check the degree of functionalization. The I_G/I_D ratio for pristine, 12h, 24h and 36h was found to be approximately 15, 8, and 12 respectively. Moreover, the width of the D peak for the functionalized SWCNTs was found to be narrower than that for the pristine SWCNTs. This is an indication of higher degree of order in functionalized SWCNTs.

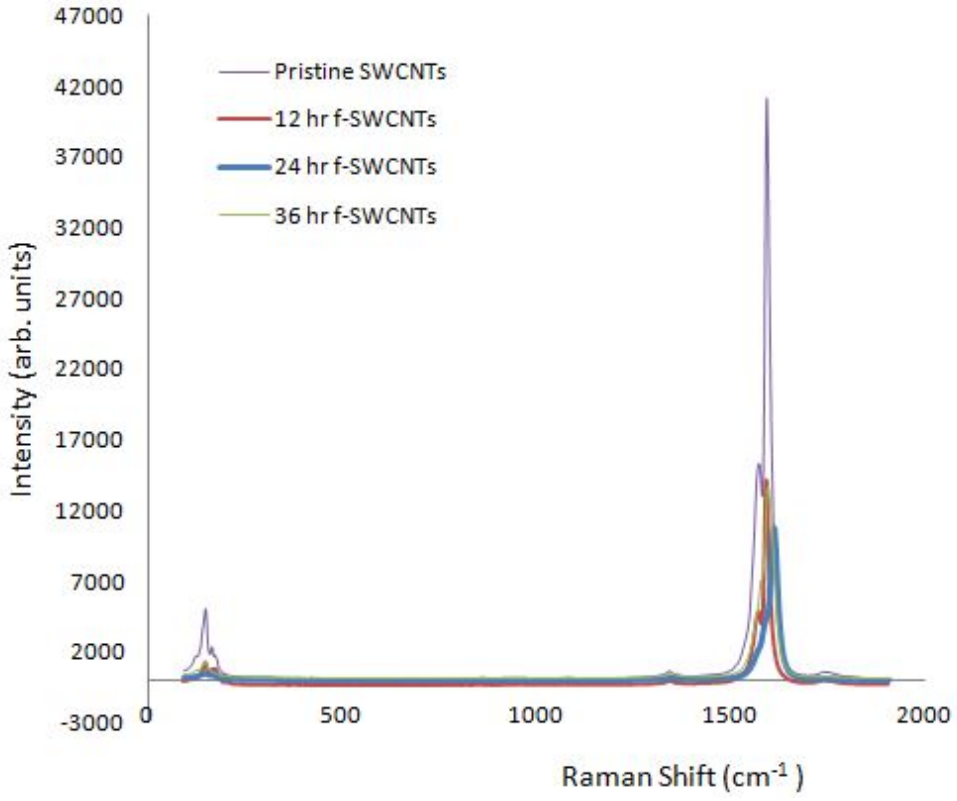

FIGURE 3.18: Raman spectrum of the pristine and functionalized SWCNTs

Furthermore, TGA was conducted on both the pristine and on the three functionalized time periods SWCNTs. The results are shown in Figure 3.19 and 3.20. Pristine SWCNTs show a residual mass of 15% which is consistent with the manufacturer's specification of 85% purity. The residual mass decreased to 10% for the functionalized SWCNTs. This behavior shows that functionalization helped purify the SWCNTs. Figure 3.19 also shows that the decomposition temperature of SWCNTs decreased with increase in functinaliszation time period from 12 h to 36 h. The pristine SWCNTs decomposed at temperature of 660°C and as the functionalization time increased to 36 h, the decomposition of SWCNTs decreased to 570°C.

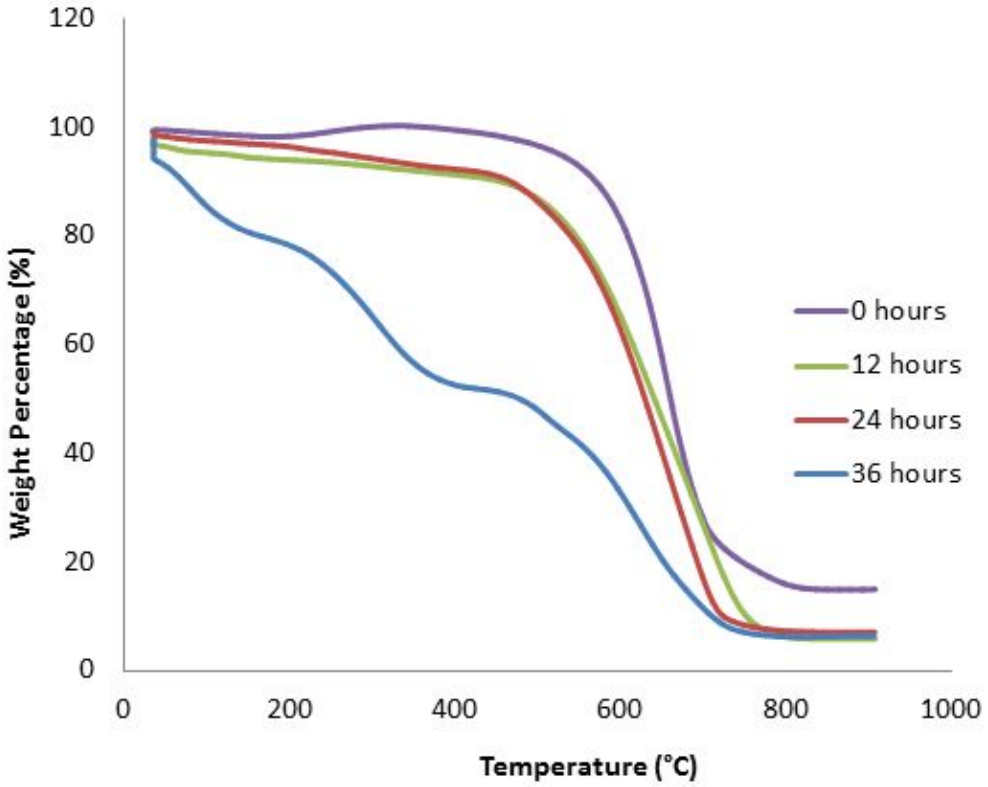

FIGURE 3.19: TGA of pristine and functionalized SWCNTs.

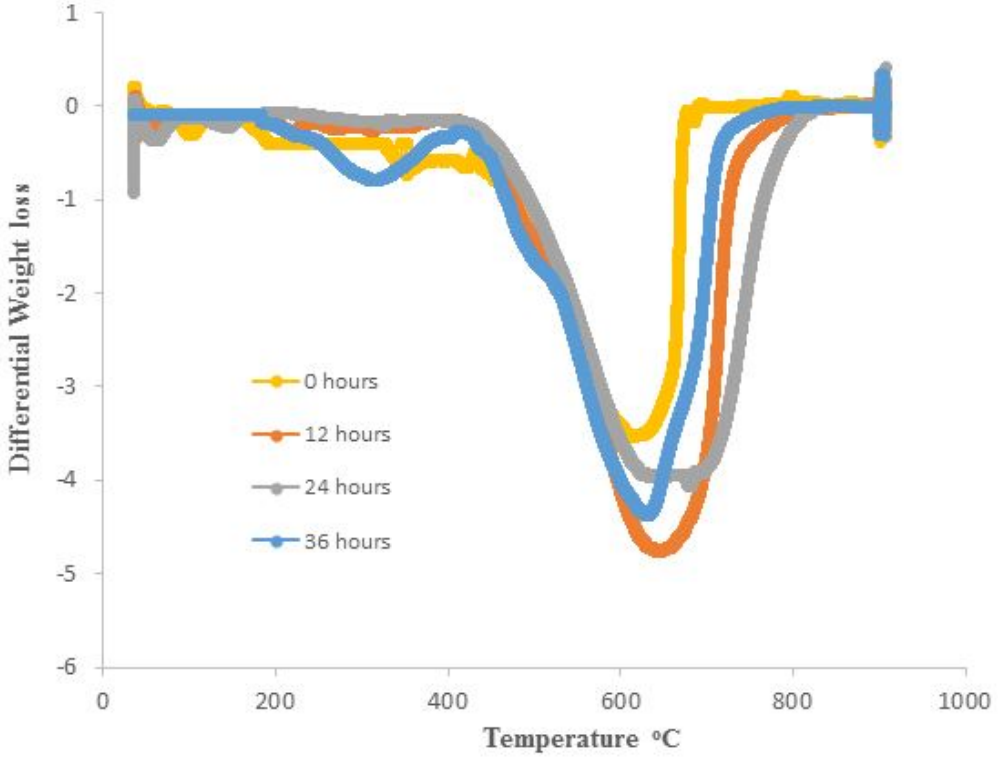

FIGURE 3.20: TGA of differential weight to temperature of pristine and functionalized SWCNTs.

Figure 3.21 shows the functionalized SWCNTs dispersed in DMF and left for over a long period (month) to settle to investigate if SWCNTs are properly dispersed. Sample 'A', 'B' and 'C' refers to the SWCNTs treated for 12 h, 24 h and 36 h respectively. The sample functionalized for 24 hours remained dispersed in DMF after a month while the one functionalized for 12 h settled quickly followed by the functionalized for 36 h. Based on these results it is clear that treatment of SWCNTs with nitric and sulphuric acid improved the dispersion of CNTs in DMF. Acid treatment of SWCNTs over a short period of time ($\leq$ 12h) results in limited functionalization and extended period of functionalization results in weakening and poor dispersion of SWCNTs.

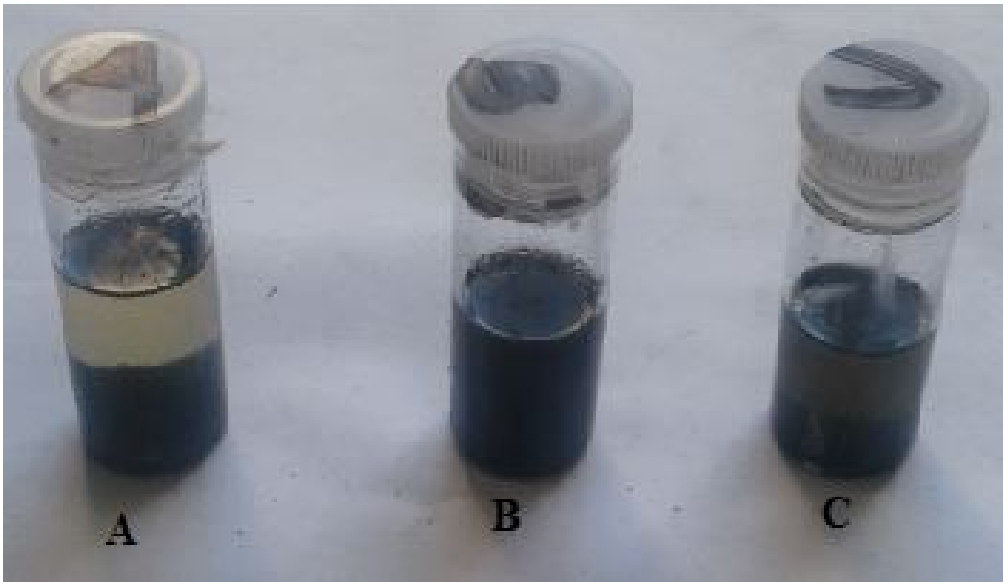

FIGURE 3.21: Functionalized SWCNTs dispersed in DMF for: a) 12 hours, b)24 hours and C) 36 hours

Fiure 3.22 shows both the non functionalized and functionalized CNT doped PAN nanomat coated aramid fibre. Small dark CNT agglomerates were observed in the non functionalized electropsun CNT doped PAN nanomatn

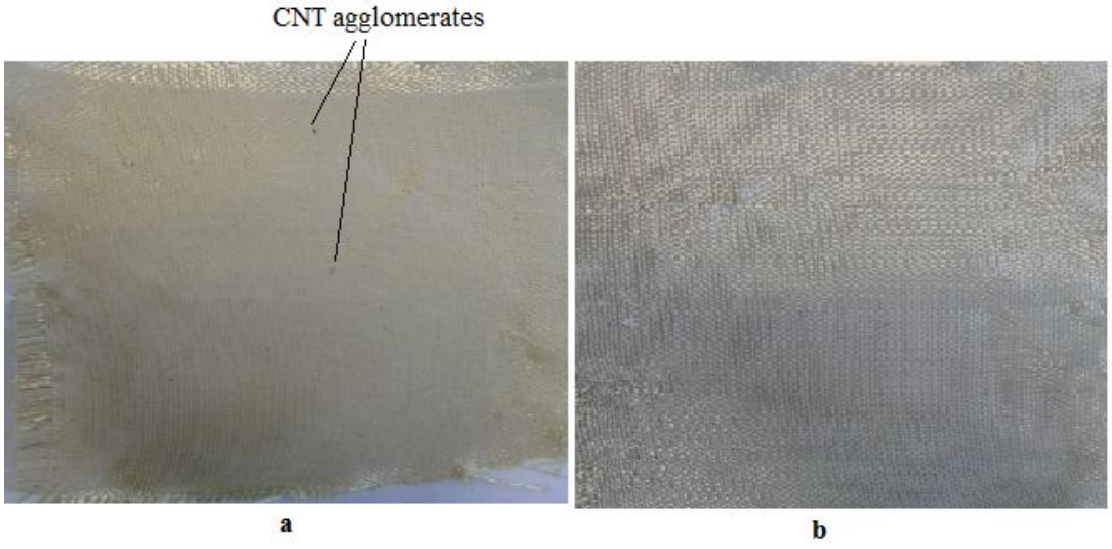

FIGURE 3.22: a) Non functionilizaed CNT doped PAN nanofibre coated Aramid fiber and b) functionalized CNT doped PAN nanofibre coated Aramid fiber.

3.3.7 CNT doped PAN Nanomat Manufacturing

The manufacturing of CNT doped PAN nanomat was carried out with 30% and 0.5% for aramid and PAN nanofibres respectively. Three CNT concentrations (0.1%, 0.25% and 0.5%) were considered for the current analysis. The CNTs were dissolved in DMF solvent and magnetically stirred until the solution was fully dissolved.

A maximum of 0.5% CNTs concentration was used because concentrations beyond this could not be electrospun as the viscosity markedly increased. There was also extreme clogging. The 0.5% PAN was then added to separate CNT/DMF mixtures and magnetically stirred for a further 24hrs to completely dissolve the PAN and evenly disperse the CNTs in the solution. Figure 3.23 shows the CNT doped PAN solution. The 0.5% and volume fraction CNT/PAN mixtures were then electrospun on to the aramid fiber.

FIGURE 3.23: CNT doped PAN solution

The same calculations applied in section 3.3.1 were used with the only difference being that the electrospinning was on the aramid fibers and not polypolypropylene sheets. The volume CNT/PAN/DMF solution for CNT concentration of 0.5% was dispensed at a speed of $0.36ml/hr$ and using 6 syringes. This volume was fully dispensed in $110mins$ and $248mins$. However, there are 9 aramid layers (30% volume fraction) per composite and thus electrospinning will take $12.2mins/sheet$. In summary the amount of CNT/PAN/DMF solution needed to be dispensed was determined by dividing the volume of PAN/DMF calculated using equation 3.9 by the dispensing speed, number of syringes and the number of sheets. The same process was also done for the functionalized CNTs.

3.4 Mechanical Characterization

The fabricated polypropylene, AF-PP composite and hybrid composite specimens were tested to determine the mechanical properties and these include the tensile test, flexural test (3 point bending test), impact test and short beam test.

3.4.1 Short Beam Test

The interlamianr shear strength is one of the most important parameters which determine the interlaminar properties of a composite. It is therefore important to accurately predict/determine its value and a number of tests have been developed. The short beam(ASTM D2344) test method, formerly know as interlaminar shear strength test (ILSS) was used to measure the inter-laminar shear strength of the fabricated composites. This test involves loading a beam under three point bending with span-to-thickness ratio of the specimen equal to 4. This ensures that the interlaminar shear failure is induced. Figure 3.24 shows the short beam test set up as per ASTM D2344. A minimum

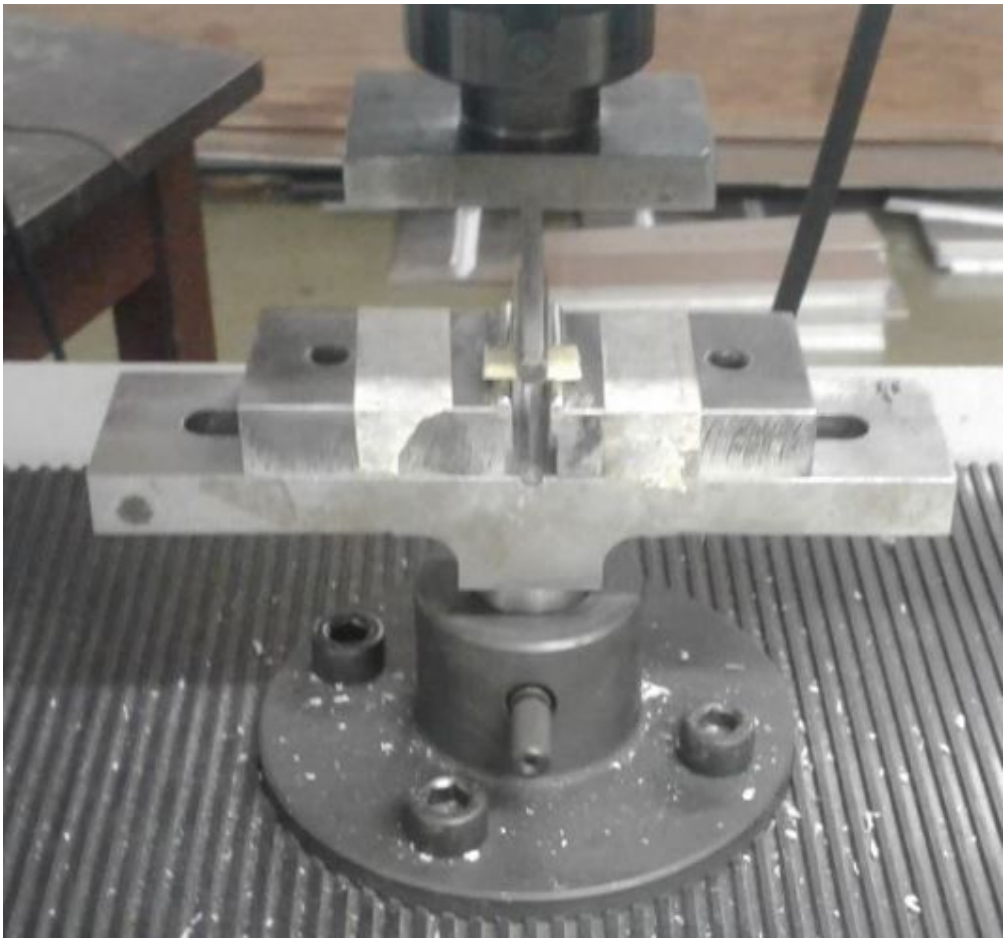

FIGURE 3.24: Short beam test setup

of 5 specimens were cut in preparation of the short beam test. The short beam test specimens are center loaded as shown in Figure 3.24. The specimen rest on two supports that allow lateral motion and the load is applied at a speed of $1mm/min$. The specimen end should overhang on the side support centers by at least the specimen thickness. The next step is to apply the load until either of the following occurs: load drop off of 30%, two piece specimen failure or head travel exceeds specimen nominal thickness [108].

The short beam strength is calculated using the following equation:

$$ILSS = F^{sbs} = \frac{0.75P_m}{bh} \tag{3.11}$$

where

F^{sbs} = short-beam strength, MPa

P_m = maximum load observed during the test, N

b = measured specimen width, mm

h = measured specimen thickness, mm

3.4.2 Tensile Test

Tensile test technique, ASTM D638:2010 was used to determine tensile strength and modulus of the hybrid composites. The preferred dimensions for the tensile test specimen as per ASTM D638:2010 is shown in Figure 3.25. Test specimens were prepared using the saw and cut into dog-bone specimens using a CNC machine and this was done in accordance with ASTM D638:2010. The specimens were tested using Shimadzu universal mechanical test machine shown in Figure 3.26.

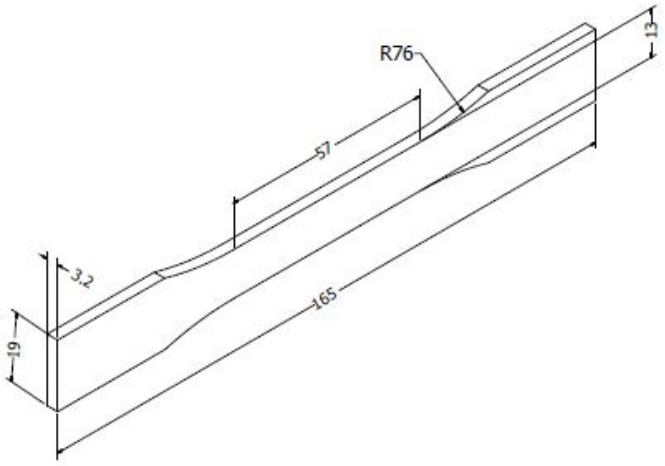

FIGURE 3.25: Tensile test specimen dimensions as per ASTM D638:2010.

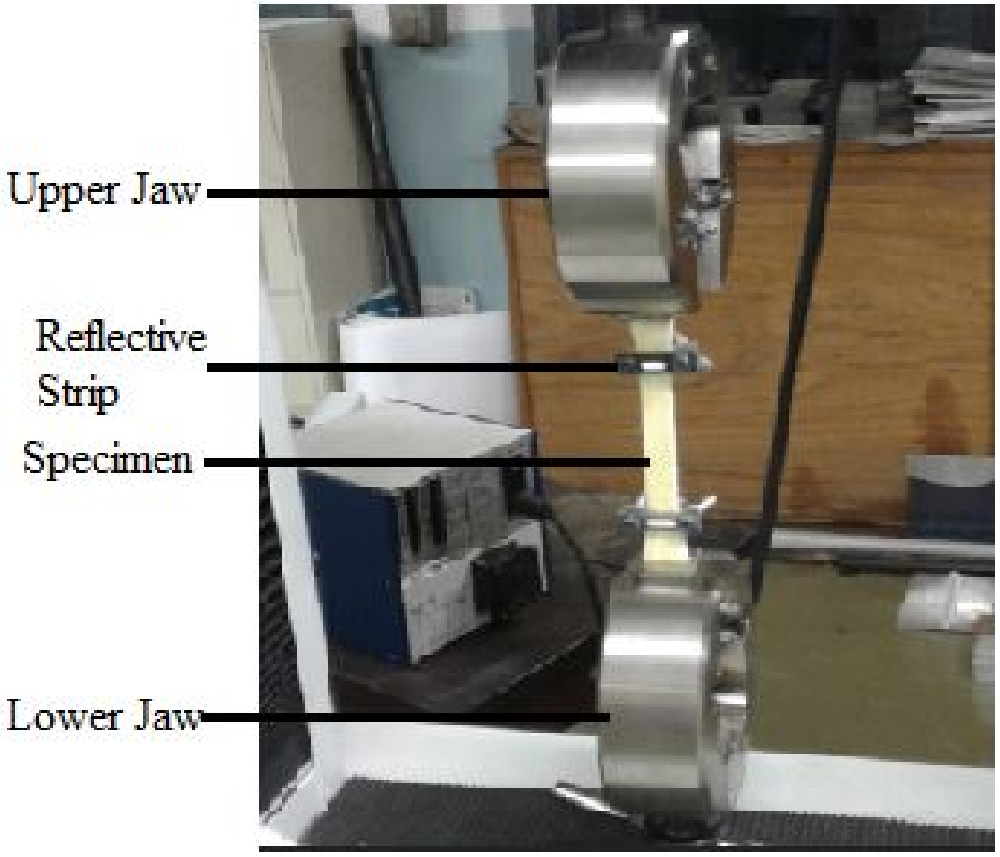

FIGURE 3.26: Tensile test setup

A minimum of 5 specimens were tested for each panel. The specimens were tested at a cross head speed of 2 mm/min and at room temperature. An external laser extensometer LE-05 obtained from Epsilon Technology Corp was used to record the change in length of the gauge section of the specimen. The experimental data was recorded to the

data acquisition software.The data recorded was then used to calculate the the tensile properties of the specimens.

The analysis procedure is outlined below. Firstly, the average cross-sectional area of the gauge test section of the tensile specimen was calculated as follows;

$$A = wt \tag{3.12}$$

where w and t is the width and thickness of the gauge test section of the dog-bone specimen.

The ultimate tensile strength was calculated by using the recorded maximum ultimate load at the point of failure and the average cross sectional area of the specimen using equation 3.13.

$$\sigma_{ult} = \frac{F_{max}}{A} \tag{3.13}$$

where F_{max} is the ultimate load and A the specimen cross sectional area.

The tensile strain was calculated using the data recorded by the extensometer as follows:

$$\epsilon = \frac{L - L_0}{L_0} \tag{3.14}$$

where L_0 is the original length of the specimen and L is the gauge length of the tensile tested specimen.

The stress-strain curves were used to obtain the elastic modulus using the following equations;

$$E = \frac{\sigma}{\epsilon} \tag{3.15}$$

where σ and ϵ are tensile stress and strain respectively.

3.4.3 Flexural Test

Flexural test was performed in accordance with the ASTM D790:2010 which makes use of the 3 point bending test. The proposed dimensions for the flexural test specimen according to the ASTM standards is shown in Figure 3.27. Figure 3.28 shows the flexural test specimem under the applied load.

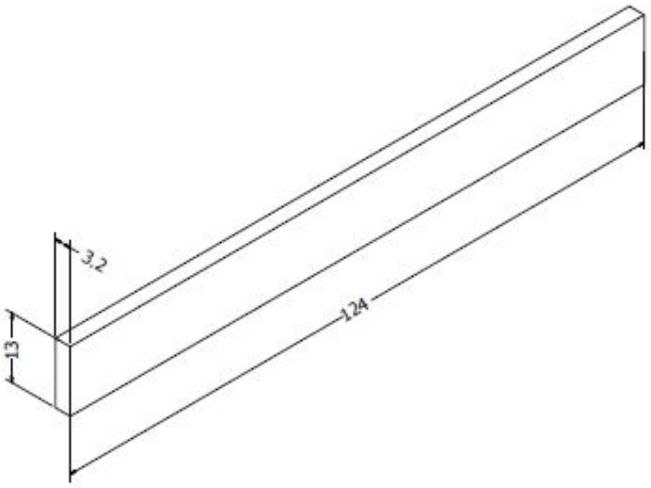

FIGURE 3.27: Flexural testing specimen dimensions

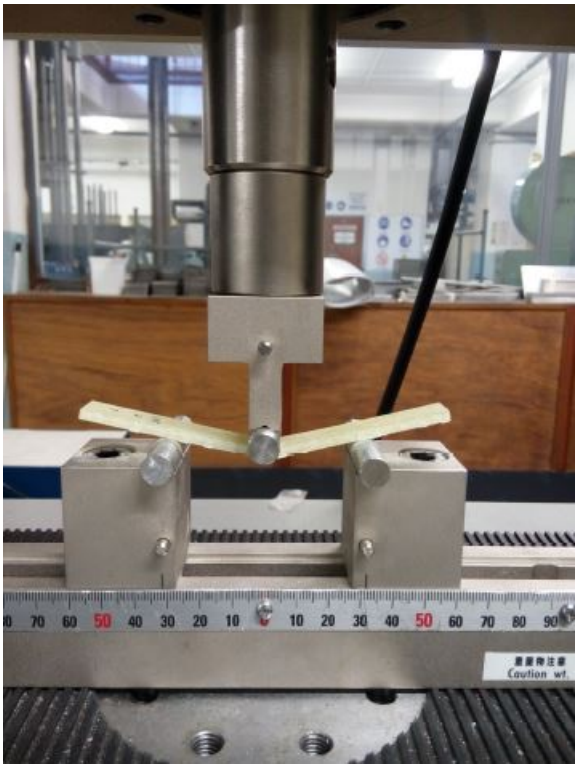

FIGURE 3.28: 3-point flexural test specimen

A minimum of 5 specimens were tested using the Shimadzu universal testing machine. The flexural strength (S) in MPa is calculated using the following equation;

$$S = \frac{3PL}{2bh^2} \tag{3.16}$$

where P is the applied load, L is the span length, b is the width and h is the thickness

of the span. The flexural strain was calculated by using the data recorded extensometer and the following equation;

$$\epsilon_f = \frac{6hD}{L^2} \tag{3.17}$$

where D is the vertical deflection of the specimen at the point of load application.

3.4.4 Impact Energy Absorption Test

The test was performed in accordance with ASTM D256:2010 which stipulates that at least five notched specimens per panel be tested. Figure 3.29 shows the impact test specimen dimensions as per ASTM standard.

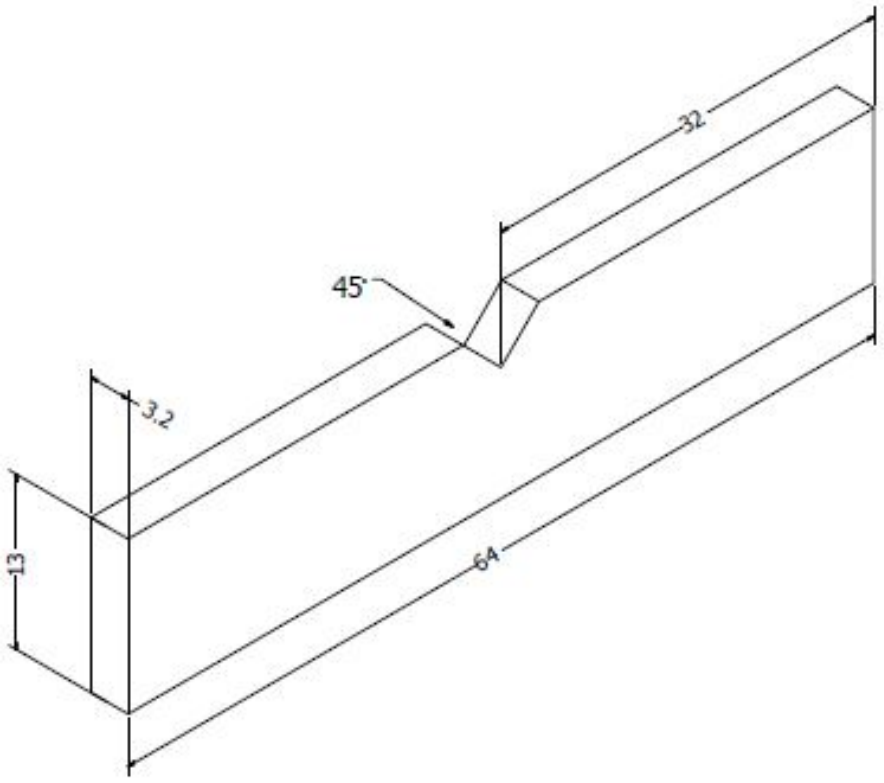

FIGURE 3.29: Impact testing specimen dimensions as per ASTM standard.

The Avery pendulum impact testing machine shown in Figure 3.30 was used to determine the toughness of the composite materials. It consists of a pendulum axe swinging at a notched sample/specimen of material. The machine has a static dial arm which is manually movable up to the 4.2 Joule marking. When the pendulum is released with no specimen being tested, the dynamic dial moves to zero mark on the absorbed energy gauge indicating that no energy was absorbed. The range of the impact testing machine is 0 to 4.2J and has a resolution of 0.025 Joules.

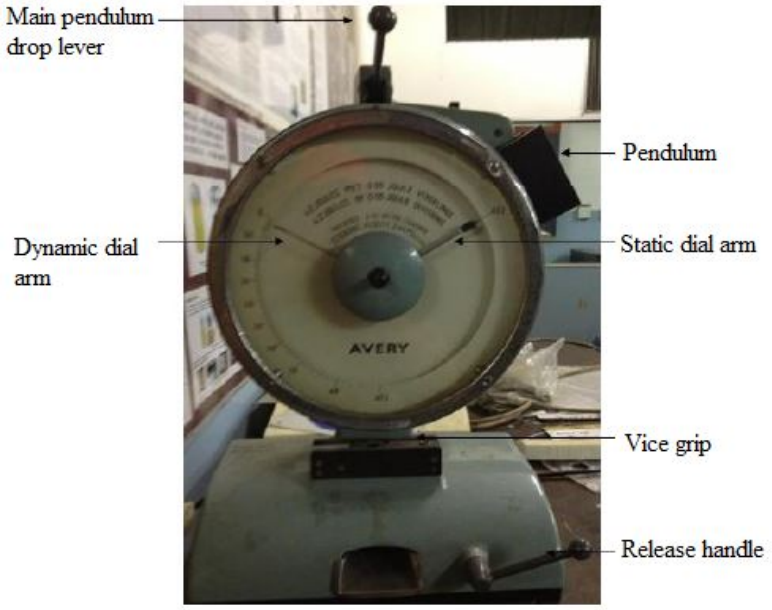

FIGURE 3.30: Impact testing specimen.

Procedure for impact test is summarised as follows; The pendulum was swung back to its maximum energy position and locked into place. The machine's lever base was then opened and the specimen placed slightly towards the left side of the grip away from the point of impact with pendulum. The next step was to turn the centre dial in order to move the static dial arm to the 4.2 Joules marking. The pendulum is then release by pulling down the release lever on the top of the machine and the resultant value that the dynamic dial corresponded to was recorded. The impact toughness was then determined using the following equation:

$$K_I = \frac{\Delta e_I}{A_I} \tag{3.18}$$

where

K_I = Impact toughness, J/m^2

Δe_I = Energy lost by pendulum due to impact, J

A_I = Cross-sectional area of impact specimen, m^2

3.5 Morphological Characterization

The microscopy used in this research include Raman Spectroscopy (RS), Thermogravimetric analysis (TGA), Scanning Eletron Microscopy (SEM) and Fourier Transform Infrared spectrometry (FTIR).

3.5.1 Scanning Electron Microscopy (SEM)

The SEM was extensively used in this study to visually inspect both the electrospun nano-fibers and to characterise the material damage mechanism by analysisng the composite's fiber and matrix structures such as fiber breakage, matrix cracks, morphology of the fiber surface. The FEI Nova 600 Nanolab FIB shown in Figure 3.31a was used to examine the electrospun nano-fiber and the specimen subjected to various mechanical tests. However, before the specimens could be analysed on SEM they needed to be coated. The samples were prepared using EMITECH K950X apparatus (3.31b) by spatter coating with 10nm carbon and 15nm gold palladium.

FIGURE 3.31: (a) FEI NOVA 600 Nanolab FBI and (b) EMITECH K950X.

3.5.2 Thermogravimetric Analysis (TGA), Raman Spectroscopy and Fourier Transform Infrared Spectrometry (FTIR)

Thermogravimetric analysis, Raman spectroscopy (RAMAN) and Fourier Transform Infrared spectrometry (FTIR) were used to analyse the raw PAN nanofibres, CNT doped PAN nanofibres, pristine and functionalized CNTs. The thermal stability of the PAN nanofibres, CNT Doped PAN, SWCNTs and the functionalized SWCNTs was determined using a Perkin-Elmer-Pyris thermo-gravimetric analyzer under an air flow of 20 mL/min. Figure 3.32a shows the TGA system used for analysis. Raman Spectroscopy shown in Figure 3.32b was used to analyse the effect of functionalization on the pure

SWCNTs, functionalized SWCNTs and SWCNTS doped PAN nanofibres. Raman spectra were acquired using the 514.5nm line of a Lexel Model 95 SHG argon ion laser and a Horiba LabRAM HR Raman spectrometer equipped with an Olympus BX41 microscope attachment. The incident beam was focused onto the sample using a 100x LWD objective. Power at the sample was kept relatively low (0.5 mW) to prevent localised heating. The backscattered light was dispersed via a 600 lines/mm grating onto a liquid nitrogen cooled CCD detector. The data was acquired using LabSpec v5 software. A Bruker Tensor 27 Fourier Transform Infrared spectrometer shown in Figure 3.32c was used to analyse the surface functionalities of nanoparticles.

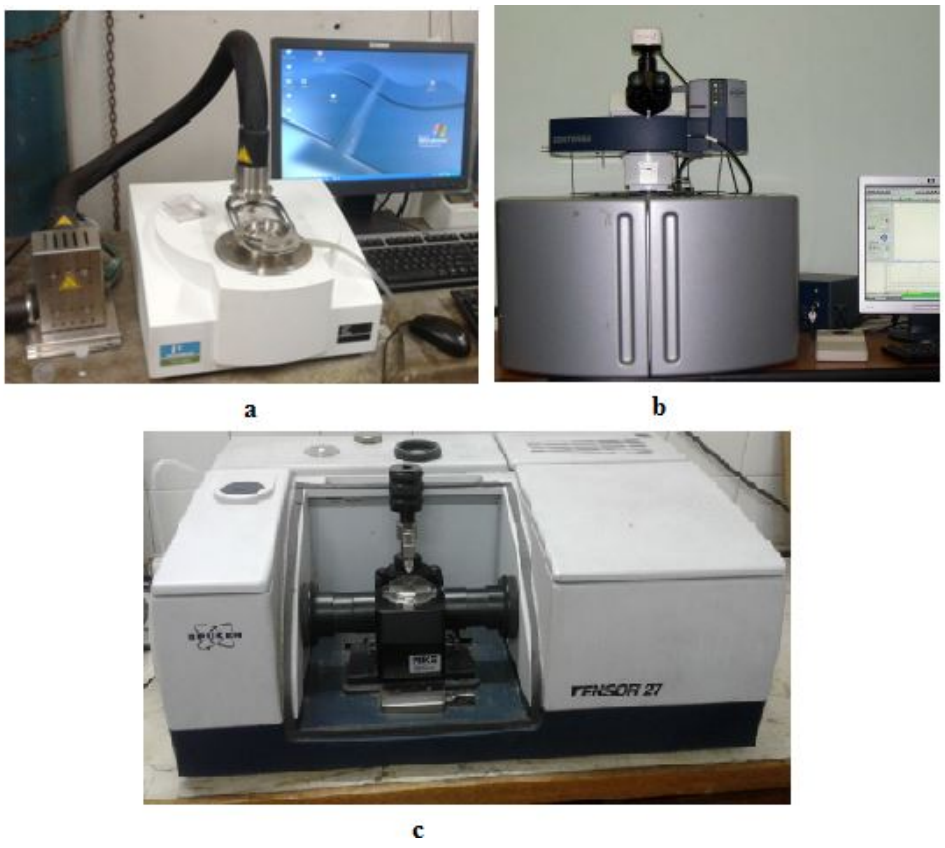

FIGURE 3.32: Microanalysis equipment: (a) Perkin-Elmer-Pyris thermo-gravimetric analyzer, (b) SENTERA Raman spectroscope, (c) TENSOR 27 Infrared spectrometer

Chapter 4

RESULTS AND DISCUSSIONS

This chapter presents the experimental results of the electrospun nanomat and CNT doped nanomat strengthened aramid-PP composites. The results are divided into three sections as listed below,

1. Effect of aramid fibre volume fraction on the mechanical properties of PP matrix composites
2. Effect of PAN nanomat on the mechanical properties of the optimized aramid fibre volume fraction of PP composite.
3. Effect of both the pristine and functionalized CNT doped PAN nanomat on the mechanical properties of aramid-PP composites

4.1 Aramid fibre Composites

The aramind reinforced polypropylene (aramid-PP) composites were fabricated with different fibre volume fractions i.e 25%, 30% and 35%. The reason for selecting these three fibre volume fractions were mainly based on the previous studies [107], [109], [110].

4.1.1 Tensile Strength and Elastic modulus

The tensile properties of the aramid fibre reinforced polypropylene composites are shown in Figure 4.1 and 4.2. It can be seen that addition of aramid fibre to the PP matrix increased the mechanical properties of the composites. The tensile strength of PP increased from 37.5 MPa to 360 MPa with the addition of 25% aramid fibre volume fraction. As the volume fraction increased, so did the tensile strength until 30% volume

fraction, which produced the highest tensile strength of 480 MPa. The increase in tensile properties could be attributed to the good matrix penetration through the fibre which resulted in good bonding between the matrix and the fibre. This led to improvement of load transfer between the matrix and aramid fibre. Beyond 30% volume fraction, the tensile strength started to decrease and this could be due to poor matrix penetration and poor bonding between fibre and matrix. The tensile strength decreased by 26% as the aramid volume fraction increased from 30% to 35%. The fracture behaviour of the aramid-PP composites is shown in Figure 4.3, which shows that the main failure mechanism was debonding and fibre fracture.

The elastic modulus followed a similar behaviour and increased to maximum of 6.7 GPa with the addition of 30% aramid fibre volume fraction. As explained before, the reason for the increase could be attributed to good fibre-matrix bonding which improved the load transfer from the matrix to the aramid fibre.

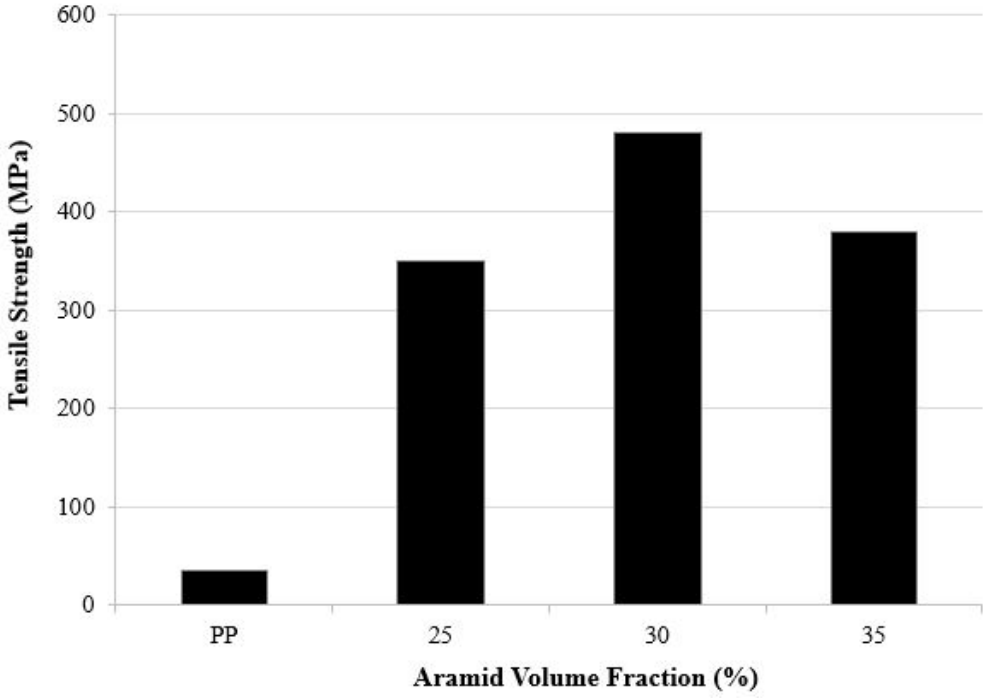

FIGURE 4.1: Tensile properties of aramid-PP composites.

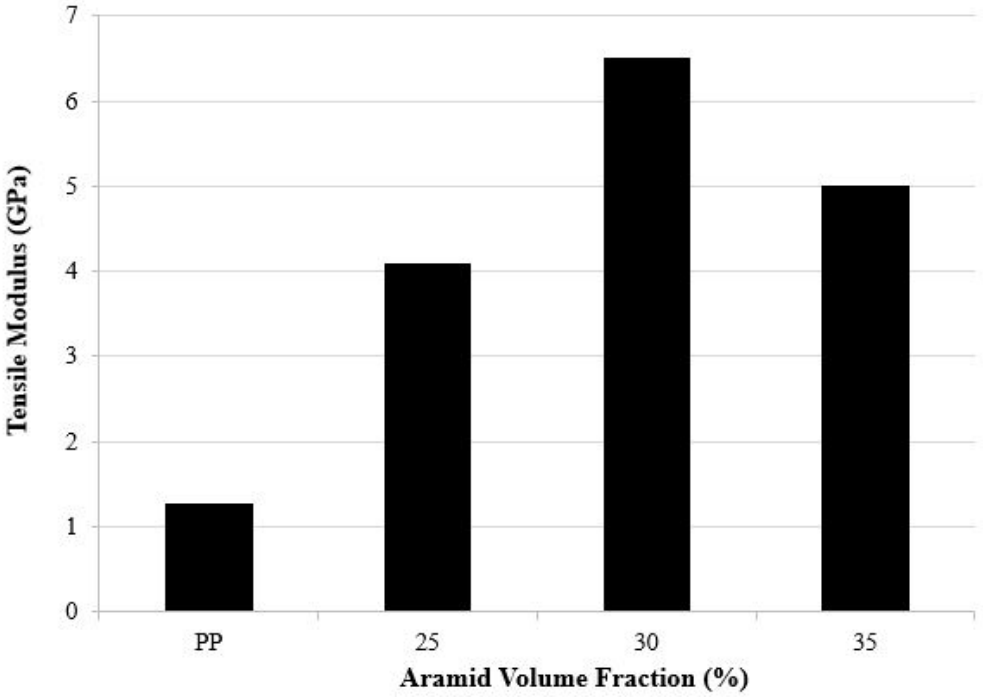

FIGURE 4.2: Tensile modulus of aramid-PP composites.

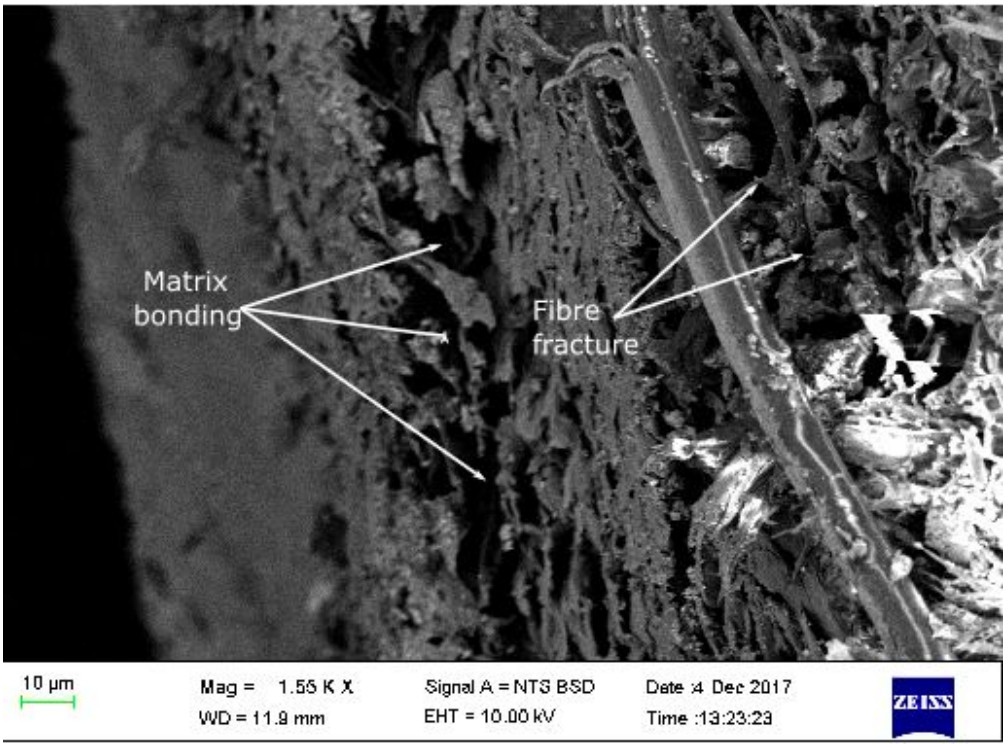

FIGURE 4.3: : SEM image of fractured surface of 30% vol. aramid-PP composites.

4.1.2 Flexural Strength and Modulus

The flexural properties of the aramid fibre composites are presented in Figure 4.4 and 4.5. The flexural strength of PP increased from 40 MPa to 80 MPa while the flexural modulus increased from 1.5 GPa to 2.8 GPa with the addition of 25% volume fraction of aramid fibre. Furthermore, the addition of the 30% fibre volume fraction produced the highest flexural strength (88 MPa) and modulus (4.2 GPa), which is approximately 10% and 50% increase in strength and modulus when compared to the 25% volume fraction. This increase could be attributed to good adhesion between the matrix and fibre. However, addition of fibre volume fraction beyond 30% resulted in the decrease of both flexural strength and modulus by 17% and 26% respectively. This could be attributed to the poor fibre-matrix interfacial adhesion leading to poor load transfer between the fibre and matrix.

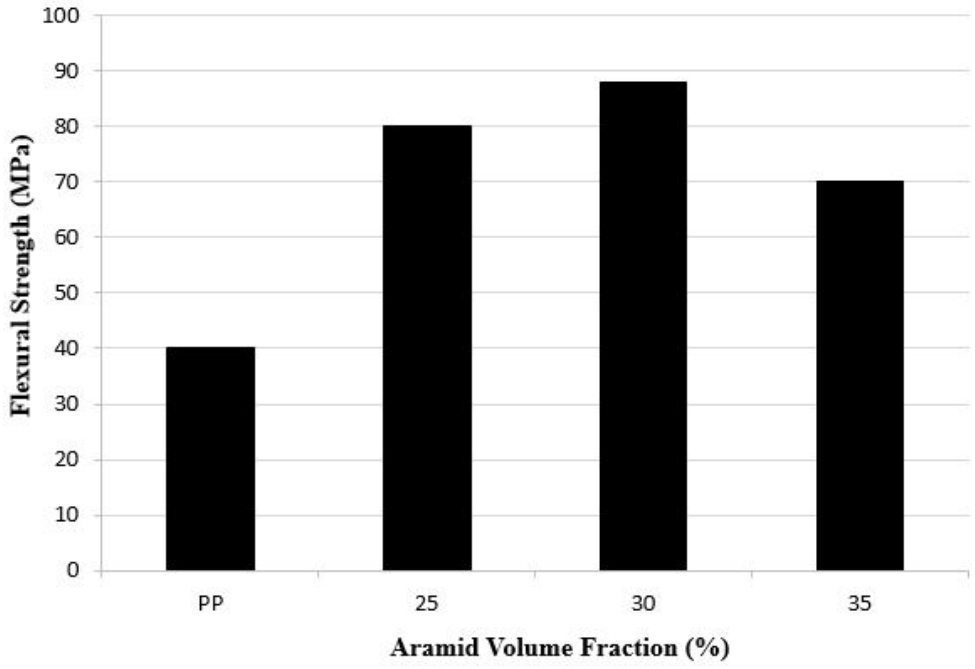

FIGURE 4.4: Flexural strength of aramid-PP composites.

The SEM image of the fractured specimen of flexural tested aramid-PP composite reinforced with 30% is shown in Figure 4.6. The fibre matrix cracking and debonding seems to be the main failure mechanism.

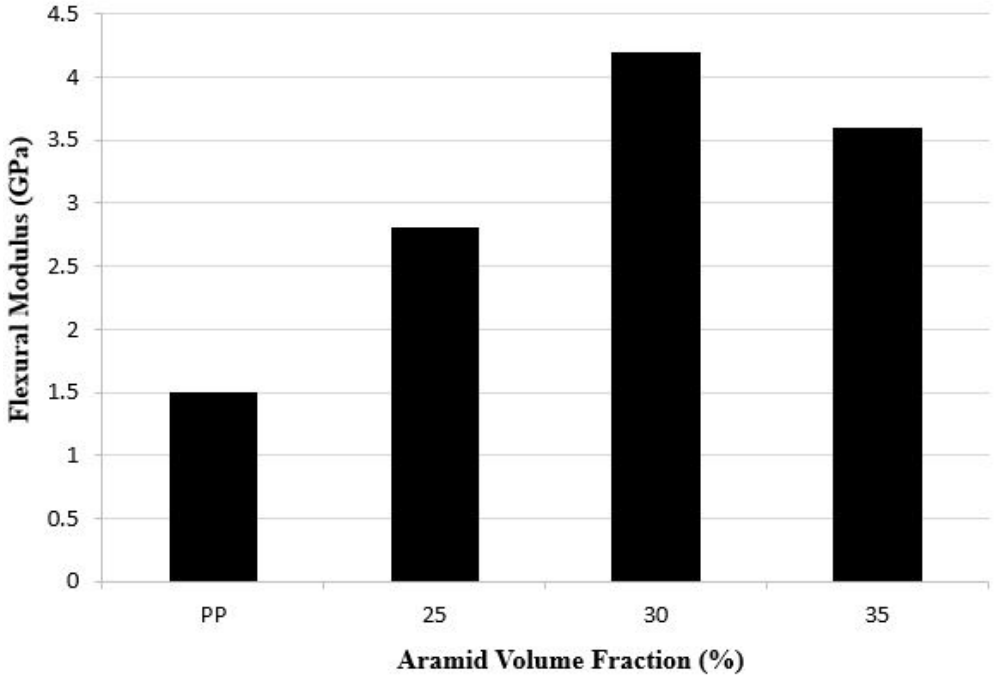

FIGURE 4.5: Flexural modulus of aramid-PP composites of varying fiber volume fractions.

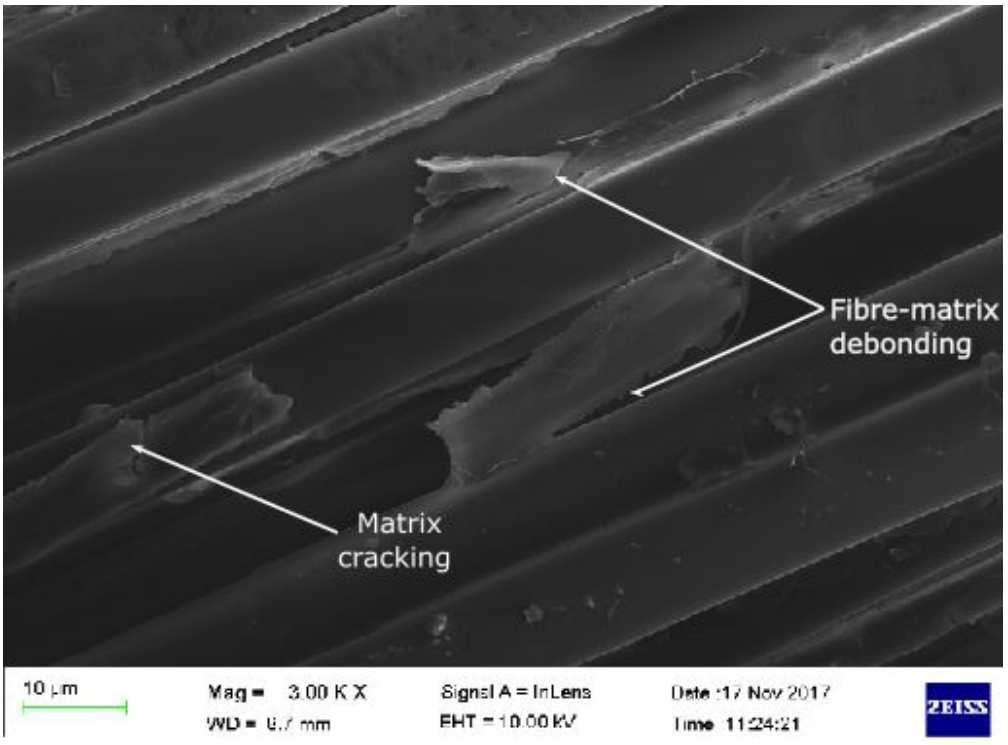

FIGURE 4.6: SEM image of fractured aramid-PP composites.

4.2 Impact Energy Absorption

The impact tests were performed to obtain the impact absorption energy properties of the aramid-PP composites and the results are shown in Figure 4.7. The addition of 25% aramid fibre volume fraction increased the impact energy of PP from 14 kJ/m^2 to 95 kJ/m^2. The 30% aramid fibre volume fraction produced the maximum impact energy absorption of 112 kJ/m^2. This was an 18% increase when compared to the 25% aramid fibre strengthened composites. The reason for this increase could be attributed to good bonding between fibre and the matrix as explained before. Further increase in fibre volume fraction to 35% led to decrease of impact energy absorption approximately to 72 kJ/m^2, which is a decrease of 56%. The decrease in impact energy absorption with the addition of fibre volume fraction beyond 30% can be attributed to insufficient bonding between fibre and the matrix.

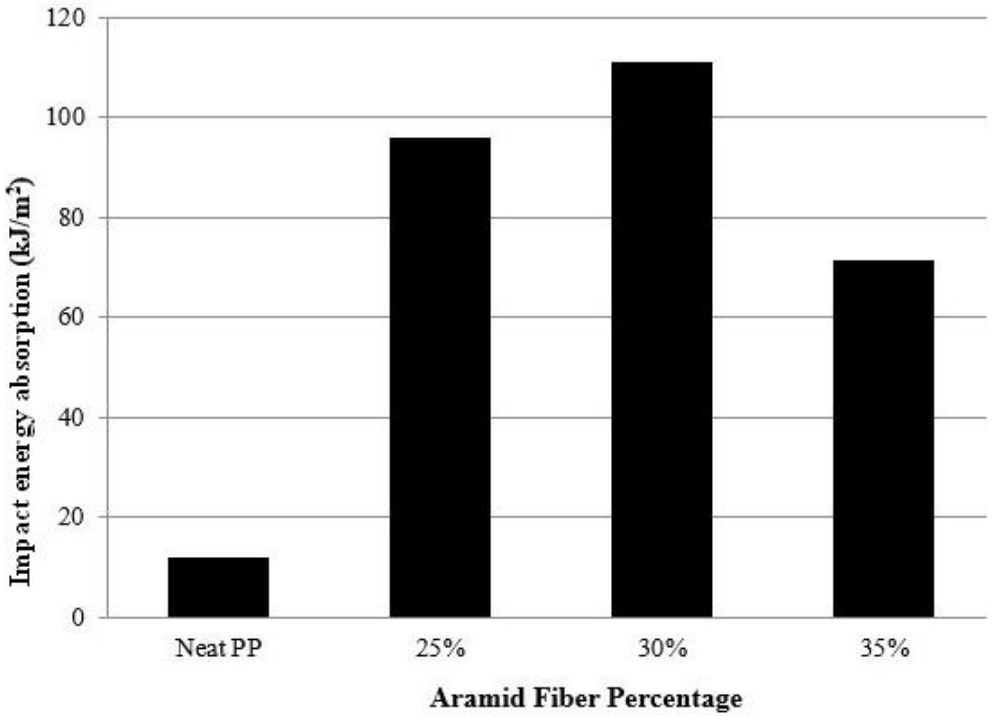

FIGURE 4.7: Impact resistance of aramid-PP hybrid composites

Figure 4.8 shows a SEM image of the impact tested fractured specimen. The main cause of failure was due to fabric/matrix debonding, which contribute to the absorption of impact energy.

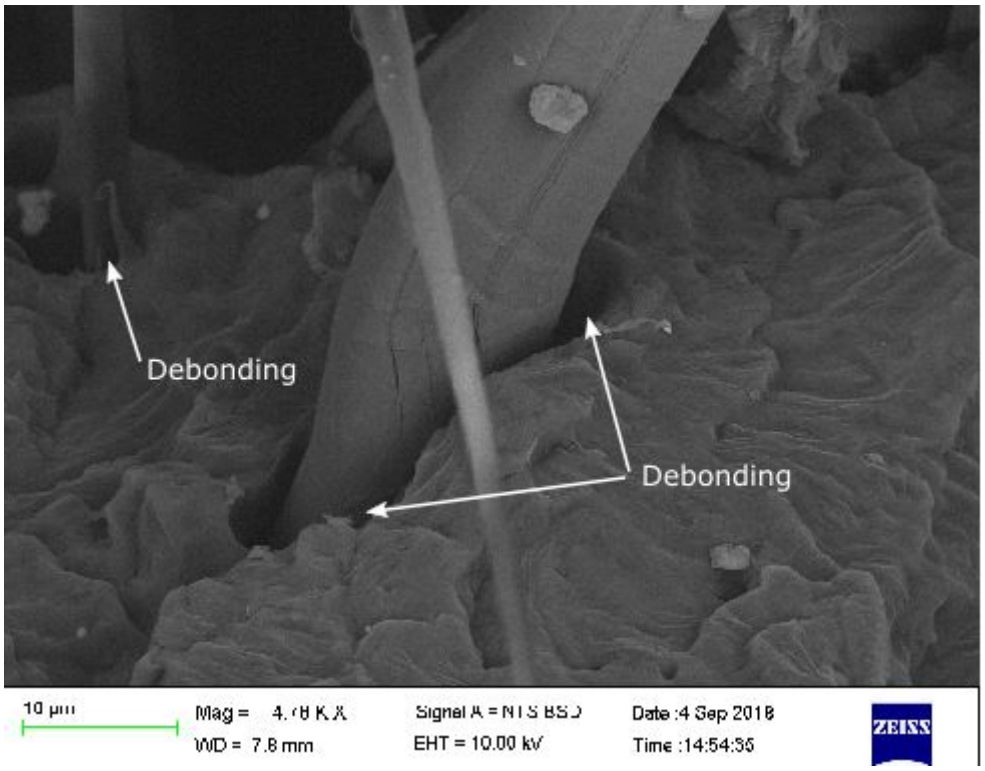

FIGURE 4.8: Fractured aramid-PP composites

4.2.1 Interlaminar Shear Strength (ILSS)

The short beam tests were performed to obtain the intalaminar properties of the aramid-PP composites and the results are presented in Figure 4.9. The ILSS of PP increased from 43 MPa to 162 MPa with the addition of 25% aramid fibre volume fraction. The addition of 30% aramid fibre volume fraction produced the highest ILSS of 183 MPa which is an increase of 13% when compared to the composites made from 25% volume fraction. The reason for this increase could be attributed to sufficient fibre bonding with the matrix which resulted in efficient load transfer. Further addition of fibre beyond 30% volume fraction, resulted in the decrease of ILSS from 183 MPa to 70 MPa. This behaviour could be due to poor interfacial adhesion between the fibre and the matrix. This led to poor load transfer which resulted in premature failure of the composites. Based on the mechanical properties of the different aramid fibre volume fractions, it was clear that the 30% volume fraction produced the best mechanical properties (tensile, flexural, impact and ILSS). Hence, it was decided that the 30% volume fraction will be used in the fabrication of hybrid composites.

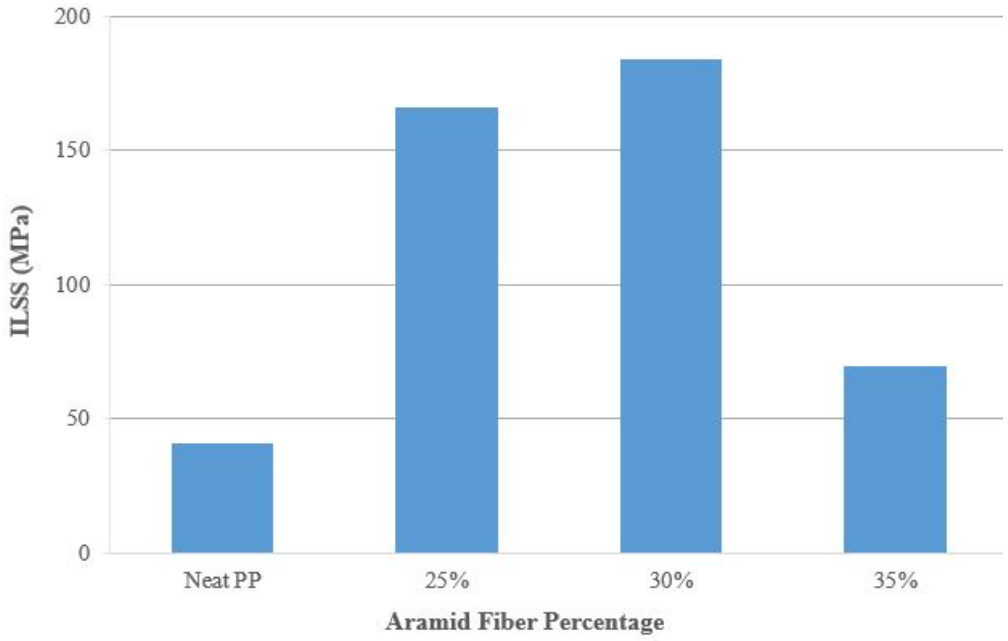

FIGURE 4.9: ILSS properties of aramid-PP composites

4.3 PAN reinforced Aramid fibre-PP composites

PAN nanomat strengthened aramid-PP hybrid composites were fabricated using the optimum fibre volume fraction of aramid with 0.1%, 0.5% and 1% PAN nanomat reinforcements. Both random and aligned PAN nanofibre strengthened aramid-PP composites were fabricated and their mechanical properties were investigated.

4.3.1 Tensile properties

The tensile properties of both aligned and randomly distributed PAN nanofibre strengthened aramid-PP composites are shown in Figure 4.10 and 4.11 respectively. As can be seen in Figure 4.10, the tensile strength gradually increased with the increase in PAN nanofibre volume fraction. The tensile strength of aramid fibre composites increased from 480 MPa to 525 MPa for the addition of 0.1% PAN nanofibre volume fraction. The increase of nanofibre volume fraction from 0.1% to 0.5% resulted in a tensile strength increase of 9%, achieving the maximum tensile strength of 570 MPa. The increase in tensile strength with the increase in PAN nanofibre volume fraction is evidence of the fact that the large surface areas and interconnected porosity of PAN nanofibres helped improve the interaction of the PP matrix with the aramid fibres. This led to the improvement of interfacial adhesion which is a requirement for efficient load transfer between the matrix and fibre.

Further increase of volume fraction beyond 0.5% resulted in a decrease in tensile strength for both aligned and randomly distributed PAN nanofibre strengthened hybrid composites. This could be due to a number of reasons. Firstly, an increase in PAN nanofibre volume fraction beyond a certain limit could result in the formation of a thick nanofibre layer, which was believed to act in a similar role like that of macro aramid fibre, resulting in poor interaction between the matrix and fibres [111]. It also could be due to formation of PAN nanofibre entanglements at high nanofibre volume fractions, which led to inefficient load transfer between the matrix and fibre by weakening the interlamaniar region.

Furthermore, an interesting observation was drawn when comparing the aligned and randomly distributed PAN nanofibre strengthened hybrid composites. Compared to the randomly distributed nanofibres, the addition of the aligned nanofibres resulted in an increase in tensile strength of 18% and 8% for PAN nanofibre volume fraction of 0.1% and 0.5% respectively. The reason for this increase could be attributed to the fact that the aligned nanofibres helped achieve higher strength and modulus as opposed to the randomly distributed nanofibres which substantially reduce the load transfer efficiency. Again, at low volume fraction, the randomly distributed nanofibres could have formed concentration sites within the hybrid composites. This is due to non uniformity formed from having areas with small amounts of nanonofibre reinforcements resulting in some large areas without nanofibre reinforcement. This results in inefficient transfer of stress between the PAN nanofibre, matrix and aramid fibre leading to premature composite failure [112].

Figure 4.11 shows the elastic modulus of PAN nanofibre reinforced hybrid composites. The addition of 0.1% volume fraction of randomly distributed PAN nanofibres resulted in a slight decrease of elastic modulus of both aligned and randomly distributed nanofibre strengthened hybrid composites. The elastic modulus of aramid-PP composites slightly decreased from 6.9 GPa to 6.7 GPa and 6.8 GPa with the addition of 0.1% volume fraction of PAN nanomat for randomly distributed and aligned nanofibres respectively. This can be attributed to uneven nanofibre distribution at very low nanomat volume fractions as some moicrofibre areas might not be coated with nanofimat. This could the result in premature failure. Thereafter, the elastic modulus increased with the increase in volume fraction for both aligned and randomly distributed nanofibres. The addition of 0.5% PAN nanofibres increased the elastic modulus to 7.1 GPa and 7.5 GPa respectively, for randomly distributed and aligned PAN nanofibres. Compared to the 30% aramid-PP composites, the elastic modulus increased by 4% and 10% for randomly distributed and aligned nanofibres respectively. As explained, the reason for increase in elastic modulus is due to the reinforcement effect of the PAN nanofibres which have large surface areas and interconnected porosity resulting in the improved interaction of

the PP matrix with the aramid fibres thereby improving the interlaminar region. This results in the improved load transfer.

Further increase of PAN nanofibre volume fraction to 1% resulted in an increase of elastic modulus while the tensile strength decreased for both randomly distributed and aligned nanofibres. The elastic modulus increased from 7.1 GPa and 7.6 GPa to 7.3 GPa and 8GPa for randomly distributed and aligned PAN nanfobres respectively. This is approximately 9% and 16% increase in comparison to aramid-PP composites which have the elastic modulus of 6.9 GPa. The reason for this phenomenon could be explained by the fact that for PAN nanofibre reinforced aramid-PP, the modulus of the PAN nanofibres ranges between 35 GPa to 55 GPa [113] which is significantly higher than that of PP matrix (ranges between 0.9 GPa to 1.2 GPa) but still less than that of aramid fibre (ranges between 80 GPa to 190 GPa). However, the extensibility of PAN nanofibres is much higher than that of aramid fibre and this allows for more elongation at break of the fibres within the composite during failure.

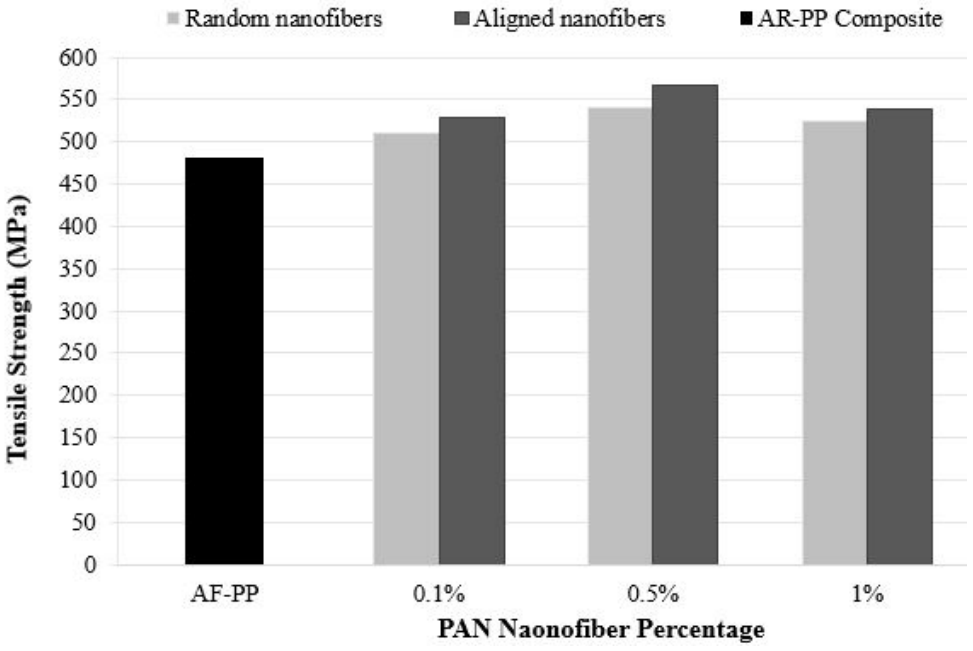

FIGURE 4.10: Tensile strength of aramid-PP hybrid composites

The SEM images of the fractured tensile samples are shown in Figure 4.12 and 4.13. The main modes of failure was both cracking and crazing of the polymer matrix as shown in Figure 4.12.

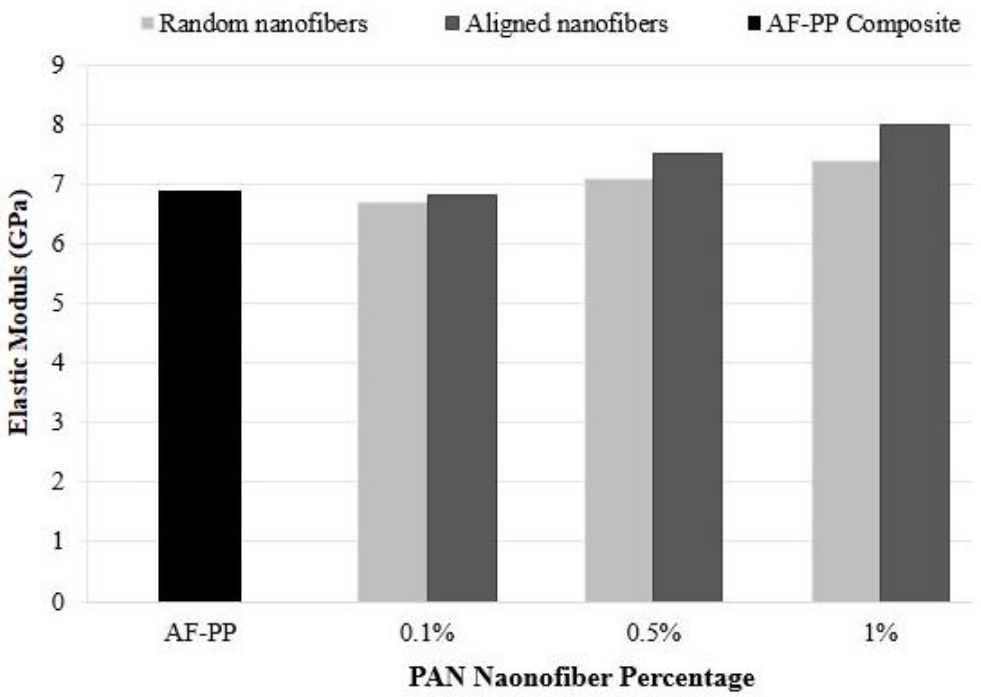

FIGURE 4.11: Elastic modulus of aramid-PP hybrid composites

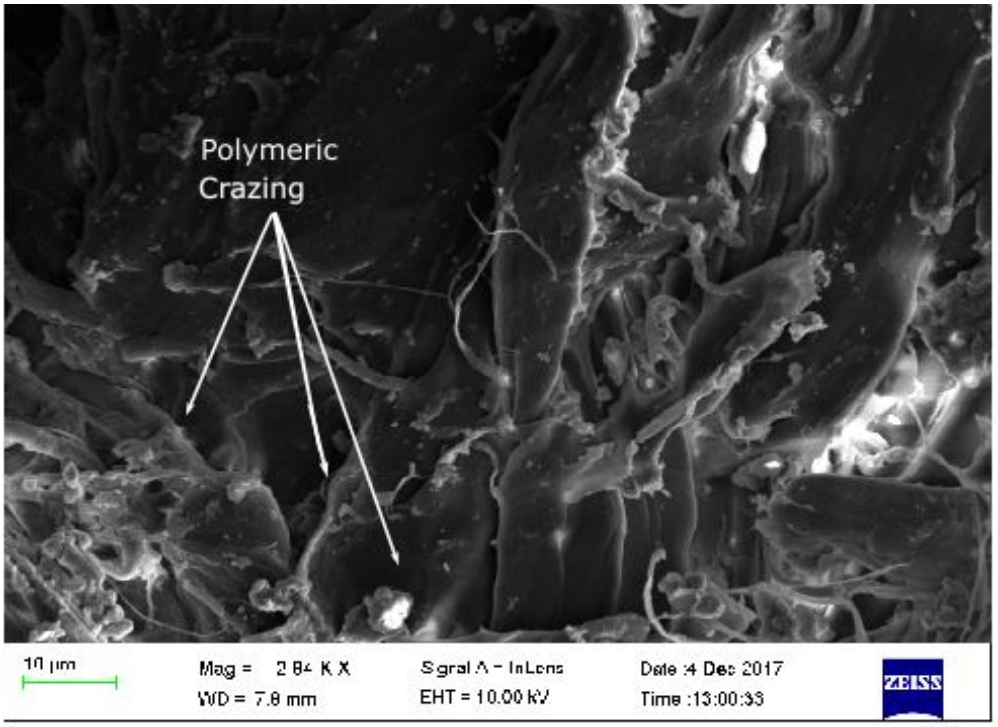

FIGURE 4.12: Fractured surface showing polymeric crazing effect under tensile stress.

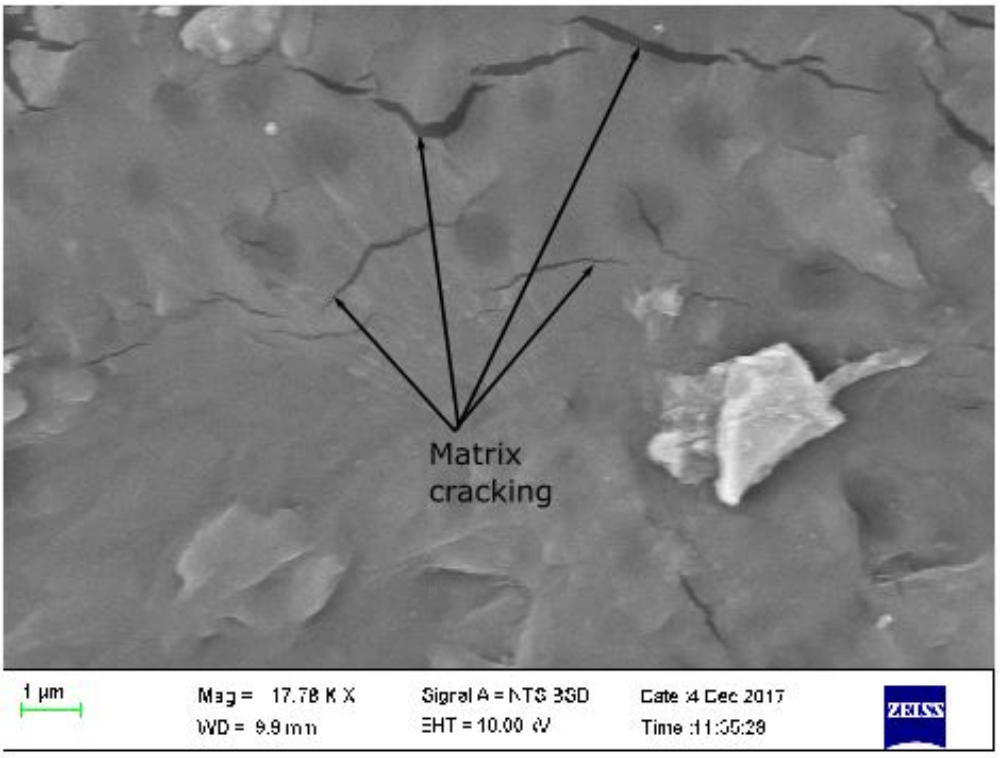

FIGURE 4.13: Fractured surface: Matrix cracking and polymeric crazing.

4.3.2 Flexural properties

Figures 4.14 and 4.15 show the flexural modulus of the randomly distributed and aligned PAN nanofibre reinforced hybrid composites. The flexural properties increased with the increase in PAN nanofibre volume fraction until the 0.5% volume fraction. The hybrid composite strengthened with 0.5% aligned PAN nanofibres produced the highest flexural strength (118 MPa) and modulus (4.9 GPa). Compared to the flexural strength (88 MPa) and modulus (3.7 GPa) of aramid-PP composites, this is a 37% and 32% increase in flexural properties. This maybe due to the reinforcement of the load transferring interlaminar region. Further increase in randomly distributed PAN nanofibre volume fraction beyond 0.5% resulted in the decrease of flexural properties. This clearly shows that the addition of PAN nanofibres beyond a certain limit has the opposite effect. This could be attributed to PAN nanofibres entangling at high volume fractions resulting in uneven distribution within the composites which could then lead to formation of defects [114]. The similar behavior was also observed for the aligned PAN nanofibre strengthened hybrid composites. This could be due to the thick PAN nanofibre layer which could be acting in a similar role to that of the micron aramid fibre. Thus, a higher nanofibre volume fraction of both aligned and randomly distributed nanofibres has negative influence on the flexural properties of the composites.

Furthermore, it must also be noted that the hybrid composites strengthened with aligned nanofibres yielded higher flexural properties when compared to those strengthened with randomly distributed nanofibres. For example, for 0.5% PAN volume fraction, the flexural strength of aligned PAN nanofibre strengthened aramid-PP composite is 12% higher than that strengthened with randomly aligned nanofibres. This could be attributed to the efficient load transfer from the matrix to the fibres in hybrid composites strengthened with aligned nanofibres. This trend is in agreement with Arinstein et al. [115], who showed that the alignment of the nanofibres has a positive effect on the mechanical properties of individual PAN nanofibres.

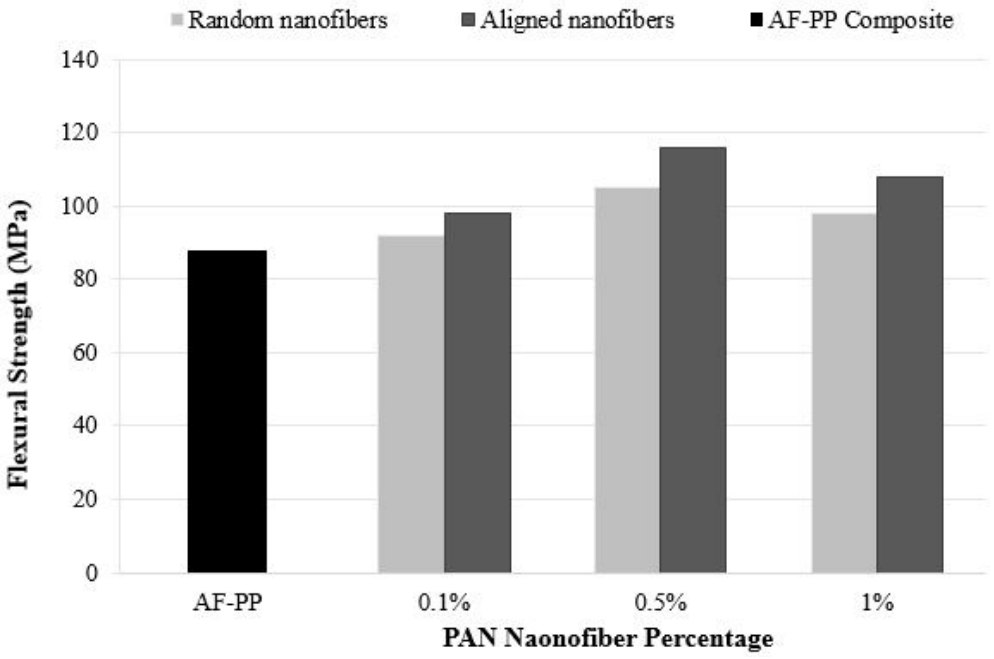

FIGURE 4.14: Flexural strength of aramid-PP hybrid composites

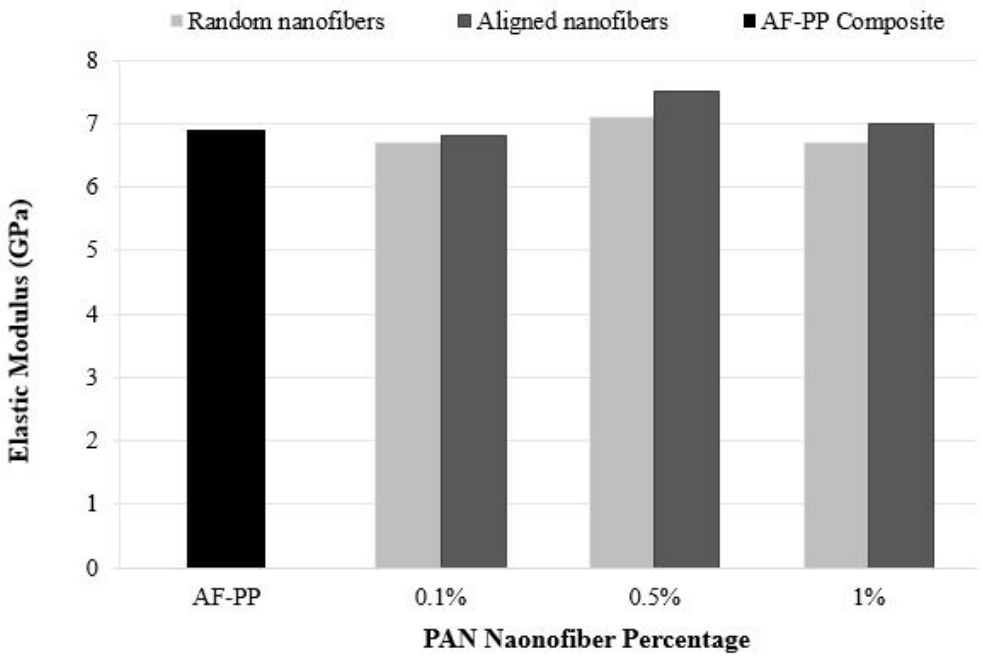

FIGURE 4.15: Fexural modulus of aramid-PP hybrid composites

4.3.3 Impact Energy Absorption

Figure 4.16 shows the impact properties of the PAN nanofibre strengthened hybrid composites. The similar behaviours to that of tensile and flexural properties were observed such as the increase in impact absorption energy with the increase in PAN nanofibre volume fraction. This could be attributed to the reinforced interlaminar region being able to absorb and transfer the maximum impact energy during loading from the matrix to the aramid fibre which has a high modulus. The 0.1% PAN nanofibre volume fraction had negligible effect on the impact energy absorption of the hybrid composites. Compared to the aramid-PP composites which has the impact energy of 110 kJ/m^2, the 0.1% nanofibre volume fraction resulted in minor impact energy absorption of 2% and 3% for both randomly distributed and aligned PAN nanofibre strengthened hybrid composites. This is due to the limited amount of nanofibres at 0.1% volume fraction, leading to a large matrix zone (weak intalaminar region) between fibres which result in poor load transfer between the matrix and fibre leading to premature composites failure.

Aligned PAN nanofibre strengthened hybrid composites had higher impact energy absorption than those strengthened with randomly distributed nanofibres. For example, at 0.5% volume fraction, the impact absorption energy of the hybrid composites strengthened with aligned nanofibres is 136 kJ/m^2 which is approximately 9% higher than that strengthened with randomly distributed nanofibres. The explanation for this is that the

alignment of nanofibres is very important to achieve high strength and modulus. Misaligned nanofibres reduce the nanofibre efficiency resulting in lower mechanical properties. The aramid-PP composites strengthened with the 0.5% aligned PAN nanofibres produced the highest impact energy absorption of 136 kJ/m^2.

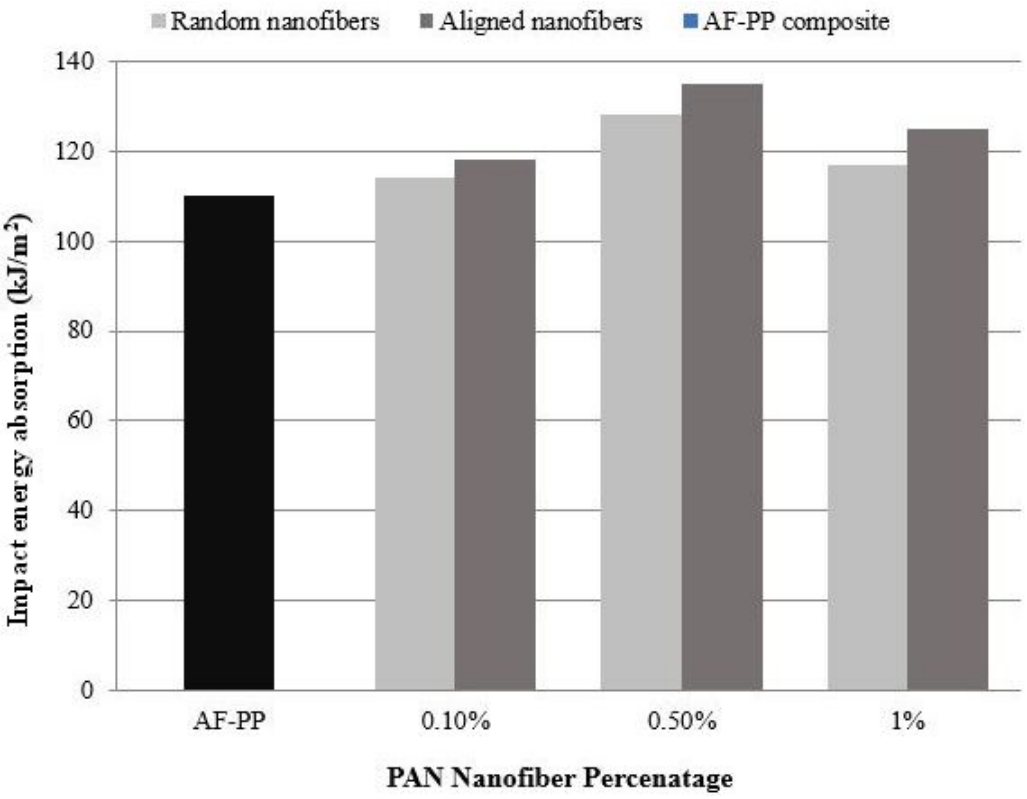

FIGURE 4.16: Impact energy absorption of aramid-PP hybrid composites

4.3.4 ILSS

The ILSS describes the resistance of the composites against interlaminar shear failure, which generally indicates free delamination in angle-ply polymer composites. Figure 4.17 shows the interlaminar shear strength results of the PAN strengthened hybrid composites. Clearly, the ILSS increased with the increase in PAN nanofibre volume fraction up to 0.5%. The ILSS of the randomly distributed PAN nanofibre strengthened hybrid composite increased by 6% and 13%, with the addition of PAN nanofibre volume fractions of 0.1% and 0.5% respectively, when compared with the aramid-PP composites. A similar behaviour was also observed for the aligned nanofibres. This increase in ILSS with an increase in nanofibre volume fraction can be attributed to the improvement of the interlaminar region as a result of adding the PAN nanofibres which act as secondary reinforcement. This result in an improved load transfer between the matrix and fibre.

Further increase in PAN volume fraction beyond 0,5% resulted in a decrease in ILSS. This could be attributed to inefficient load transfer between the nanofibre and the matrix at high PAN volume fraction. The nanofibres might be entangling (Figure 4.18) at high volume fractions which could result in uneven distribution in composites. It was also noticed that aligned nanofibre reinforced hybrid composites produced higher ILSS when compared to randomly distributed nanofibre strengthened hybrid composites. This could be attributed to efficient load transfer between the matrix and aligned PAN nanofibres.

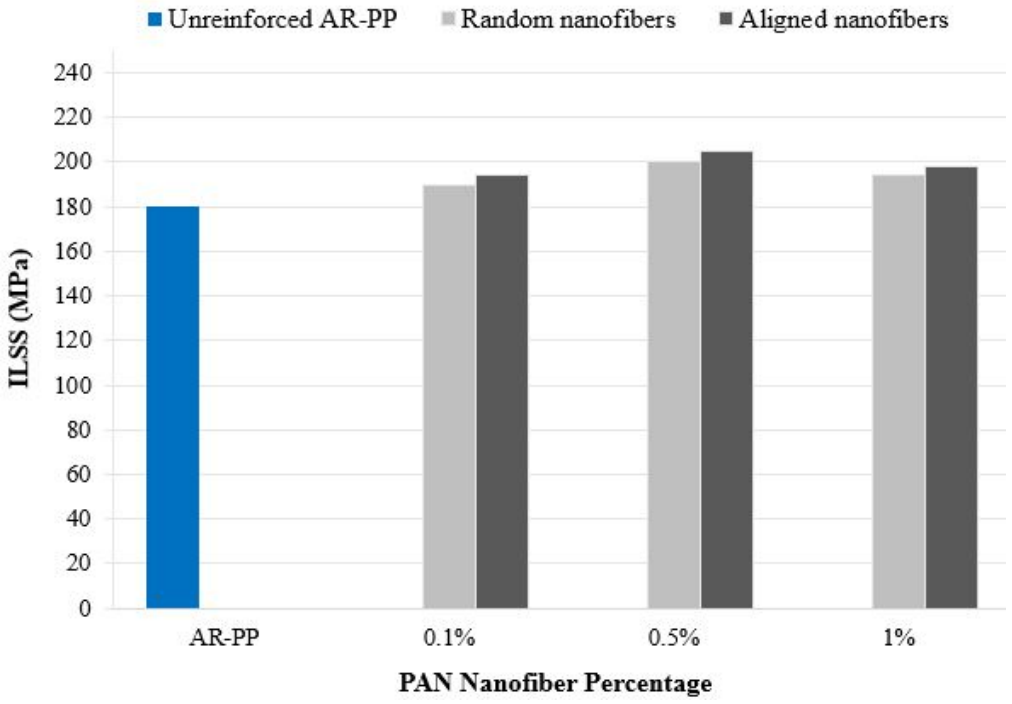

FIGURE 4.17: ILSS properties on aramid-PP hybrid composite

The tensile, flexural, impact and ILSS test results of the 30% aramid fibre reinforced with 0.5% aligned PAN nanofibres composites achieved optimum properties.

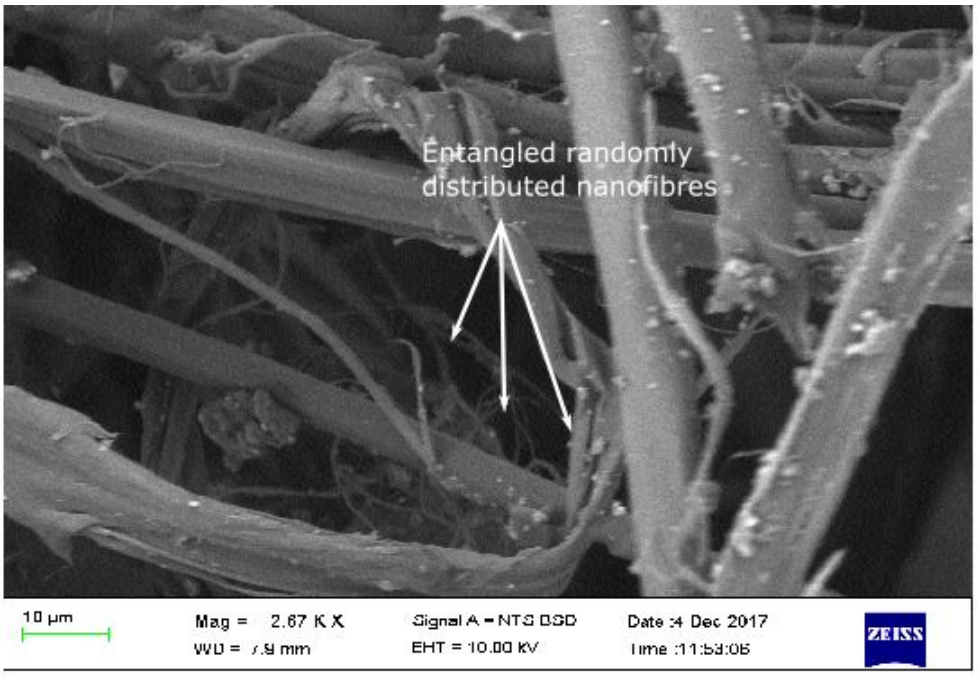

FIGURE 4.18: Fractured surface: 0.5% randomly dispersed PAN nanomat strengthened hybrid composite ILSS sample

4.4 CNT doped PAN Nanomat Reinforced Aramid-PP Composites

CNT doped PAN nanomat strengthened hybrid composites were fabricated using 30% aramid fibre and 0.5% PAN nanomat doped with 0.1%, 0.25% and 0.5% SWCNTs respectively. Both functionalized and non functionalized SWCNT's were used for doping with PAN nanofibre and the hybrid composites were investigated further.

4.4.1 Tensile Properties

Figure 4.19 shows the tensile strength of the SWCNT doped PAN nanomat strengthened hybrid composites. There is very small change in tensile strength for both the pristine and functinalized SWCNT doped PAN nanofibre hybrid composites for 0.1 $wt\%$ SWCNTs. This suggests that the quantity of CNTs incorporated into the matrix at 0.1% weight fraction is inadequate to improve the strength of the material as the load is predominantly still carried by the matrix. Thereafter, the tensile strength increased significantly with the increase in CNT weight fractions for both pristine and functinalized CNTs. The addition of 0.25 $wt\%$ of pristine and functionalized SWCNT doped PAN nanomat at the interlaminar region increased the tensile strength to 625 MPa and 645

MPa respectively. This could be attributed to the improved interlaminar region as a result of incorporation of SWCNTs.

Furthermore, it was noted that the reinforcing effect of functionalized SWCNT doped PAN nanofibre was better than that of pristine SWCNTs. Compared to the pristine SWCNT doped PAN nanofibre strengthened hybrid composites, the tensile strength of functionalized SWCNT doped PAN nanofibre strengthened hybrid composites increased by 4% and 5% with the addition of 0.1 $wt\%$ and 0.25 $wt\%$ of SWCNTs respectively. The reason for this could be attributed to the improved dispersion of the CNTs in the polymer solution (PAN) and enhanced interfacial bonding between the CNT doped PAN nanofibres and the PP matrix which was achieved through the functionalization of SWCNTs.

It was also noted that the addition of 0.5% weight fraction of pristine SWCNTs, resulted in a substantial decrease in tensile strength to 590 MPa, which is still higher that that of aramid-PP composite without nanofibres (470 MPa). This phenomenon could be attributed to SWCNTs agglomerating inside the PAN nanofibres leading to the formation of defects in the hybrid composites. The 0.5% weight fraction of functionalized SWCNTs produced the highest tensile strength (675 MPa) which is approximately 13% higher than the pristine SWCNTs strengthened hybrid composites. This clearly shows the importance of functionalization in enhancing the SWCNTs dispersion and their interaction with the matrix. Figure 4.20 shows the SEM image of the tensile test specimen of the 0.5% functionalized SWCNT doped PAN nanofibre hybrid composite after fracture. A closer look of the image shows the crack propagation. The hybrid composites strength is seen by its ability to control the crack initiation and propagation in the interlaminar region. A weak interlaminar region allows for quick crack propagation once a micro crack has been initiated. The strengthening of the interlaminar region with SWCNTs helps resist the initiated crack from propagating thus improve the properties of the composites. If the crack overcomes this resistance, it propagates until the composite fails either by fibre pull out or fracture.

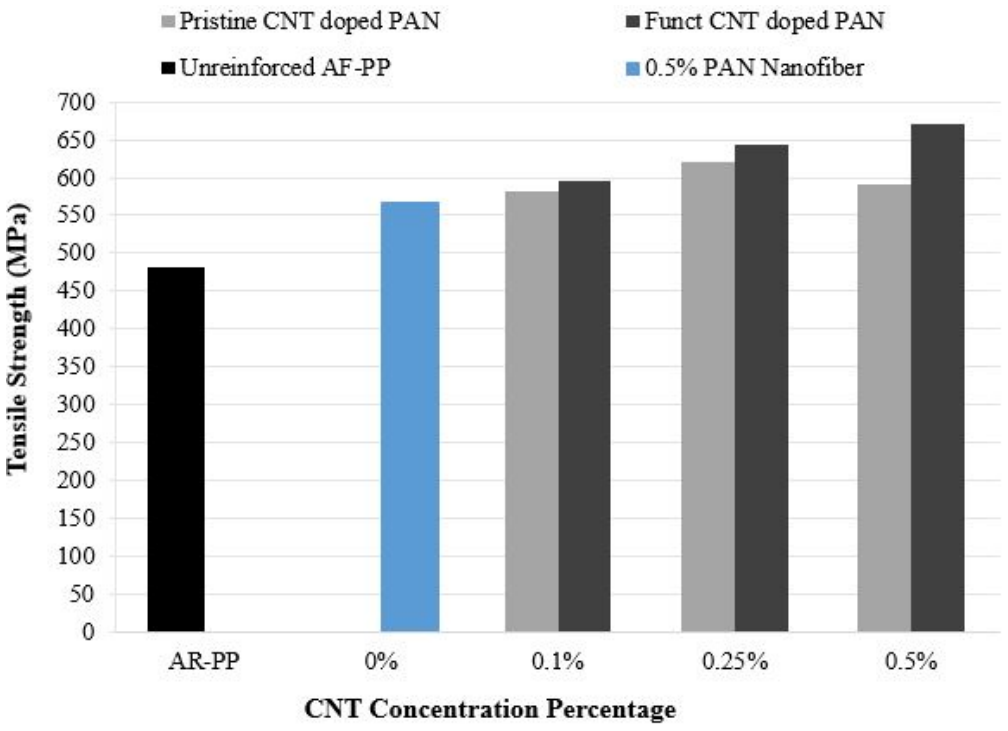

FIGURE 4.19: Tensile strength of CNT doped PAN nanomat strengthened aramid-PP hybrid composites.

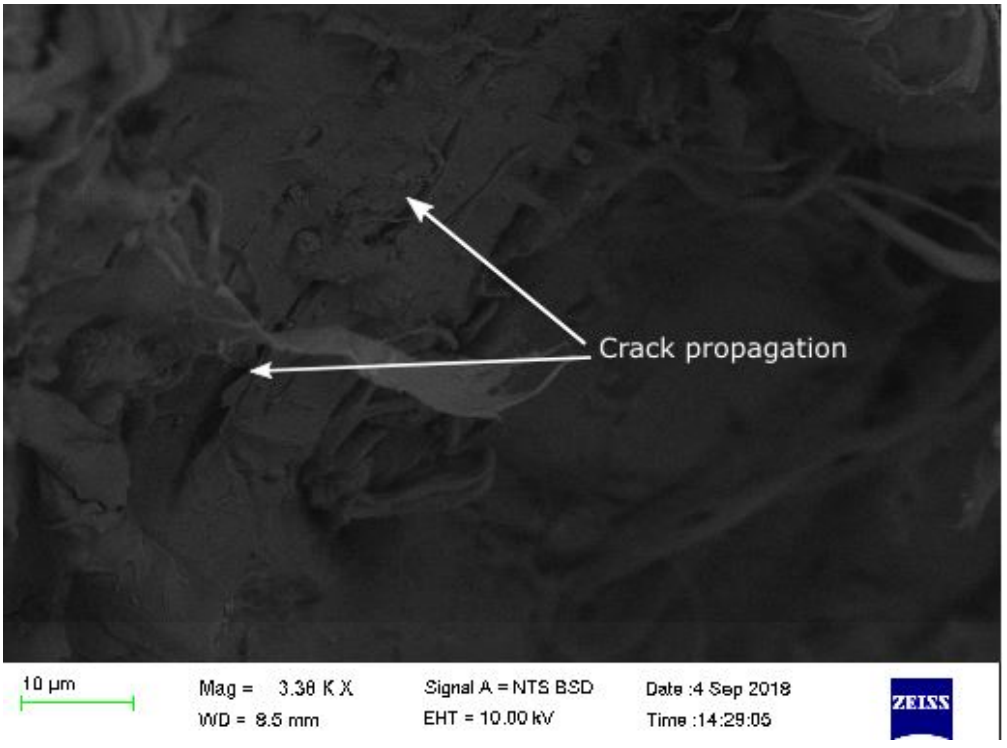

FIGURE 4.20: SEM image of the the 0.5% fucntionalized CNT doped PAN nanofibre strengthened hybrid composite

4.4.2 Flexural properties

Figure 4.21 shows the flexural strength of the CNT doped PAN nanofibre reinforced aramid-PP composites. There is a slight increase in flexural strength when the hybrid composite is strengthened with 0.1% weight fraction of both pristine and functionalized SWCNTs. Thereafter, the increase of SWCNTs weight fraction to 0.25% led to substantial increase of flexural strength to 160 MPa and 176 MPa for pristine and functionalized SWCNTs respectively. The 0.5% weight fraction of functionalized SWCNTs produced the highest flexural strength of 185 MPa. This could be attributed to high strength of CNTs as a secondary reinforcement and the improvement of interfacial adhesion between the matrix and fibres enhanced by SWCNTs.

Furthermore, it is apparent that the flexural strength of functionalized SWCNT doped PAN nanofibre aramid-PP composites are higher than those strengthened with pristine SWCNTs. For example, the flexural strength of functionalized SWCNT strengthened hybrid composite is approximately 11% higher than that of pristine SWCNTs strengthened composites. This can be attributed to the functionalization of SWCNTs which could have led to better fibre-matrix interaction leading to improved interfacial adhesion between the fibres and matrix. Muthu et al. [116] showed that the improved interfacial load transfer could be obtained by the uniform distribution of the functionalized carbon nanotubes within the matrix and the formation of matrix coating around the nanotubes.

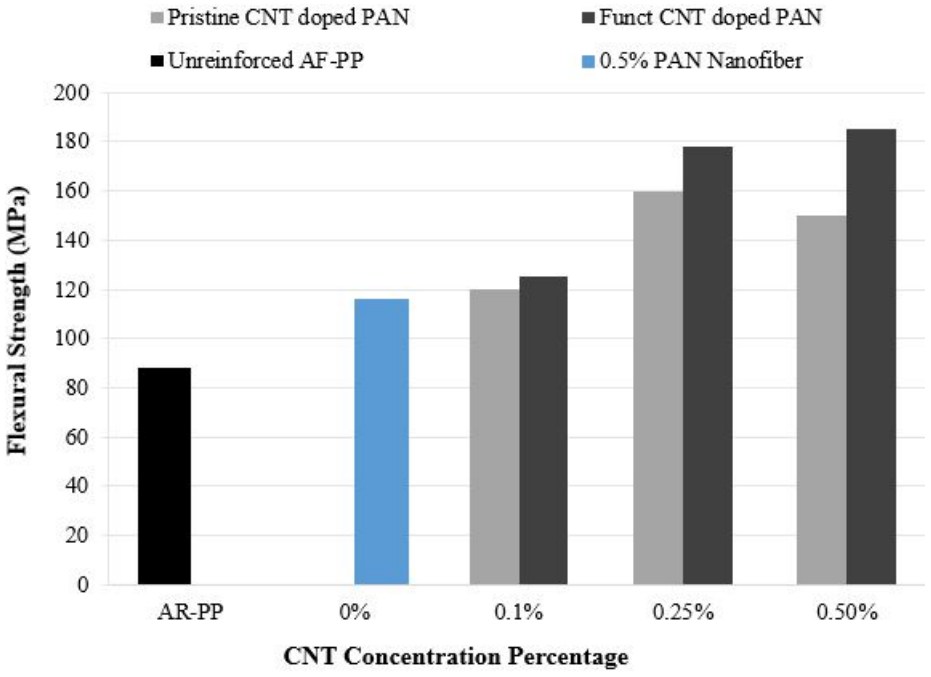

FIGURE 4.21: Flexural strength of CNT doped PAN nanomat strengthened aramid-PP hybrid composites.

4.4.3 Impact energy absorption

Figure 4.22 shows the impact strength of the SWCNT doped PAN nanofibre strengthened hybrid composites. It increased with the increase in the SWCNTs weight fraction. The impact energy absorption of the functionalized SWCNT doped PAN nanofibre hybrid increased to 147 MPa, 171 MPa and 183 MPa for SWCNTs weight fractions of 0.1%, 0.25% and 0.5% weight fractions respectively. The increase in impact energy absorption could be attributed to the presence of SWCNTs which have exceptional mechanical properties and their reinforcing effect contributing to the impact strength of the SWCNT doped PAN nanofibre strengthened AR-PP hybrid composite.

Furthermore, the functionalization of SWCNTs adds active functional groups on its surface which contributes to enhanced interaction with the matrix which improves interfacial compatibility. This improvement allows for elastic deformation of the hybrid composite under an impact loading. The impact energy is absorbed by this deformation leading to toughening of the composites, thus increasing the impact resistance. However, the impact energy absorption of 0.5% pristine SWCNTs strengthened hybrid composites decreased by 6%. As discussed before, this phenomenon could be attributed to both poor dispersion of pristine SWCNTs in the polymer solution (PAN) which resulted in the formation of agglomerates of SWCNTs inside PAN nanofibres at high weight fraction. This may lead to a decrease in mechanical properties as the agglomerates act as defects which contribute to premature composite failure.

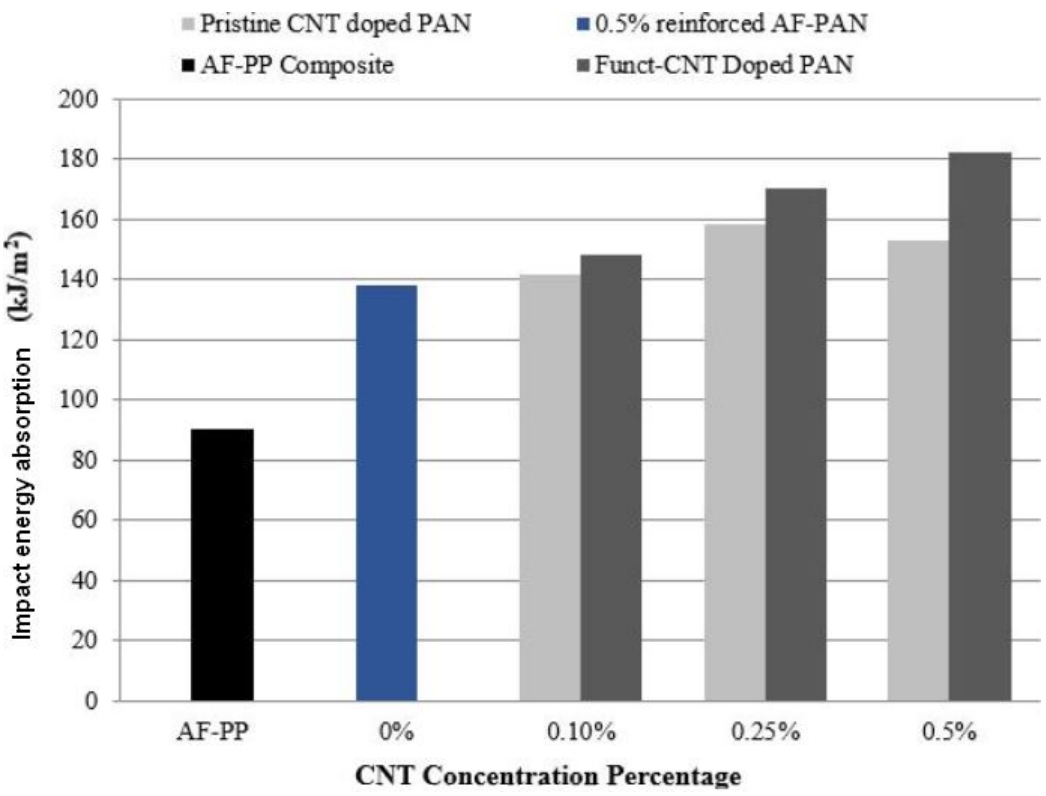

FIGURE 4.22: Impact energy absorption of SWCNT doped PAN nanomat strengthened aramid-PP hybrid composites.

4.4.4 ILSS

Figure 4.23 shows the intrelamninar strength properties of the SWCNT doped PAN strengthened nanofibre aramid fibre hybrid composites. The ILSS gradually increased with the increase in weight fraction of the pristine and functionalized SWCNTs. The initial increase in ILSS when SWCNTs were added to PAN reinforced AR-PP hybrid composite was negligible as seen by addition of 0.1% pristine and functionalized SWCNTs weight fraction. This was clear evidence that the low weight fraction (0.1%) of SWCNTs incorporated into the matrix is inadequate to improve the strength of the material. Upon addition of 0.25% SWCNT weight fraction, the ILSS increased to 221 MPa and 228 MPa for pristine and functionalized CNTs respectively which is an increase of 8% and 11% when compared to the PAN strengthened hybrid composites which have ILSS of 205 MPa. As explained before, this increase in ILSS is due to the addition of SWCNTs which improves the intelaminar region [116]. The improved interfacial adhesion results in the increase in energy absorption during crack propagation which leads to the significant improvement in the ILSS. The presence of CNTs in the interfacial region also plays a significant role in controlling the shrinkage in the polymer composites and this prevents the delamination at the interfacial region.

By comparison, the hybrid composites reinforced with functionalized SWCNTs showed visibly higher ILSS than those reinforced with pristine SWCNTs. This suggest the success of functionalization of SWCNTs as they interact better with the matrix and thus enhancing the load transfer from the matrix to the fibre.

The addition of 0.5% weight fraction of functionalized SWCNTs resulted in an appreciable increase of ILSS to 280 MPa. This could be attributed to the fact that at high weight fractions, the functionalized SWCNTs form a continuous layer around the aramid fibre which increases the interfacial surface due to high aspect ratio of the CNTs. However, the addition of 0.5% pristine SWCNTs weight fraction led to a decrease of ILSS to 215 MPa, which is still much higher that both the PAN nanofibre reinforced hybrid composite and the aramid-PP composite without nanofibres. As explained before, this may be due to unfunctionalized SWCNTs agglomeration and voids which act as defects.

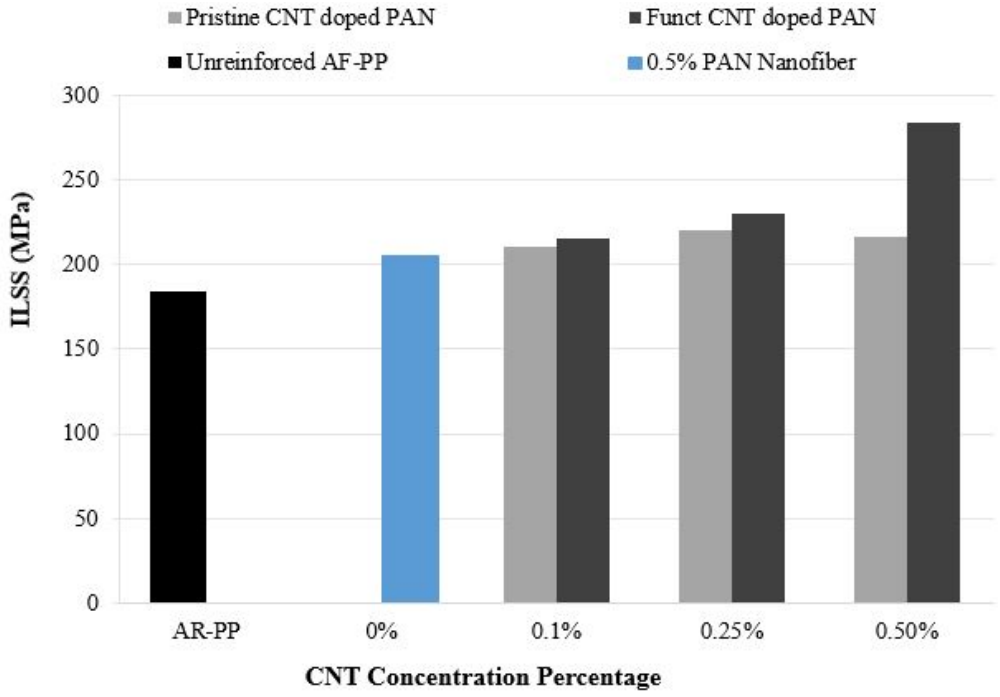

FIGURE 4.23: ILSS properties of CNT doped PAN nanomat strengthened aramid-PP hybrid composites.

Figure 4.24a and b) show the SEM image of the fracture surfaces of the short beam test specimens of the aramid fibre composite (30% volume of aramid fibre) and aramid hybrid composite containing 0.5% of CNT doped PAN nanofibres. Figure 4.24a) shows the clean, debonded fibres with very little polypropylene matrix on the fibre surfaces. The main failure is due to poor adhesion between fibre and matrix which is associated with poor resistance to crack propagation. In contrast, the SEM micrograph of the functionalized SWCNT doped PAN nanofibre strengthened hybrid composite fracture surface (4.24b) shows fibres with a lot of PP matrix when compared to the aramid

fibre composite. This indicates that the incorporation of functinalized SWCNTs helped improved the interalaminar region by improving the adhesion of the fibre and matrix.

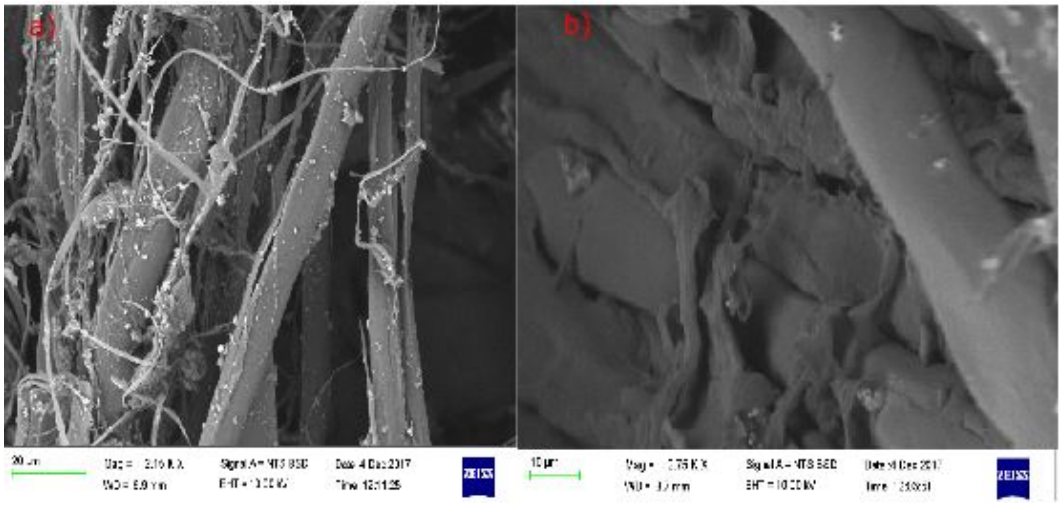

FIGURE 4.24: SEM images of the fractured surfaces of the a) short beam tests specimens of the aramid fibre composite and b) functionalized SWCNT doped PAN nanofibre reinforced aramid-PP composite.

Finally, it must be noted that only a maximum of 0.5% CNT weight fraction could be dissolved in the PAN/DMF solution. Beyond this concentration the solution became extremely viscous, making it difficult to electrospin. Thus, it is very difficult to predict what could have happened if the CNT concentration of over 0.5% was used. However, Dhakate et al.[111] found that the ILSS decreased continuously when strengthened with CNT doped PAN nanofibres above 1.1 $wt\%$.

Chapter 5

Conclusion

The research focused on improving the mechanical properties of hybrid multiscale composites using the secondary reinforcements. The mechanical properties of at least some of the derived composites have fallen short of predicted values and only marginal interlaminar property improvements have been achieved due to poor dispersion of the CNTs into the polymer matrix, improper alignment of CNTs, weak interfacial bond between nano-particle reinforcement and the matrix. The dispersion and alignment issue was addressed by optimization and modification of the electrospinning equipment. The interfacial adhesion of the nanoparticles was enhanced through functionalization of CNTs.

The results of the mechanical tests and microscopic examinations discussed in the preceding chapters, allow the following conclusions to be drawn:

1. Smooth aligned electrospun nanofibres were produced using the electrospinning equipment modified by introducing two electrodes.

2. The coupling of calendering and compression molding manufacturing techniques led to the fabrication of good quality composites without voids

3. The strengthening of aramid-PP composites with aligned PAN nanofibres resulted in a significant improvement in mechanical properties. Compared with randomly distributed PAN nanofibres, the optimum volume fraction (0.5%) of aligned PAN nanofibre reinforced aramid-PP composites improved the tensile strength by 17%, flexural strength by 18%, impact energy absorption by 21% and ILSS by 14% respectively.

4. Doping of electrospun PAN nanofibers with SWCNTs significantly increased the mechanical properties (tensile, flexural, impact and interlaminar shear strength)

of the AR-PP composites. The results showed that the mechanical properties increased with the increase in SWCNT weight fraction. The optimal concentration could not be determined as the CNT/PAN/DMF solution became too viscous and could not be electrospun beyond the CNT concentration of 0.5%. Fibre fracture and delamination were the prevalent failure modes in fiber dominated regions. In matrix dominated regions, matrix cracking was the main failure mode. Interfacial debonding of matrix from the fiber was shown to be the dominant mechanism for shear failure of composites without CNTs.

5. Functionalization of SWCNTs improved both their dispersion in the polymer matrix and interaction with the matrix leading to improved interfacial adhesion. The strengthening of hybrid composites with 0.5 wt% of functonalized SWCNTs resulted in an increase in tensile strength, flexural strength, impact energy absorption and ILSS by 14%, 21%, 17% and 29% respectively, when compare with 0.5% of pristine SWCNTs.

The study conducted found that functionalization, good alignment and dispersion of CNTs significantly improve the mechanical properties of the multiscale hybrid composites. However more research still needs to be done to achieve even better results. The following recommendations are proposed:

1. Further research needs to be done into finding the best possible CNT/PAN/DMF which will allow for an increase in CNT weight fraction beyond 0.5%. Currently, CNT weight fraction beyond 0.5% could not be electrospun as the solution became extremely viscous.

2. Further research on the calendering manufacturing technique needs to be conducted in order to understand its impact on the mechanical properties of composites. The designed and fabricated calendaring equipment might need to be modified and made less manually intensive.

3. Further experimentation should be performed with different primary fiber reinforcements and various matrices to confirm the results found from this investigation. This could also involve the use of other manufacturing techniques.

4. Research other functionalization methods and their effect on the SWCNTs.

Bibliography

[1] M A Masuelli. Introduction of fibre-reinforced polymers- polymers and composites: Concepts, properties and processes. In *Fiber Reinforced Polymers-The Technology Applied for Concrete Repair*. Intech, 2013.

[2] M J Hinton, A S Kaddour, and P D Soden. *Failure criteria in fibre reinforced polymer composites: the world-wide failure exercise*. Elsevier, 2004.

[3] DN Saheb, Jyoti P Jog, et al. Natural fiber polymer composites: a review. *Advances in polymer technology*, 18(4):351–363, 1999.

[4] P Green. Fibre volume fraction determination of carbon-epoxy composites using an acid digestion bomb. *Journal of materials science letters*, 10(19):1162–1164, 1991.

[5] MJ John, RD Anandjiwala, and S Thomas. Lignocellulosic fiber reinforced rubber composites. *School of Chemical Sciences, Mahatma Gandhi University, Kottayam, Kerala, India*, 2009.

[6] RB Mathur, S Chatterjee, and BP Singh. Growth of carbon nanotubes on carbon fibre substrates to produce hybrid/phenolic composites with improved mechanical properties. *Composites Science and Technology*, 68(7):1608–1615, 2008.

[7] F Inam, DWY Wong, M Kuwata, and T Peijs. Multiscale hybrid micro-nanocomposites based on carbon nanotubes and carbon fibers. *Journal of Nanomaterials*, 2010:9, 2010.

[8] RH Baughman, AA Zakhidov, and WA De Heer. Carbon nanotubes–the route toward applications. *science*, 297(5582):787–792, 2002.

[9] A Aqel, KMMA El-Nour, RAA Ammar, and A Al-Warthan. Carbon nanotubes, science and technology part (i) structure, synthesis and characterisation. *Arabian Journal of Chemistry*, 5(1):1–23, 2012.

[10] LY Yeo and JR Friend. Electrospinning carbon nanotube polymer composite nanofibers. *Journal of experimental nanoscience*, 1(2):177–209, 2006.

[11] AS Aricò, Peter Bruce, B Scrosati, J-M Tarascon, and W Van Schalkwijk. Nanostructured materials for advanced energy conversion and storage devices. *Nature materials*, 4(5):366–377, 2005.

[12] BP Singh, V Choudhary, P Saini, and RB Mathur. Designing of epoxy composites reinforced with carbon nanotubes grown carbon fiber fabric for improved electromagnetic interference shielding. *Aip Advances*, 2(2):022151, 2012.

[13] L Mei, Y Li, R Wang, C Wang, Q Peng, and X He. Multiscale carbon nanotube-carbon fiber reinforcement for advanced epoxy composites with high interfacial strength. *Polymers & polymer composites*, 19(2/3):107, 2011.

[14] B-S Lee and W-R Yu. Pa6/mwnt nanocomposites fabricated using electrospun nanofibers containing mwnt. *Macromolecular research*, 18(2):162–169, 2010.

[15] Y Song, Z Sun, L Xu, and Z Shao. Preparation and characterization of highly aligned carbon nanotubes/polyacrylonitrile composite nanofibers. *Polymers*, 9(1): 1, 2017.

[16] D H Reneker, AL Yarin, H Fong, and S Koombhongse. Bending instability of electrically charged liquid jets of polymer solutions in electrospinning. *Journal of Applied physics*, 87(9):4531–4547, 2000.

[17] A L Yarin, S Koombhongse, and D H Reneker. Taylor cone and jetting from liquid droplets in electrospinning of nanofibers. *Journal of applied physics*, 90(9): 4836–4846, 2001.

[18] Z Su, J Ding, and G Wei. Electrospinning: A facile technique for fabricating polymeric nanofibers doped with carbon nanotubes and metallic nanoparticles for sensor applications. *RSC Advances*, 4(94):52598–52610, 2014.

[19] P Bradley. *Characterisation of the structural properties of ECNF embedded pan nanomat reinforced glass fiber hybrid composites*. PhD thesis, 2016.

[20] V Choudhary, BP Singh, and RB Mathur. Carbon nanotubes and their composites. In *Syntheses and applications of carbon nanotubes and their composites*. InTech, 2013.

[21] H-Y Liu, L Xu, and N Si. Effect of magnetic intensity on diameter of charged jets in electrospinning. *Thermal Science*, 18(5):1451–1454, 2014.

[22] X Ma, J Liu, C Ni, DC Martin, DB Chase, and JF Rabolt. Molecular orientation in electrospun poly (vinylidene fluoride) fibers. *ACS Macro Letters*, 1(3):428–431, 2012.

[23] O Regev, PNB ElKati, J Loos, and CE Koning. Preparation of conductive nanotube–polymer composites using latex technology. *Advanced Materials*, 16 (3):248–251, 2004.

[24] M Shim, N W Shi Kam, RJ Chen, Y Li, and H Dai. Functionalization of carbon nanotubes for biocompatibility and biomolecular recognition. *Nano Letters*, 2(4): 285–288, 2002.

[25] P-C Ma, NA Siddiqui, G Marom, and J-K Kim. Dispersion and functionalization of carbon nanotubes for polymer-based nanocomposites: a review. *Composites Part A: Applied Science and Manufacturing*, 41(10):1345–1367, 2010.

[26] M Li, Y Gu, Y Liu, Y Li, and Z Zhang. Interfacial improvement of carbon fiber/epoxy composites using a simple process for depositing commercially functionalized carbon nanotubes on the fibers. *Carbon*, 52:109–121, 2013.

[27] T Ramanathan, H Liu, and LC Brinson. Functionalized swnt/polymer nanocomposites for dramatic property improvement. *Journal of Polymer Science Part B: Polymer Physics*, 43(17):2269–2279, 2005.

[28] J Gao, ME Itkis, A Yu, E Bekyarova, B Zhao, and RC Haddon. Continuous spinning of a single-walled carbon nanotube- nylon composite fiber. *Journal of the American Chemical Society*, 127(11):3847–3854, 2005.

[29] O Asumani. *Characterization of the mechanical and moisture absorption properties of kenaf reinforced polypropylene composites*. PhD thesis, 2014.

[30] RM Rowell, RA Young, and JK Rowell. Paper and composites from agro-based resources, 1997. *Ch*, 7:257.

[31] MR Barone and DA Caulk. The effect of deformation and thermoset cure on heat conduction in a chopped-fiber reinforced polyester during compression molding. *International Journal of Heat and Mass Transfer*, 22(7):1021–1032, 1979.

[32] M Tehrani, A Yari Boroujen, C Luhrs, J Phillips, and MS Al-Haik. Hybrid composites based on carbon fiber/carbon nanofilament reinforcement. *Materials*, 7(6): 4182–4195, 2014.

[33] DM Bigg and EJ Bradbury. The impact performance of thermoplastic sheet composites. *Polymer Engineering & Science*, 32(4):287–297, 1992.

[34] NE Merter. Effects of processing parameters on the mechanical behavior of continuous glass fiber/polypropylene composites. Master's thesis, İzmir Institute of Technology, 2009.

[35] P Frontera, A Malara, S Stelitano, E Fazio, F Neri, L Scarpino, PL Antonucci, and S Santangelo. A new approach to the synthesis of titania nano-powders enriched with very high contents of carbon nanotubes by electro-spinning. *Materials Chemistry and Physics*, 153:338–345, 2015.

[36] FC Campbell Jr. *Manufacturing technology for aerospace structural materials*. Elsevier, 2011.

[37] L Sorrentino, G Simeoli, S Iannace, and P Russo. Mechanical performance optimization through interface strength gradation in pp/glass fibre reinforced composites. *Composites Part B: Engineering*, 76:201–208, 2015.

[38] DV Rosato and DV Rosato. *Reinforced plastics handbook*. Elsevier, 2004.

[39] V Cech, E Palesch, and J Lukes. The glass fiber–polymer matrix interface/interphase characterized by nanoscale imaging techniques. *Composites Science and Technology*, 83:22–26, 2013.

[40] M Jassal and S Ghosh. Aramid fibres-an overview. 2002.

[41] BD Agarwal and LJ Broutman. Analysis and performance of fiber composites. 1990.

[42] J Varga, GW Ehrenstein, and AK Schlarb. Vibration welding of alpha and beta isotactic polypropylenes: mechanical properties and structure. *Express Polym Lett*, 2(3):148–156, 2008.

[43] LF Cai, YL Mai, MZ Rong, WH Ruan, and MQ Zhang. Interfacial effects in nanosilica/polypropylene composites fabricated by in-situ chemical blowing. *eXPRESS Polym. Lett*, 1(1):2–7, 2007.

[44] S C Turmanova, SD Genieva, AS Dimitrova, and LT Vlaev. Non-isothermal degradation kinetics of filled with rise husk ash polypropene composites. *Express Polymer Letters*, 2(2):133–146, 2008.

[45] P-C Ma and Y Zhang. Perspectives of carbon nanotubes/polymer nanocomposites for wind blade materials. *Renewable and Sustainable Energy Reviews*, 30:651–660, 2014.

[46] CC Chamis and RF Lark. Hybrid composites, state-of-the-art review: Analysis, design, application and fabrication. 1977.

[47] PK Mallick. *Fiber-reinforced composites: materials, manufacturing, and design*. CRC press, 2007.

[48] WM Banks and D Semple. A review of fibre reinforced plastics applications–past, present and future. *HKIE Transactions*, 4(2-3):44–48, 1997.

[49] J Zhang, K Chaisombat, S He, and CH Wang. Hybrid composite laminates reinforced with glass/carbon woven fabrics for lightweight load bearing structures. *Materials & Design (1980-2015)*, 36:75–80, 2012.

[50] Y Li, XJ Xian, CL Choy, M Guo, and Z Zhang. Compressive and flexural behavior of ultra-high-modulus polyethylene fiber and carbon fiber hybrid composites. *Composites science and technology*, 59(1):13–18, 1999.

[51] NK Naik, R Ramasimha, H Arya, SV Prabhu, and N ShamaRao. Impact response and damage tolerance characteristics of glass–carbon/epoxy hybrid composite plates. *Composites Part B: Engineering*, 32(7):565–574, 2001.

[52] E Bekyarova, ET Thostenson, A Yu, H Kim, J Gao, J Tang, HT Hahn, T-W Chou, ME Itkis, and RC Haddon. Multiscale carbon nanotube- carbon fiber reinforcement for advanced epoxy composites. *Langmuir*, 23(7):3970–3974, 2007.

[53] ET Thostenson, WZ Li, DZ Wang, ZF Ren, and TW Chou. Carbon nanotube/-carbon fiber hybrid multiscale composites. *Journal of Applied physics*, 91(9):6034–6037, 2002.

[54] BI Yakobson and RE Smalley. Fullerene nanotubes: C 1,000,000 and beyond: Some unusual new moleculeslong, hollow fibers with tantalizing electronic and mechanical propertieshave joined diamonds and graphite in the carbon family. *American Scientist*, 85(4):324–337, 1997.

[55] K Balasubramanian and M Burghard. Chemically functionalized carbon nanotubes. *Small*, 1(2):180–192, 2005.

[56] R Andrews, D Jacques, D Qian, and T Rantell. Multiwall carbon nanotubes: synthesis and application. *Accounts of Chemical Research*, 35(12):1008–1017, 2002.

[57] JN Coleman, U Khan, WJ Blau, and YK Gunko. Small but strong: a review of the mechanical properties of carbon nanotube–polymer composites. *Carbon*, 44 (9):1624–1652, 2006.

[58] G Siqueira, J Bras, and A Dufresne. Cellulose whiskers versus microfibrils: influence of the nature of the nanoparticle and its surface functionalization on the thermal and mechanical properties of nanocomposites. *Biomacromolecules*, 10(2): 425–432, 2008.

[59] E Hammel, X Tang, M Trampert, T Schmitt, K Mauthner, A Eder, and P Pötschke. Carbon nanofibers for composite applications. *Carbon*, 42(5):1153–1158, 2004.

[60] J-P Salvetat, J-M Bonard, NH Thomson, AJ Kulik, L Forro, W Benoit, and L Zuppiroli. Mechanical properties of carbon nanotubes. *Applied Physics A*, 69 (3):255–260, 1999.

[61] CT White, J Li, D Gunlycke, and JW Mintmire. Hidden one-electron interactions in carbon nanotubes revealed in graphene nanostrips. *Nano letters*, 7(3):825–830, 2007.

[62] T Belin and F Epron. Characterization methods of carbon nanotubes: a review. *Materials Science and Engineering: B*, 119(2):105–118, 2005.

[63] VN Popov. Carbon nanotubes: properties and application. *Materials Science and Engineering: R: Reports*, 43(3):61–102, 2004.

[64] S-P Han and WA Goddard III. Coupling of raman radial breathing modes in double-wall carbon nanotubes and bundles of nanotubes. *The Journal of Physical Chemistry B*, 113(20):7199–7204, 2009.

[65] OV Kharissova and BI Kharisov. Variations of interlayer spacing in carbon nanotubes. *Rsc Advances*, 4(58):30807–30815, 2014.

[66] MR Kamal and J Uribe-Calderon. Nanoparticles and polymer nanocomposites. *Graphite, Graphene, and Their Polymer Nanocomposites*, page 353, 2012.

[67] S Shokoohi, G Naderi, and A Davoodi. Mechanical properties of nanomaterials. *Nanocomposite Materials: Synthesis, Properties and Applications*, 2016.

[68] G Cicala and C Lo Faro. Material selection: Polymeric composites matrix. *Wiley Encyclopedia of Composites*.

[69] S Mallakpour and E Khadem. Hybrid optically active polymer/metal oxide composites. *Hybrid Polymer Composite Materials: Properties and Characterisation*, page 379, 2017.

[70] OI Okoli and GF Smith. Failure modes of fibre reinforced composites: The effects of strain rate and fibre content. *Journal of Materials Science*, 33(22):5415–5422, 1998.

[71] X-F Wu, A Rahman, Z Zhou, DD Pelot, Suman S-R, Bin Chen, S Payne, and AL Yarin. Electrospinning core-shell nanofibers for interfacial toughening and self-healing of carbon-fiber/epoxy composites. *Journal of Applied Polymer Science*, 129 (3):1383–1393, 2013.

[72] F Shalchy and N Rahbar. Nanostructural characteristics and interfacial properties of polymer fibers in cement matrix. *ACS applied materials & interfaces*, 7(31): 17278–17286, 2015.

[73] MJ Yacamán, MC Hersam, TM Pollock, EJ Lavernia, and G Rijnders. A. 7. nanostructured materials and nanotechnology.

[74] LT Drzal, N Sugiura, and D Hook. The role of chemical bonding and surface topography in adhesion between carbon fibers and epoxy matrices. *Composite Interfaces*, 4(5):337–354, 1996.

[75] W-C Choi, S-J Jang, and H-D Yun. Interface bond characterization between fiber and cementitious matrix. *International Journal of Polymer Science*, 2015, 2015.

[76] M Etcheverry and SE Barbosa. Glass fiber reinforced polypropylene mechanical properties enhancement by adhesion improvement. *Materials*, 5(6):1084–1113, 2012.

[77] LA Utracki and CA Wilkie. *Polymer blends handbook*, volume 1. Springer, 2002.

[78] P Gatenholm and J Felix. Wood fiber/polymer composites: fundamental concepts, process, and material options. *Forest Product Society, Madison*, 1993.

[79] A Hirsch. Functionalization of single-walled carbon nanotubes. *Angewandte Chemie International Edition*, 41(11):1853–1859, 2002.

[80] A Hirsch and O Vostrowsky. Functionalization of carbon nanotubes. In *Functional molecular nanostructures*, pages 193–237. Springer, 2005.

[81] V Georgakilas, M Otyepka, AB Bourlinos, V Chandra, N Kim, KC Kemp, P Hobza, Radek Zboril, and Kwang S Kim. Functionalization of graphene: covalent and non-covalent approaches, derivatives and applications. *Chem. Rev*, 112 (11):6156–6214, 2012.

[82] Z Akram, A Kausar, and M Siddiq. Review on polymer/carbon nanotube composite focusing polystyrene microsphere and polystyrene microsphere/modified cnt composite: preparation, properties, and significance. *Polymer-Plastics Technology and Engineering*, 55(6):582–603, 2016.

[83] R Krajcik, A Jung, A Hirsch, W Neuhuber, and O Zolk. Functionalization of carbon nanotubes enables non-covalent binding and intracellular delivery of small interfering rna for efficient knock-down of genes. *Biochemical and biophysical research communications*, 369(2):595–602, 2008.

[84] S-Y Yang, C-CM Ma, C-C Teng, Y-W Huang, S-H Liao, Y-L Huang, H-W Tien, T-M Lee, and K-C Chiou. Effect of functionalized carbon nanotubes on the thermal conductivity of epoxy composites. *Carbon*, 48(3):592–603, 2010.

[85] RA Vaia, S Vasudevan, W Krawiec, LG Scanlon, and EP Giannelis. New polymer electrolyte nanocomposites: Melt intercalation of poly (ethylene oxide) in mica-type silicates. *Advanced Materials*, 7(2):154–156, 1995.

[86] MC Paiva, B Zhou, KAS Fernando, Y Lin, JM Kennedy, and Y-P Sun. Mechanical and morphological characterization of polymer–carbon nanocomposites from functionalized carbon nanotubes. *Carbon*, 42(14):2849–2854, 2004.

[87] K Tohji, H Takahashi, Y Shinoda, N Shimizu, B Jeyadevan, I Matsuoka, Y Saito, A Kasuya, S Ito, and Y Nishina. Purification procedure for single-walled nanotubes. *The Journal of Physical Chemistry B*, 101(11):1974–1978, 1997.

[88] S Bandow, S Asaka, Y Saito, AM Rao, L Grigorian, Eklund Richter, and PC Eklund. Effect of the growth temperature on the diameter distribution and chirality of single-wall carbon nanotubes. *Physical Review Letters*, 80(17):3779, 1998.

[89] AV Eletskii. Carbon nanotubes and their emission properties. *Physics-uspekhi*, 45 (4):369, 2002.

[90] S Ramakrishna, K Fujihara, W-E Teo, T Yong, Z Ma, and R Ramaseshan. Electrospun nanofibers: solving global issues. *Materials today*, 9(3):40–50, 2006.

[91] C-H Weng, H-C Su, C-S Yang, K-Y Shin, K-C Leou, and C-H Tsai. Direct synthesis of single-walled carbon nanotubes selectively suspended on tips of vertically aligned silicon nanostructures fabricated by hydrogen plasma etching. *Nanotechnology*, 17(22):5644, 2006.

[92] J-H Kim, J Noh, H Choi, J-Y Lee, and T-S Kim. Mechanical properties of polymer–fullerene bulk heterojunction films: Role of nanomorphology of composite films. *Chemistry of Materials*, 29(9):3954–3961, 2017.

[93] R Hensleigh. Suspension electrospinning carbon nanotube doped poly (vinyl alcohol) nanowires. 2015.

[94] DC Davis and BD Whelan. An experimental study of interlaminar shear fracture toughness of a nanotube reinforced composite. *Composites Part B: Engineering*, 42(1):105–116, 2011.

[95] ET Thostenson, Z Ren, and T-W Chou. Advances in the science and technology of carbon nanotubes and their composites: a review. *Composites science and technology*, 61(13):1899–1912, 2001.

[96] P-C Ma, M-Y Liu, H Zhang, S-Q Wang, R Wang, K Wang, Y-K Wong, B-Z Tang, S-H Hong, K-W Paik, et al. Enhanced electrical conductivity of nanocomposites containing hybrid fillers of carbon nanotubes and carbon black. *ACS applied materials & interfaces*, 1(5):1090–1096, 2009.

[97] SW Kim, T Kim, Yern S Kim, HS Choi, HJ Lim, SJ Yang, and CR Park. Surface modifications for the effective dispersion of carbon nanotubes in solvents and polymers. *Carbon*, 50(1):3–33, 2012.

[98] PG Osborn, DWJ Osmond, and BJ Thorpe. Inorganic reinforcing phase dispersed and bonded to polymer matrix, February 17 1981. US Patent 4,251,576.

[99] M Moniruzzaman and KI Winey. Polymer nanocomposites containing carbon nanotubes. *Macromolecules*, 39(16):5194–5205, 2006.

[100] SY Yang and YC Chen. Experimental study of injection-charged compression molding of thermoplastics. *Advances in Polymer Technology: Journal of the Polymer Processing Institute*, 17(4):353–360, 1998.

[101] G Kasaliwal, A Göldel, and P Pötschke. Influence of processing conditions in small-scale melt mixing and compression molding on the resistivity and morphology of polycarbonate–mwnt composites. *Journal of Applied Polymer Science*, 112(6): 3494–3509, 2009.

[102] X Cheng and JS Wiggins. Novel techniques for the preparation of different epoxy/thermoplastic blends. 2015.

[103] PJ Andersen and SK Hodson. Articles of manufacture and methods for manufacturing laminate structures including inorganically filled sheets, November 3 1998. US Patent 5,830,548.

[104] W Haselrieder, S Ivanov, DK Christen, H Bockholt, and A Kwade. Impact of the calendering process on the interfacial structure and the related electrochemical performance of secondary lithium-ion batteries. *ECS Transactions*, 50(26):59–70, 2013.

[105] S Rockstedt. Multi-screw, continuous mixing and kneading machine with polygonal kneading elements for plasticizable compounds, December 7 1993. US Patent 5,267,788.

[106] J-G Racine. Method and apparatus for high density paper, May 31 1994. US Patent 5,316,624.

[107] IIK Jinasena. *Electrospun nano-mat strengthened aramid fibre hybrid composites improved mechanical properties by continuous nanofibres.* PhD thesis, 2016.

[108] ASTM Standard. Standard test method for short-beam strength of polymer matrix composite materials and their laminates. *Annual book of ASTM standards, West Conshohocken*, 15:54–60, 2007.

[109] AK Bandaru, S Patel, Y Sachan, S Ahmad, R Alagirusamy, and N Bhatnagar. Mechanical behavior of kevlar/basalt reinforced polypropylene composites. *Composites Part A: Applied Science and Manufacturing*, 90:642–652, 2016.

[110] J Maity, C Jacob, CK Das, AP Kharitonov, RP Singh, and S Alam. Fluorinated aramid fiber reinforced polypropylene composites and their characterization. *Polymer Composites*, 28(4):462–469, 2007.

[111] SR Dhakate, A Chaudhary, A Gupta, AK Pathak, BP Singh, KM Subhedar, and T Yokozeki. Excellent mechanical properties of carbon fiber semi-aligned electrospun carbon nanofiber hybrid polymer composites. *RSC Advances*, 6(43): 36715–36722, 2016.

[112] H Saghafi, R Palazzetti, A Zucchelli, and G Minak. Influence of electrospun nanofibers on the interlaminar properties of unidirectional epoxy resin/glass fiber composite laminates. *Journal of Reinforced Plastics and Composites*, 34(11):907–914, 2015.

[113] J Yao, CWM Bastiaansen, and T Peijs. High strength and high modulus electrospun nanofibers. *Fibers*, 2(2):158–186, 2014.

[114] F Yuan, R-X Ou, Y-J Xie, and Q-W Wang. Reinforcing effects of modified kevlar® fiber on the mechanical properties of wood-flour/polypropylene composites. *Journal of forestry research*, 24(1):149–153, 2013.

[115] A Arinstein and E Zussman. Electrospun polymer nanofibers: mechanical and thermodynamic perspectives. *Journal of Polymer Science Part B: Polymer Physics*, 49(10):691–707, 2011.

[116] JSD Muthu and R Paskaramoorthy. Double-wall carbon nanotube-reinforced polyester nanocomposites: Improved dispersion and mechanical properties. *Polymer composites*, 33(6):866–871, 2012.